THE HIGHER TECHNICAL INSTITUTE

HTI REVIEW 2005-2006

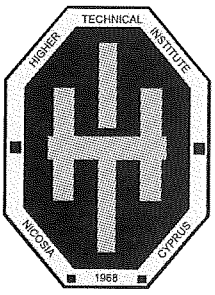

THE HIGHER TECHNICAL INSTITUTE

THE HIGHER TECHNICAL INSTITUTE REVIEW 2005-2006

No 35, November 2006, Nicosia - Cyprus

The Higher Technical Institute (HTI) was established in 1968 as a Government of Cyprus project with assistance by the United Nations Special Fund (UNDP), the United Nations-Education-Scientific and Cultural Organisation (UNESCO) and the International Labour Office (ILO). Cyprus Government Executing Agency: The Ministry of Labour and Social Insurance.

HTI Review is published by the Press and Information Office in co-operation with the Higher Technical Institute, Nicosia. It accepts articles which promote and further new developments and knowledge in technology especially with reference to Industries of Cyprus. Requests for further copies of the magazine and information concernig the published articles should be made to:

The Editors
HTI Review Higher Technical Institute
P.O.Box 20423, 2152 Nicosia - Cyprus
Tel.: 22 406300, Fax: 22 494953/22 406545
e-mail: registry@hti.ac.cy
website: www.hti.ac.cy

P.I.O. 382/2006-1.000 ISSN 1 019-7354
Published by: Press and Information Office
Designed by: CHROMAsyn Ltd
Printed by : THEOPRESS Ltd

CONTENTS

FROM THE EDITORS' DESK...

Dear Readers,

We would like to welcome you to our latest edition of the HTI Review. The development and adoption of new technologies is inevitable and of prominent importance and this will naturally occur through research activity.

The aim of this publication therefore, is to reflect this contemporary research and present it as reported by our members of staff.

The articles presented in this current issue cover a wide range of topics encompassing a broad spectrum of engineering and academic disciplines, including articles on thermal energy, tele-echography, noise pollution, solar water heaters and artificial neural networks, technology and language, and others.

Furthermore, the continuous professional development has always been a primary goal amongst staff and this is illustrated through their wide participation both locally and abroad in courses, seminars, staff exchange and European programmes.

We hope that the material presented in this publication will provide ground for further discussion and prompt possibly further research.

While this issue was prepared with much care and enthusiasm, we would always welcome feedback and suggestions that could improve future publications.

The Editors

NOISE POLLUTION IN SCHOOLS: A STUDY OF REDUCTION OF REVERBERATION TIME IN A LYCEUM IN NICOSIA

By Dr Ioannis Angeli, Higher Technical Institute, Nicosia
George Tsikalas, Apostolos Varnavas Lyceum, Strovolos

SUMMARY

The aim of present research work (which is a continuation of the last year work (the noise pollution in the school classes and the repercussions in the performance of students) was the study of acoustics of teaching rooms thought the systematic recording of time of reverberation as well as to identify ways of reducing this time. The research that lasted roughly one and a half year became from a team of students of Apostle Barnabas Lyceum at Strovolos, under the supervision and collaboration of the authors.

The time of reverberation is the time the sound remains in the class-room, because of the multiple reflections is doing that time. The basic method of communication in the schools is through the speech. This means that the size of coverage has distinguished importance. When the time of reverberation is big the coverage of speech is decreased. This make uncomfortable conditions particularly to teachers and students and influences the training operations into which obviously or inconspicuously speech enters, even when the noise levels are low.

With the present study an effort have been made, to record the levels of reverberation time in school teaching rooms, during the lessons. The time of reverberation was calculated in 10 teaching rooms and in 2 special rooms. The reverberation time was calculated using the related theory (theoretical approach) and using special software (experimental approach). Then comparison was made of the measurements with the internationally acceptable limits. This was followed by an effort to improve the acoustics of teaching room, with the appropriate selection and the placement of sound absorbing materials. New measurements were then taken to evaluate the effect of the above taken actions. The basic results and conclusions of present study are following:

• The students receive lessons in classes which the acoustics are far away from the acceptable specifications that are proposed for educational activities. According to the measurements results, the time of reverberation in all classrooms inspected is high.

• The reverberation time almost in all the teaching rooms , in which measurements were taken, exceeded the 1 second when the admissible limit for such rooms, that belong in the category of regular acoustic comfort, is hardly 0,4 seconds .

• The cost for the acoustic improvement of a teaching room is not prohibitory. The research team achieved impressive reduction of reverberation time from 1 second to 0, 48 seconds with the use 20m^2 of a suitable sound absorbing material at a cost of CP150.

RESEARCH DESCRIPTION

A) Introduction to sound pollution and world wide related studies

From the analysis of international bibliography effortlessly the results let to the conclusion that the bad acoustics conditions in the rooms of teaching are incriminated for training difficulties of children and in a lot of cases for low records in the examinations that become in noisy rooms.

The research that was carried out in the region Tirol of Austria supports that noise pollution influences negatively the intellectual health of children. The scientists led to the conclusion that the noise pollution influenced children behaviour and attention during lessons and the communication with the social unit (Occupational and Environmental Medicine).

A research of the Vice-president of the Greek Institute of Acoustics, Associate Professor Dimitri Skarlatou, shows that the students are receiving lessons in conditions of noise that are very far from the acceptable specifications of noise that are proposed for the particular educational activities. The research was held in 32 rooms of 11 schools in Padres and lasted five days. According to the results, the equivalent level of noise during lessons was above of the equivalent acceptable level and it was 71-89 dB while during noise activity was almost zero (during exams) the sound level drops to 52 dB. The proposed limits of level of noise that are proposed by the Building Regulation for such rooms that belong in the category of regular acoustic comfort, are hardly 32 dB. The reverberation time is presented equally increased. According to the estimates of researchers, in a room with 25 students the reverberation time was 1, 52 seconds, while it would not exceeds the 0,8s. "The delayed reflections assist the perception so the students conceive the sound, but it is difficult to them to understand words" (Newspaper, the NEWS 31-10-03.)

In Spain the Delgado Perera and Santiago measured the suitability of each place of rooms, which was included in their research. Same other researchers faced the problem of stress caused by noise in her region of Valencia. The main discovery of those researches is that the professors believed that the problem is limited in their own class and to the near ones.

In 1993 the World Organism of Health (WHO) adopted a series of measures for the design of new rooms or for the improvement of existing ones based on related researches (Anderson, Mr L., "The Sound of Learning", Crandell, C. C., "Pilot studies of speech communication in elementary school classroom", Acoustical Society of America 1997, Madell, I. R., "Managing classroom amplification" 1990.) So is proposed short time of reverberation < 0, 6 s in the region of frequencies from 125 until 4000

Hz. Children has larger sensitivity in big reverberation time from the adults. Existing reports, supports that individuals with small loss hearing 10-15 dB, have larger important problems of understanding, from the individuals with regular hearing'. Even individuals with regular hearing can pass a certain periods of light decreased of hearing, when for example have flew. With this thoughtful, it is proposed that the reverberation should not exceed the reverberation time of 0, 4 s.

B) The problem of noise pollution in schools

The increased levels of noise pollution and their negative repercussions in all the expressions of our daily life, was the main reason of initiating present study.

The last years the scientific community has led to the conclusion that the noise pollution is responsible for many problems of the modern person which have direct impact to his health as well to his quality of life. Problems such as the cardiac diseases, the accumulation of stresses in the already heavy loaded human organism and the incalculable cases of hearing damages worldwide, lead to the conclusion that is rendered henceforth imperative the adoption of ways facing the phenomenon of noise pollution. "Invisible threat", therefore, the noise for the human being, constitutes one of the most important factors of polluting of environment and consequently the quality of life. The pollution from noises affects henceforth the one third of population of European Union and has detrimental repercussions in the human health. The undesirable noise increases the pressure, causes tiredness, decreases the sleep, increases the stress, influences negatively the digestion and impedes the concentration.

In the children the sound pollution and the acoustics of teaching rooms, can influence the capability of concentration and learning. It constitutes a common secret that in the great majority of classrooms of secondary education, there are students with "weakness of concentration" that they make noise without reason" and generally they try so much to take the attention of the others so what, in certain cases the teaching becomes impossible. The teacher's efforts to tackle and overcome these types of conditions have repercussions in their health.

It appears therefore that the bad records in the schools are justified connected with the ergonomic conditions that exist in the teaching rooms. The paradox it is that, while in almost in every country there is an entire body of legislated regulations on the protection of adults from the noise in the working place, there is a big cup for children. The most likely reason for this lack of regulations is the direct connection of young population with noisy activities and accordingly the opinion that it is useless to regulate by law the protection from the noise. It is proved however that the educational processes are sensitive to noise as well as the mental health of young population.

In spite of that the problem of noise in the education is a worldwide problem; the public have no information for that. We could say that is given too much attention in the social conditions and the physiological types of behaviour in the education than in the natural factors which are mainly ignored, with a result the teaching staff and students suffer from noise that prevail in the teaching rooms.

This question is not covered sufficiently by researches. In all the educational rungs the issue of noise is an important factor, which has not been given the adequate importance. In Cyprus there are no systematic measurements to estimate of classrooms conditions with regard to their acoustic adequacy.

The last year analysis of results of the research on the subject *«the noise pollution in the school rooms and their repercussions in the students performance»*, which was developed from the same team, showed that it is necessarily the further investigation of the problem of noise pollution in classrooms.

According to the results of that research, the equivalent noise level during lessons was very high. In all the classrooms that measurements were taken , the mean equivalent noise level exceeded the 60dB when the level limits of noise that are proposed by the Building Regulation for such rooms that belong in the category of regular acoustic comfort, are hardly 32 dB. Also the team identify that there was a problem with low acceptability.

The acceptability of speech is one of the basic acoustic parameter of teaching rooms. It has been proved scientifically that better acoustic teaching environment, helps to a large extent in the process of learning. The improvement of acceptability of speech is achieved mainly with the control of the reverberation time and noise in the interior of school rooms. When a sound is released in air by a point, a series of round waves is created which are propagated outwards in the form of spheres with the same centre. Those sound spheres are getting bigger and bigger resulting continues loss of energy in every point and because the distance from the source increases. Finally if there no obstacles the sound is becoming weaker so that it could be considered as negligible.

On the contrary, when the distribution of sound is prevented by the limits that specify a space, then a part of the sound wave goes through those limits, another is absorbed and another one is reflected. When a listener finds itself, in such a space accepts as in fiqure I below, (a) the direct sound and (b) the reflected sound. The reflected sound again, is the one that is coming from the first reflections and the ones that are becoming later.

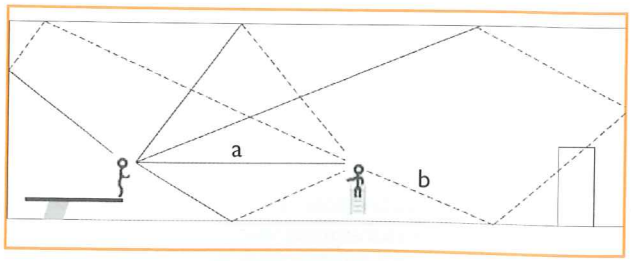

Figure 1: The propagation of sound waves

METHODOLOGY THAT WAS FOLLOWED

Collaboration of the participants:

The members of the research team even during the preparatory stages as well during the approval of the

implementation of the research, dealt with extensive bibliographic research and research in the internet. This research was consecrated on similar work in the subject as well in the acquisition of any other relative information. It initially became in individual level or in small teams and followed discussion and exchange of information.

After the training of the selected software for measuring reverberation time, some of the team members started measuring the dimensions of the class rooms as well as surfaces of all the reflecting materials, windows, doors furniture, roof, floor etc. All those measurements were inputted in Microsoft Excel in order to calculate the reverberation time using formula. Figure 2 shows how reverberation time was calculated in Microsoft Excel. From the results it was clear that there was a problem with the reverberation time, so measures should be taken to improve the acoustics of the classrooms.

Implementation of the study:

In order to have the first estimation of acoustic behaviour of the teaching rooms, the dimensions were measured in ten rooms of teaching and in two special rooms as explained above .Then the reverberation time was calculated, in the recommended frequency of 500Hz, as shown on figure 2.

The calculations were made using the method of Sabine who at the 19th century calculated the reverberation time (RT) in seconds, using the following formula:

$$RT \approx 0.161 \left(\frac{V}{A}\right)$$

Where: $A = aS = a_1S_1 + a_2S_2 + a_3S_3 + \ldots$, the total absorption in "Sabine» units and V the volume of the room in m^3 . a = abortion coefficient, S = surface area

For finding the total absorption (A), a detail recording and calculation of the surface area (S) was made of the materials the walls is covered, the ceiling and the floor in each room as shown in figure 2. Also various objects that existed in the rooms were recorded (desks, chairs, tables etc.); there surface area was calculated and from what materials they were made .The absorption coefficient for each material, was taken from internationally accepted tables.

The number of students in each teaching room plays an important role in the increase of absorption of sound and accordingly in the reduction of the reverberation time is resulting to the improvement of the acoustics of the classroom. Thus the reverberation time was calculated assuming that there were on average 20 students in each class. This number was assumed from a study of the number of students in each class during the current year and the previous one.

At this point it should be noted that during the last years there has been intense criticism for the Sabine's formula, which is considered insufficient for the modern acoustics requirements and some ways of calculating reverberation time have been proposed. The main weakness of Sabine's formula is that it does not considering the aspect of the distribution of the noise reduction materials in the various surfaces, while it is already known that this distribution plays an important role. Also the formula considers that the reflected sound in a room is diffused uniformly. However it is generally acceptable that, as a first estimate of the acoustics of space, the formula of Sabine gives satisfactory results.

After the first calculations of the reverberation time, which gave big values, the research team decided that further investigation should be made. Thus as more reliable method it was selected to measure the reverberation time. This could be accomplished by using computer and a special software for sound analysis. The selected open code software (audacity 1.3), except that it is sold free of charge in internet (http://audacity sourceforge.net/), it was judged satisfactorily reliable, for the needs of present research. Detail instructions that concern the use of the software in the measurement of reverberation time of space, are given by the designers in the relative web page. The way of calculations is also given for reverberation time (RT) with the exploitation

3	**Αίθουσα:1**			**(20 μαθητές)**	
4	**Διαστάσεις:**	**Μήκος x=**	**7,34 m**	**162,7 m^3**	
5		**Πλάτος y=**	**7,15 m**		
6		**Ύψος z=**	**3,1 m**		
7					
8	**Περιγραφή επιφάνειας**		**Εμβαδόν (S) m^2**	**Συντελεστής(α)**	**α·S**
9	Καρέκλες (κενές)		2	0,03	0,06
10	Καρέκλες (κατειλειμένες)		20	0,7	14
11	12 θρανία		21,6	0,03	0,648
12	2 πίνακες		4,33	0,04	0,1732
13	1 πινακίδα		4,1	0,1	0,41
14	1 κρεμάστρα ρούχων		0,28	0,04	0,0112
15	1 ρολόϊ		0,07	0,04	0,0028
16	3 σώματα θέρμανσης		5,7	0,01	0,057
17	1 πάγκος		5	0,05	0,25
18	16 Παράθυρα (μεγάλα 1τμ)		16	0,18	2,88
19	6 Παράθυρα (μικρά 0,65τ.μ)		3,9	0,18	0,702
20	2 Πόρτες(1,8τμ)		3,6	0,12	0,432
21	Πάτωμα(μάρμαρο)		50	0,01	0,5
22	Τοίχοι (μπετόν βαμμένο)		26	0,06	1,56
23	Τοίχοι (επένδυση πετροβάμβακα)		22	0,9	19,8
24	Οροφή(μπετόν βαμμένο)		56,5	0,06	3,39
25				$A=\bar{a}S=a_1S_1+a_2S_2+a_3S_3+..=$	44,876
26					
27				$t=0.161\left(\frac{V}{A}\right)=$	0,58

Figure 2: Calculation of reverberation time 't' using formulas in Microsoft Excel

of graphic representations performed with the help of computational audacity (see figure 3).

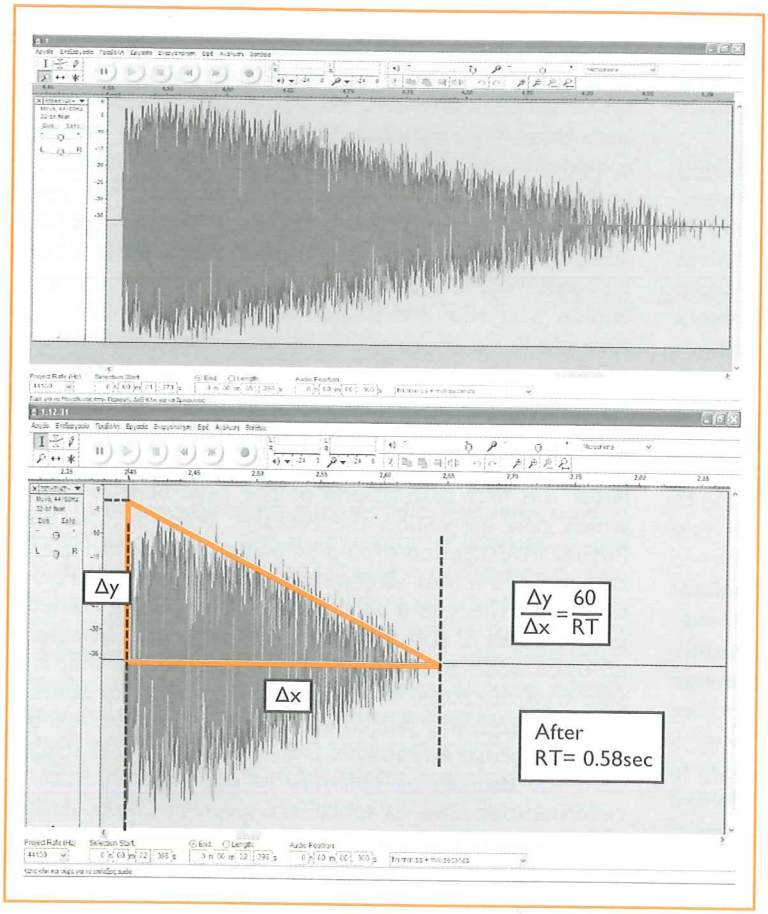

Figure 3: Calculation of reverberation time before and after the addition of sound absorbing sheets

The reverberation times measured in each room (table I) with the software were compared with those calculated with the Sabine's formula. The comparison did not show important differences but confirmed the existence of a serious problem in the room's acoustics. So the next step was to try to improve the acoustics of problematic teaching rooms. For this purpose room I was selected which was in the centre of the Lyceum and the efforts were initiated to identify the appropriate sound absorption material. The basic selection criteria were the sound absorption coefficient /performance output, the cost and the difficulty of placement the material on the classroom walls. With the active participation and the help of experienced researcher the members of the resèarch team evaluate and select the most appropriate material. The selected material was 60x60cm sheets of mining fibres called petrovamvakas which was fixed on 22m^2 of classroom walls. The method of fixing as well as the final view of the classroom I is shown on figure 4.

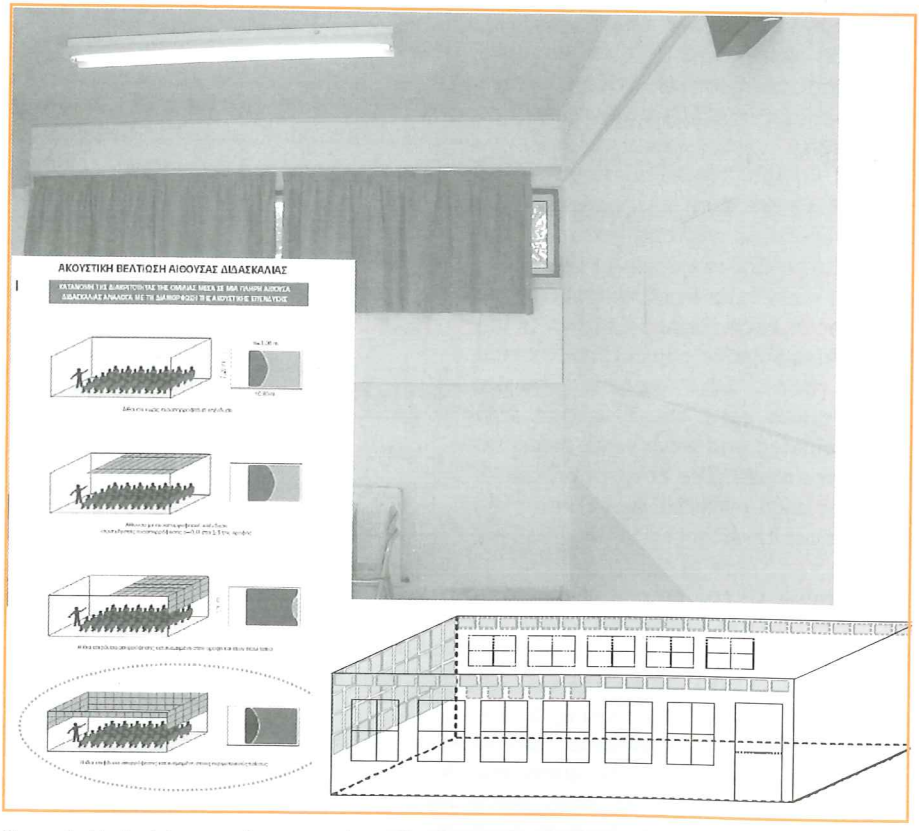

Figure 4: Methodology used to cover the walls of a teaching room with sound absorbing material

The absorption coefficient of the material used was a = 0, 9 and the one of the wall was 0, 06. The expected time of reverberation using the Sabine formula was calculated to be 0,58sec.The measurement of the reverberation time with audacity software showed impressive improvement of the acoustics of the room as it is shown on figure 3. The two values (Sabine and audacity) were almost the same.

The next step was the extensive discussion of the results of the research, the cost analysis for the improvement of acoustics of all the teaching rooms of the Lyceum and finally an attempt was made to diffuse the experiences and knowledge that had been acquired, in the form of suggestions and proposals to the School management and the ministry of Education.

SUMMARY OF RESULTS

The theoretical calculations and the experimental measurements of reverberation time, investigated in this research work, showed that the acoustics of the teaching rooms that have been investigated are problematic. Table I presents the results of the theoretical calculations and the measurements of the computer. The reverberation time as appears in table I in both cases in all the rooms exceeds I second.

The above mentioned values can be characterized as particularly high for school teaching rooms, in comparison with the proposed reverberation time values for such spaces, ranging from

0, 4 up to 0, 6 seconds. The lower value of reverberation time in the special room 31 is due to the coverage of relatively big surfaces, of this room, with various materials which are not used in the common teaching rooms. The floor of room 31 is covered with carpet which has a coefficient of absorption of roughly 0, 4. This coefficient is 400 times bigger than the coefficient of marble which the floor of the common teaching rooms are covered. Nevertheless the acoustics of the particular room is not satisfactory. This is because there are big desks and many wooden constructions, with very smooth surfaces, with very small coefficient of absorption.

Table 1: Reverberation time in teaching rooms investigated

Room no (with 20 students)	RT(Sabine)	RT(audacity)
1	0,99	0,98
2	1,10	1,08
8	1,20	0,96
9	1,08	0,95
21	1,03	0,98
22	1,19	1,11
23	1,10	1,10
24	1,20	1,13
25	1,13	1,10
32	1,20	1,04
3	0,98	0,95
31	0,76	0,73
Mean	1,08	1,01

The reduction of reverberation time in room 1 after the placement of sound absorbing sheets, as it is shown on figure 4, was impressive. Taking into consideration the volume of the particular room the ideal reverberation time is 0, 4 seconds. The reverberation time was reduced to 0,48 seconds, so it can be said that this room even thought the room does not have the ideal conditions ceased to have problematic acoustics.

At this point is good to mention that immediately after the installation of the absorbing material in room 1, students and teachers, realised big difference in the acceptability of speech. It was in deed noticed, as it was expected the phenomenon most students and teachers raising unconsciously the intensity of their voice. This phenomenon is due to the reduction on sound reflections which gives the impression to the speakers that they are not heard and thus are required some time of adaptation in the new acoustics conditions.

MAIN CONCLUSIONS

All the students of St Apostolos Varnavas Lyceum worked intensively as a team under the supervision and assistance of their supervisor for the succesful accomplishment of the research work with all the well known benefits to them. The systematic and scientific approach in solving a problem or proving a hypothesis was well established.

Summarising the results, the applicability of the study should be noted first. The main questions and hypothesis of the research were confirmed completely. Unfortunately the students receive lessons in teaching rooms which their acoustics are far away from the acceptable specifications that are proposed internationally for the educational activities.

Also it became obvious that an acoustic intervention in the rooms of teaching is not only feasible but rather easy and relatively at low cost. The cost for the spectacular improvements of the acoustics of rooms in which the students and their teachers are called to participate in the learning process, is not bigger than 2 CP per student. For the Lyceum under investigation with roughly 800 students, 40 teaching rooms and cost per room 200CP, the cost roughly is 40 x 200=8000 CP. Considering the life time of the sound absorbing material only 5 years, there is a cost of ((8000/800)/5 years) equal to CP2 per student). Even if the above calculations can be characterized as unsophisticated or ease the authors believe that they are not far away from the reality.

Due to the limited time spend for the study and the limited resources it was not feasible to conduct multiple repetitions, as well as the study of the phenomenon for an extended period of time (school year duration), in a larger number of teaching rooms and with other materials. Thus the conclusions of the present research even if they cannot be considered final, it is believed that they are reliable enough to draw the attention and put the people involved in education to think about it.

With the conviction that an educational policy, that respects the educational process, it should pay attention to the achievement of excellent acoustic quality in the teaching rooms, we hope that the announcement of findings of present research will contribute positively in the sensitization of the interested parties. It is our hope that the school rooms that are designed and erected from now on, have the right and satisfactory acoustics.

For the above reason the main objective of the research team is to distribute the results to the appropriate bodies and interested parties. (Ministry of education, Nicosia schools council, the Lyceum management, and to present a paper at 2nd Eco – Forum). Already the lyceum management, where the research has been conducted, is very much interested for full implementation. That is why an investigation has been initiated to find ways for financing a major project for the improvement of the acoustics of all teaching rooms.

BIBLIOGRAPHY AND SOURCES

1. Delgado, C., Perera, P., Santiago, P., "Influence of different acoustic parameters in the speech intelligibility", Institute National de Recherche sur les Transports et leur Securiti, Nice 1993
2. Garcia, A., Garcia, A. M., Romero, I., "Effects of environmental comprehended in Spanish schools", Acoustics Bulletin 1993,
3. Acoustics Dr. H. Brockmayer, Giessen
4. United States Department of Transportation, ` Keeping noise Down: Highway Traffic noise Barriers', Federal Highway Administration (FHWA). (2001).
5. Ntais, P. A., ` Forestry of Cities, Aristotelian University Thessalonica, Department of Publications Academic Printing-house, Thessalonica, (1998-1999).
6. Health and Safety Office (HSO), ` noise', Sheffield, Hallam University. (2001).
7. Occupational and Environmental Medicine
8. Newspaper "News" (31/10/03)
9. Greek Building regulation Sound insulation – sound reduction(article 12 decision 3046/304/301/3.2.1989)
10. Greek Presidential decree YP' NO 85/91
11. www.rockfon.com

INTRAPARTICLE MASS TRANSFER RATE IN ADSORPTION PROCESSES

Andreas Georgiou[1], Paul Christodoulides[2] and Krzysztof Kupiec[3]
[1]Frederick Institute of Technology, Limassol, Cyprus
[2]Higher Technical Institute, General Studies Department, Nicosia, Cyprus
[3]Technical University of Cracow, Institute of Chemical Engineering and Physical Chemistry, Cracow, Poland

Abstract. A second-order approximation of adsorbate uptake rate is presented. The derivation of this approximation is based on the methodology developed by Georgiou & Kupiec (1996). Computations can be performed for different pellet geometries and boundary conditions for which analytical solutions are available.

1. INTRODUCTION

Modeling of many transient mass and/or heat transfer processes leads to coupled partial differential equations involving time and spatial variables. The unsteady-state diffusion and adsorption in particles is described by the following equation.

$$a\frac{\partial Q}{\partial t} = D\frac{1}{r^{m-1}}\frac{\partial}{\partial r}\left(r^{m-1}\frac{\partial Q}{\partial r}\right). \qquad (1.1)$$

The meaning of variables and parameters in (1.1) depends on the diffusion model and is given in Table 1 below.

Table 1. Definitions of variables and parameters in diffusion model (1.1)

Variables / Parameters	Pore diffusion model	Solid diffusion model
Q	C	q
D	D_p	D_s
a	$\varepsilon_p + K$	1

Analytical solutions of equation (1.1) are available (Crank 1956) for a number of initial and boundary conditions. These solutions are often in the form of infinite series and are not easy to use. The substantial simplification of computations is achieved by the use of driving-force approximations of the form

$$\frac{d\bar{Q}}{dt} = f(Q_R, \bar{Q}) \qquad (1.2)$$

and has motivated numerous studies for the development of such models.

The first and most widely used driving-force approximation is the Linear Driving-Force (LDF) approximation suggested by Glueckauf & Coates (1947) as follows.

$$\frac{dA}{d\tau} = m(m+2)(1-A). \qquad (1.3)$$

Further developments on the LDF model were later presented by Glueckauf (1955), Liaw et al. (1979), Yao (1991) and Yao & Tien (1992), Hills (1986), Yang (1987) Do & Mayfield (1987) and Do & Rice (1986). Do & Rice (1986) suggested a quartic profile approximation.

Tomida & McCoy (1987) considered a polynomial concentration profile of the form

$$C(r,t) = \sum_{n=0}^{N} a_{2n}(t) r^{2n} \qquad (1.4)$$

and showed that as the degree of the polynomial increases indefinitely, the polynomial profile equates to the exact solution.

Buzanowski & Yang (1989) derived an extended linear driving-force approximation based on a cubic intraparticle concentration profile. The extra coefficient in this case is an adjustable parameter. This approximation is valid both for large and small times. However, Kikkinides & Yang (1993) have shown that the cubic profile is mathematically unacceptable to satisfy equation (1.1).

Vermeulen (1953) formulated the following QDF approximation.

$$\frac{d\bar{Y}}{d\tau} = \pi^2 \frac{Y_1^2 - \bar{Y}^2}{2\bar{Y}}. \qquad (1.5)$$

Do & Mayfield (1987) considered the following intraparticle concentration profile.

$$Q = a_0 + a_n x^n, \qquad (1.6)$$

where, a_0, a_n and n are functions of time. This profile approximation leads to a Quadratic Driving-Force (QDF) expression for the uptake rate:

$$\frac{dA}{d\tau} = 9\left[(1-A) + 0.533\frac{(1-A)^2}{A}\right], \qquad (1.7)$$

resembling Vermeulen's (1953) QDF model (equation 1.5). Model (1.7) is valid for $\tau > 0.003$.

Yao & Tien (1993) presented new approximations of the uptake rate that are valid both at small and large times. These approximations were obtained by making the assumption that the significant part of the concentration profile within a pellet may be represented by a parabolic profile over a spatial domain that expands with time. This profile is given by

$$Q - Q_0 = \begin{cases} a_0 + a_1 r + a_2 r^2, & R-\delta \le r \le R \\ 0, & 0 \le r \le R-\delta \end{cases} \qquad (1.8)$$

where a_0, a_1, a_2 and δ (the concentration layer thickness) are functions of time.

Georgiou & Kupiec (1995) applied an exponential approximation of the intraparticle concentration profile and developed a new driving-force model given by following equation.

$$\frac{dA}{d\tau} = (\pi^2 + \frac{18}{\pi}\frac{1-A}{A})(1-A). \qquad (1.9)$$

The same authors presented a new methodology for the derivation of driving-force approximations based on an analysis of exact analytical solutions for the particular case of negligible external mass-transfer resistances. This methodology allowed for the derivation of approximate models for all basic pellet geometries (Georgiou & Kupiec 1996).

The purpose of the work presented here is to obtain a second-order driving force approximation using the methodology of Georgiou & Kupiec (1996). It is shown that the model obtained is (analytically) integrable and is applicable to all three basic pellet geometries, namely: slab, infinite cylinder and sphere, with a substantial superiority on the accuracy of the new model as compared with other available approximations being demonstrated.

2. MODEL OF THE PROCESS. EXACT SOLUTIONS AND APPROXIMATIONS

We consider the case of a particle with a uniform initial concentration Q_0 subject to a unit-step change of the concentration at $r = R$. In this case, the system is described by equation (1.1) with the following initial and boundary conditions.

$$t = 0, \qquad Q = Q_0; \qquad (2.1a)$$

$$r = 0, \qquad \frac{\partial Q}{\partial r} = 0; \qquad (2.1b)$$

$$r = \mathrm{R}, \qquad Q = Q_R. \qquad (2.1c)$$

The following change of variables in (1.1) and (2.1):

$$Y = \frac{Q - Q_0}{Q_R - Q_0}, \qquad x = \frac{r}{R} \quad \text{and} \quad \tau = \frac{D}{R^2 a}t$$

leads to equation

$$\frac{\partial Y}{\partial \tau} = \frac{1}{x^{m-1}}\frac{\partial}{\partial x}(x^{m-1}\frac{\partial Y}{\partial x}), \qquad (2.2)$$

with conditions

$$\tau = 0, \qquad Y = 0; \qquad (2.3a)$$

$$x = 0, \qquad \frac{\partial Y}{\partial x} = 0; \qquad (2.3b)$$

$$x = 1, \qquad Y = 1. \qquad (2.3c)$$

The analytical solution in this case (Crank 1956) is given by

$$A = 1 - 2m\sum_{n=1}^{\infty} a_n^{-2} e^{-a_n^2 \tau}, \qquad (2.4)$$

where a_n depend on the pellet geometry and A is the volume-averaged value of Y, i.e.

$$A = \frac{m_t}{m_\infty} = \frac{\iiint_V Y dV}{\iiint_V dV}. \qquad (2.5)$$

At short times, upon a step change, the particle may be treated as a semi-infinite medium and this assumption leads to the following approximation (Crank 1956).

$$A = 2m\sqrt{\frac{\tau}{\pi}}, \qquad (2.6)$$

applicable for $\tau < 0.01$. At large times, the series in equation (2.4) converges rapidly and, by retaining only the first term, the fractional uptake can be estimated with satisfactory accuracy.

Following the methodology of Georgiou & Kupiec (1996), we define the following function.

$$F(\tau) = \frac{dA/d\tau}{1-A} \qquad (2.7)$$

or, equivalently (using 2.4)

$$F(\tau) = \frac{\sum_{n=1}^{\infty} e^{-a_n^2 \tau}}{\sum_{n=1}^{\infty} a_n^{-2} e^{-a_n^2 \tau}}. \qquad (2.8)$$

Then, it is not difficult to show that

$$\lim_{\tau \to \infty} F(\tau) = a_1^2. \qquad (2.9)$$

(Note that since F = F(τ) and A = A(τ), we can obtain dependency F = F(A)).

We next define another function as follows.

$$G(\tau) = (\frac{dA/d\tau}{1-A} - a_1^2)\frac{A}{1-A}. \qquad (2.10)$$

It follows (using 2.6) that

$$G_0 = \lim_{\tau \to 0} G(\tau) = \frac{2m^2}{\pi} \qquad (2.11)$$

and (using 2.10)

$$\lim_{\tau \to \infty} G(\tau) = 0. \qquad (2.12)$$

In figure 1 below is shown the dependency $G = G(A)$ for the three basic pellet geometries.

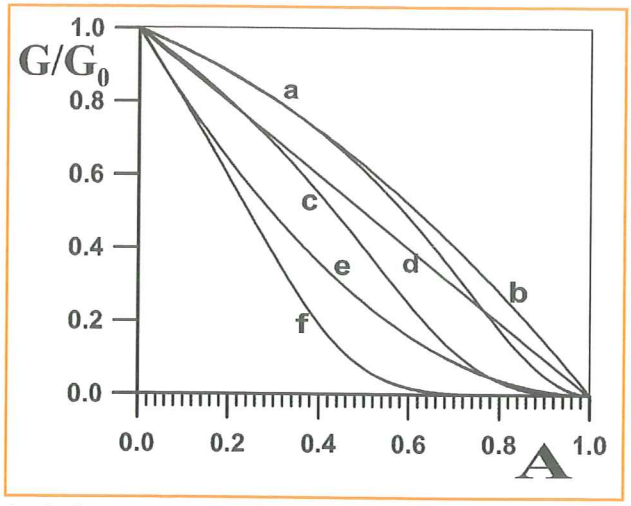

Fig. 1: Comparison of exact and approximate G(A) functions. (a) Exact - sphere, (b) approximate - sphere, (c) exact - cylinder, (d) approximate - cylinder, (e) exact - slab, (f) approximate - slab.

Some earlier published approximations along with a proposed second-order approximation may be considered as resulting from suitable approximations of function G(A).

A. Zeroth-order approximations

I. Linear driving-force approximation

The LDF model is equivalent to the approximation

$$G(A) \approx 0. \tag{2.13}$$

II. Vermeulen's QDF approximation

The QDF model (equation 1.7) is applicable only to spherical particles and it is equivalent to the approximation

$$G(A) \approx \frac{\pi^2}{2} \approx 4.934 \tag{2.14}$$

III. Do and Mayfield approximation

The DM model (equation 1.5) is applicable only to spherical particles and it is equivalent to the approximation

$$G(A) \approx 4.797. \tag{2.15}$$

IV. Georgiou and Kupiec approximation

The GK model (equation 1.8) is also applicable only to spherical particles and it is equivalent to the approximation

$$G(A) \approx \frac{18}{\pi}\,. \tag{2.16}$$

B. First-order approximation

Georgiou & Kupiec (1996) developed the following first-order approximation (see figure 1).

$$\frac{dA}{d\tau} = \{\alpha_1^2 + \frac{2m^2}{\pi}\frac{(1-A)^{2.}}{A}\}(1-A). \tag{2.17}$$

This is equivalent to

$$G(A) = \frac{2m^2}{\pi}(1-A). \tag{2.18}$$

C. Second-order approximation

A second-order approximation of function $G(A)$ is now proposed as follows.

$$G(A) \approx \frac{2m^2}{\pi}[1+\frac{2(m-2)}{m+1}A](1-A). \tag{2.19}$$

A comparison of this second-order approximation with the exact function (2.10) is shown in figure 1.

The resulting driving-force model is therefore given by equation

$$\frac{dA}{d\tau} = \{\alpha_1^2 + \frac{2m^2}{\pi}[1+\frac{2(m-2)}{m+1}A]\frac{(1-A)^{2.}}{A}\}(1-A) \tag{2.20}$$

with initial condition $A(0) = 0$.

3. ANALYTICAL SOLUTION

The proposed model (2.20) may be solved analytically as follows.

Introducing $z = 1 - A$, *(2.20)* yields

$$(1-z)\frac{dz}{d\tau} = MzP(z) \quad (\text{with } z(0) = 1), \tag{3.1}$$

where

$$M = \frac{4m^2(m-2)}{\pi(m+1)}, \qquad \mu = \frac{3(m-1)}{2(m-2)} \tag{3.2}$$

and

$$P(z) = z^3 - \mu z^2 + \frac{\alpha_1^2}{M}z - \frac{\alpha_1^2}{M},$$

on condition

$$m \neq 2. \tag{3.3}$$

The first root of cubic polynomial P(z) is given by

$$z_1 = S + T + \frac{1}{3}\mu,$$

where

$$S = \sqrt[3]{V + \sqrt{U^3 + V^2}}, \quad T = \sqrt[3]{V - \sqrt{U^3 + V^2}},$$

$$U = \frac{\alpha_1^2}{3M} - \frac{1}{9}\mu^2, \qquad V = -\frac{\mu\alpha_1^2}{6M} + \frac{\alpha_1^2}{2M} + \frac{1}{27}\mu^3.$$

It follows polynomial (3.2) may be factorized as

$$P(z) = (z - z_1)[z^2 + (z_1 - \mu)z + \frac{\alpha_1^2}{M} + W],$$

where

$$W = (S+T)^2 - \frac{1}{3}(S+T)\mu - \frac{2}{9}\mu^2.$$

Now, separation of variables in (3.1) yields

$$\int d\tau = \int \frac{M^{-1}(1-z)}{zP(z)}dz = \int \frac{M^{-1}(1-z)}{z(z-z_1)[z^2+(z_1-\mu)z+\alpha_1^2/M+W]}dz. \tag{3.4}$$

Decomposing the integrand in right-hand side of (3.4) into partial fractions yields

$$\frac{M^{-1}(1-z)}{z(z-z_1)[z^2+(z_1-\mu)z+\alpha_1^2/M+W]} = \frac{B_1}{z} + \frac{B_2}{z-z_1} + \frac{B_3 z + B_4}{z^2+(z_1-\mu)z+\alpha_1^2/M+W},$$

where

$$B_1 = -\frac{1}{M(\alpha_1^2/M+W)z_1},$$

$$B_2 = \frac{1-z_1}{Mz_1(z_1^2+(z_1-\mu)z_1+\alpha_1^2/M+W},$$

$$B_3 = -\frac{1}{M(1+z_1)} - B_1(1+\alpha_1^2/M+W) + \frac{1}{1-z_1^2}B_2[1+(z_1-\mu)z_1+\alpha_1^2/M+W],$$

and

$$B_4 = \frac{1}{M(1+z_1)} - B_1(z_1-\mu) - \frac{1}{1-z_1^2}B_2[z_1+(z_1-\mu)+(\alpha_1^2/M+W)z_1].$$

It then follows that (3.4) yields,

$\tau = \Phi(z)$

$$\equiv B_1 \ln|z| + B_2 \ln|z-z_1| + \frac{1}{2}B_3 \ln\left|z^2+(z_1-\mu)z+\frac{\alpha_1^2}{M}+W\right| + \frac{B_5}{B_6}\tan^{-1}\frac{2z-(z_1-\mu)}{2B_6} + \kappa, \tag{3.5}$$

where

$$B_5 = B_4 - \frac{1}{2}(z_1-\mu)$$

and

$$B_6^2 = \alpha_1^2/M + W - \frac{1}{4}(z_1-\mu)^2 \text{ (with condition } B_6^2 > 0).$$

4. FUTURE RESEARCH

The obtained approximate expression can be applied to batch adsorption systems for various pellet geometries (see sphere, cylinder, slab). Some early results have been compared with the exact analytical solution of each problem and it can been shown that the maximum errors do not exceed 2.5%, with the accuracy being even better in the small-time region. Furthermore, the proposed model can be applied to kinetic parameters estimation using experimental data from literature. These estimated kinetic parameters can be used for the accurate prediction of the fractional uptake curves. All this will be presented in the future.

NOTATION

a	defined in table I
A	fractional uptake
C	gas-phase concentration
D	defined in table I
D_p	effective pore diffusion coefficient
D_s	effective surface diffusion coefficient
K	linear equilibrium adsorption constant
m	geometry factor
q	solid-phase concentration
Q	defined in table I
r	radial coordinate
R	particle radius
t	time
t_d	diffusion time
x	dimensionless spatial variable
Y	dimensionless solid phase concentration

Greek letters

ε	percent-relative error
ε_p	porosity of particle
τ	dimensionless time

Subscripts

0	value at $\tau = 0$
1	value at surface
∞	value at $\tau \rightarrow \infty$
R	value at $r = R$

Superscripts

$\bar{}$	volume-averaged quantity

REFERENCES

[1] Buzanowski, M. A. and Yang, R. T., 1989, Chem. Eng. Sci. **44**, 2683-2689.

[2] Crank, J., 1956, The Mathematics of Diffusion, Oxford University Press, Oxford.

[3] Do, D.D. and Mayfield, P.L.J., 1987, A.I.Ch.E.J. **33**, 1397-1400.

[4] Do, D.D. and Rice, R.G., 1986, A.I.Ch.E.J. **32**, 149-154.

[5] Georgiou A. and Kupiec K., 1995, Inz. Chem. Proc. **16**(1), 75-94.

[6] Georgiou A. and Kupiec K., 1996, Int. Comm. in Heat Mass Transfer **23**(3), 367-376.

[7] Glueckauf, E., 1955, Trans. Faraday Soc. **51**, 1540-1551.

[8] Glueckauf, E. and Coates, J.I., 1947, J. Chem. Soc., 1308-1314.

[9] Hills, J.H., 1986, Chem. Eng. Sci. **41**, 2779-2785.

[10] Kikkinides, E.S. and Yang, R.T., 1993, Chem. Eng. Sci. **48**, 1169-1173.

[11] Liaw, C.H., Wang, J.S.P., Greencorn, R.A. and Chao, K.C., 1979, A.I.Ch.E.J. **25**, 376-381.

[12] Prinz, D. and Riekert, L., 1986, Ber. Buns. Phys. Chem. **20**, 413-417.

[13] Tomida, T. and McCoy, B.J., 1987, A.I.Ch.E.J. **33**, 1908-1911.

[14] Vermeulen, T., 1953, Ind. Eng. Chem. **45**, 1664-1670.

[15] Yang, R.T., 1987, Gas Separation by Adsorption Processes, Butterworths, Boston-Wellington.

[16] Yao, C., 1991, A study of a few problems in adsorption, PhD Dissertation, Syracuse University, Syracuse, New York.

[17] Yao, C. and Tien, C., 1992, Chem. Eng. Sci. **47**, 457-464.

[18] Yao, C. and Tien, C., 1993, Chem. Eng. Sci. **48**, 187-198.

[19] Yucel, H., Ruthren, D.M., 1980, J. Chem. Soc. Far. Trans. **76**, 60-70.

ANNEALING AND TEMPERATURE COEFFICIENT STUDY OF TYPE IA FIBRE BRAGG GRATINGS INSCRIBED UNDER STRAIN AND NO STRAIN - IMPLICATIONS TO OPTICAL FIBRE COMPONENT RELIABILITY

Kyriacos Kalli[1], George Simpson[2], Helen Dobb[2], Michael Komodromos[3], David Webb[2] and Ian Bennion[2]*
[1] *Higher Technical Institute, C. Kavafi Street, Nicosia, 2152 Cyprus*
[2] *Photonics Research Group, Aston University, Birmingham B4 7ET United Kingdom*
[3] *Frederick Research Centre, 7 Filokyprou, Nicosia, Cyprus*

ABSTRACT

The annealing properties of Type IA Bragg gratings are investigated and compared with Type I and Type IIA Bragg gratings. The transmission properties (mean and modulated wavelength components) of gratings held at predetermined temperatures are recorded from which decay characteristics are inferred. Our data show critical results concerning the high temperature stability of Type IA gratings, as they undergo a drastic initial decay at 100°C, with a consequent mean index change that is severely reduced at this temperature However, the modulated index change of IA gratings remains stable at lower annealing temperatures of 80°C, and the mean index change decays at a comparable rate to Type I gratings at 80°C. Extending this work to include the thermal decay of Type IA gratings inscribed under strain shows that the application of strain quite dramatically transforms the temperature characteristics of the Type IA grating, modifying the temperature coefficient and annealing curves, with the grating showing a remarkable improvement in high temperature stability, leading to a robust grating that can survive temperatures exceeding 180°C. Under conditions of inscription under strain it is found that the temperature coefficient increases, but is maintained at a value considerably different to the Type I grating. Therefore, the combination of Type I and IA (strained) gratings make it possible to decouple temperature and strain over larger temperature excursions.

Keywords: Fibre reliability, fibre Bragg gratings, annealing, Type IA grating, photosensitivity

1. INTRODUCTION

Type IA fibre Bragg gratings have attracted interest within the sensor community based on their unique spectral and physical characteristics. They are readily identified by their spectral attribute of a large red shift in the Bragg wavelength (λ_{BR}) of the grating during inscription that accompanies an increase in the mean core index [1]. It is recognised that this red shift is dependent on fibre type and hydrogenation conditions, and for a highly doped fibre, such as B/Ge codoped fibre, is typically 15-20nm, whereas the wavelength shift for SMF28 is lower at 5-8nm [2]. The maximum wavelength shift translates to an increase in the mean index of up to $2x10^{-2}$. A strong correlation between the growth of the OH absorption band formation in the optical fibre during prolonged UV exposure and the increase in the mean index change of the fibre grating has been reported, resulting in a fundamental material modification so that Type I and Type IA gratings have been written in the same fibre with a common phase mask, yet with central reflecting peaks more than 14nm apart after annealing [3].

2. INSCRIPTION PROCEDURE

Gratings were inscribed using the scanning phase mask technique and the fibre was illuminated with a cw UV Coherent Sabre FreD laser source operating at 244nm, Figure 1. A 1mm aperture ensured an accurate top-hat exposure profile along the length of the grating [3]. The stage was scanned at $1mms^{-1}$ with 130mW optical power delivered to the fibre.

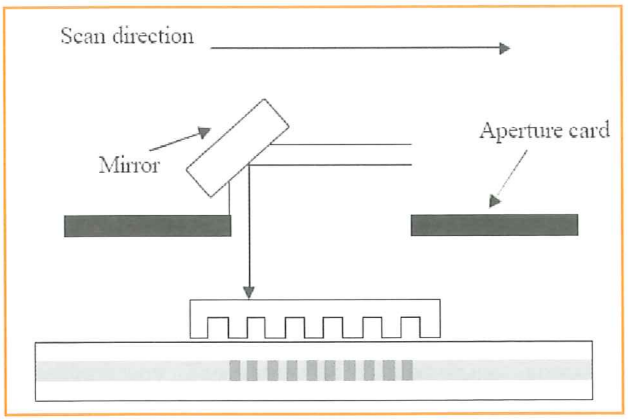

Figure 1. Scanning beam inscription setup using a phase mask and an aperture card to ensure uniform grating exposure.

The grating manufacture was a two-step process; first the phase mask was removed and the UV beam scanned along the fibre length to give a blank beam exposure. The mask was then reintroduced and a grating written into the UV pre-exposed section of fibre. This has proven the most successful way of inscribing Type IA gratings with a clean wavelength spectrum. The fibre underwent hydrogenation as follows; two identical batches of fibre were prepared and each batch consisted of SMF28 (standard corning fiber), B/Ge co-doped fibre (FibercorePS1250/1500 B/Ge co-doped single mode fibre) and two different samples of Ge-only doped fibre (Verillion 12mol%Ge and 21mol%Ge). One batch was hydrogenated at 80°c, 190bar for 93 hours and cooled to room temperature over 24 hours by which time the pressure was 160bar; the other batch was hydrogenated in excess of four months at 180bar and at room temperature. The hydrogen concentration [4] within the fibre samples based on the hydrogenation conditions outlined above is 11400 and 21000 ppm, respectively.

In order that the IA gratings have a reference grating whose properties are well understood, a 1mm Type I grating was written within the same section of each fibre. Figure 2 shows the spectra of each sample before (upper) and after (lower) annealing at 80°C for 96 hours, and highlights a number of differences between the fabricated gratings; notable examples are the gratings written in Verillion B/Ge co-doped fibre, where both the IA andl gratings differ significantly in amplitude and the Type grating would seem to be slightly offset in wavelength. The gratings in SMF28 are comparable in hot and cold hydrogenated samples and do not exhibit any significant spectral characteristics.

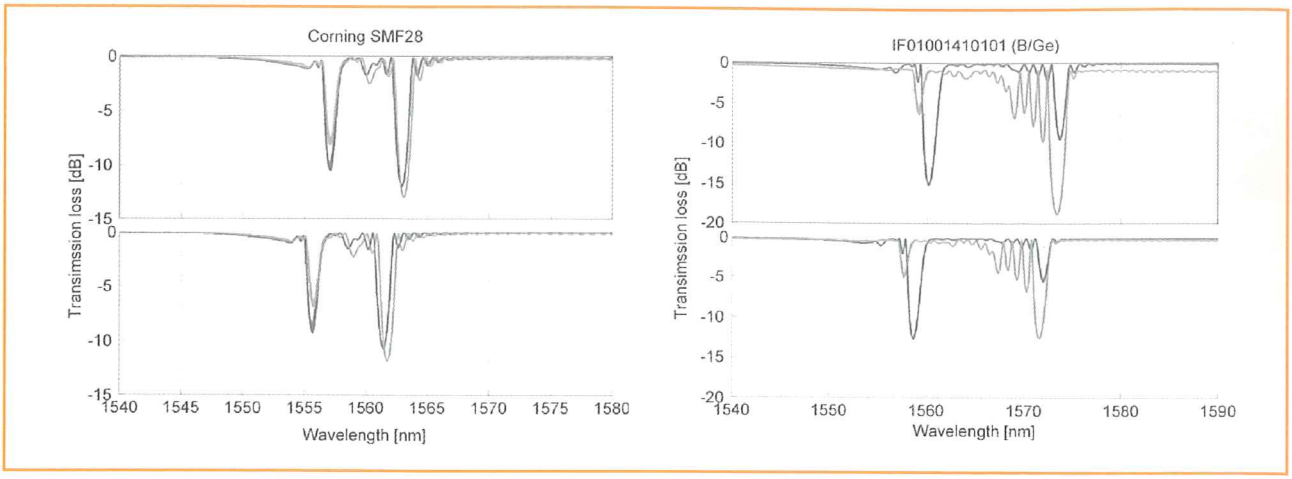

Figure 2. Pre- (upper traces) and post- (lower traces) annealing spectra for Type I and Type IA gratings written in the indicated fibre types for hot (grey) and cold (black) hydrogenation conditions.

3. DECAY OF UV INDUCED GERMANOSILICATE GRATINGS

Williams and Smith [5] studied the thermal stability of strong and weak gratings. They showed that proper stabilisation by annealing ensures that the gratings remain extremely stable and may be expected to last at least 25 years, this result was confirmed by Kannan et al [6] among others. Ishikawa et al [7] proposed a model by which the proper annealing time may be calculated. Patrick et al [8] compared the stability of hydrogenated and non hydrogenated germanosilicate fibres and concluded that gratings written in hydrogen free fibre were significantly more stable at elevated temperatures. Aslund et al [9] showed that presensitised fibres are more thermally stable than hydrogenated fibres. Niay et al [10] showed that UV grating inscription using either CW or pulsed sources resulted in gratings possessing the same elevated temperature stability properties (for the same grating types, and after proper annealing).

3.1 Modulated index changes during annealing

The modulated index change may be represented by the integrated coupling constant (ICC) in preference to reflectivity or peak transmission loss because this quantity is proportional to the UV-induced refractive index change, even for cases where the gratings are non-uniform. This quantity may be calculated according to [11]:

$$ICC = \tanh^{-1}\sqrt{1 - T_{\min}} \qquad (1)$$

where T_{min} is the transmission minimum, i.e. the grating peak reflectance R = 1 – T. It is possible to normalise ICC plots according to grating length,

$$ICC' = \frac{ICC}{L} \qquad (2)$$

or initial amplitude,

$$ICC''(t) = \frac{ICC_{t=0}}{ICC(t)} = \eta \qquad (3)$$

or both which enables the direct comparison of gratings with different lengths or initial reflectance. Erdogan et al [11] showed that initially gratings decay extremely quickly which is followed by a substantial decrease in the rate of decay at longer times. They concluded that this behaviour was indicative of a power law dependence on time and could be fitted according to [11]:

$$\eta = \frac{1}{1 + A\left(t/t_1\right)^{\alpha}} \qquad (4)$$

where the factor A and exponent α depend on temperature and are dimensionless, whilst t_1 = 1min in order to keep dimensions consistent. Baker *et al* [12] confirmed the power law thermal decay model holds well for non-hydrogenated fibres but went on to suggest that for hydrogenated fibres it was a poor fit, relying instead on a log time representation that was indicative of a broader trap distribution with a top hat profile,

$$\eta = 1 - K\log\left(\frac{t}{\tau}\right) \qquad (5)$$

where K and τ are constants and τ is temperature dependent obeying a classic Arrhenius relationship

$$\tau = Ae^{E_a/RT} \qquad (6)$$

which is characteristic of the aging of glass.

3.2 Mean index changes during annealing

A study of the wavelength shift of FBGs manufactured in hydrogenated germanosilicate (Corning SMF28) fibre by Masuda *et al* [13] showed that the wavelength shift during annealing was solely due to the out-gassing of H_2 from the fibre. This was shown by annealing a specimen grating then re-hydrogenating it and then annealing it again. During both annealing processes the wavelength evolution was shown to be the same, and hence they concluded their result. However, Chisholm *et al* [14] have showed that for boron germanium co-doped silica fibres, the wavelength decay still occurred after the hydrogen had out-gassed. Pal *et al* [15] have showed that the power law model used to model modulated index decay may be modified to model the decay in mean index.

4. ANNEALING STUDY

4.1 Experimental arrangement for monitoring annealing

The annealing properties of Type IA gratings were studied in order to investigate their thermal stability and any simi-

larities to the annealing properties of other grating types. The transmission profile of several gratings was recorded at predetermined temperatures using an 8 channel DWDM test system comprising a tuneable laser with 5pm step size, a wavemeter, launch power meter and a rack of 8 InGaAs photodiodes with >100dB dynamic range. The tuneable laser was connected to the wavemeter, before feeding the samples such that a highly accurate measure of the discrete wavelength might be obtained. The samples were placed in a Sanyo environmental chamber (-40°C to 180°C range). This apparatus is shown schematically in Figure 3. After running such an experiment the individual traces were processed using another custom software program which calculated the Bragg wavelength and peak transmission loss for each dataset.

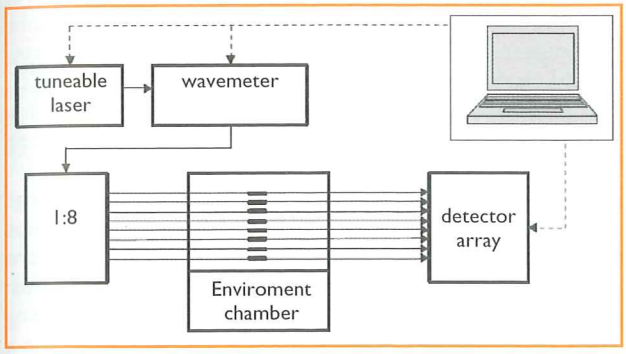

Figure 3. Schematic showing the tuneable laser system used to characterise the gratings during the heating cycle in the tubular oven. This system enabled 5pm resolution with 100dB dynamic range on all 8 channels.

4.2 Standard annealing at 80°C of IA-I dual sensors

This subsection details the annealing data for 8 IA-I dual grating sensors manufactured in B/Ge fibre (Verillion IF01001410101), hydrogenated at 200Bar / 80°C for 64 hours. The Type I grating was 1mm long and was written at 0.5mms^{-1} whereas the Type IA grating was 4mm long and written at 0.05mms^{-1} after 200 blank beam scans at 1mms^{-1} to induce the mature IA index change.

The gratings were annealed at 80°C for 70 hours. Figure 4 shows the annealing curves for an example grating (FBG7). In Figure 4a the annealing curves for the two gratings in terms of ICC.mm^{-1}. This plot explicitly shows that the Type I grating anneals significantly more slowly than the IA grating. Figure 4b shows the decay of the mean index during the annealing process as metered by the Bragg wavelength of the grating during the annealing. This figure shows that in this case, both Type I and IA gratings undergo the same rate of mean index change. The data indicates that their mean indices anneal similarly and this is principally due to hydrogen out-gassing that is set by the conditions of the environment chamber. After 70 hours we observe the reversible wavelength shift that results from the temperature decrease. Figure 4c confirms that the annealing curves for many samples of both grating types show significant differences between them.

It is well documented that gratings written in hydrogenated fibres have a broader trap distribution and this is manifest from the larger index change observed for gratings in this fiber type. The actual distribution is not apparent, although studies by Rathje et al [16] point to decay from two different defects. Our study shows that both the Type I and Type IA gratings are characterized by a second order exponential decay but with different time constants. The current annealing data indicates that standard Type I gratings are more robust than their Type IA counterparts at an elevated temperature. In general, amorphous materials display multiple relaxation mechanisms, described by a summation of exponential equations; the

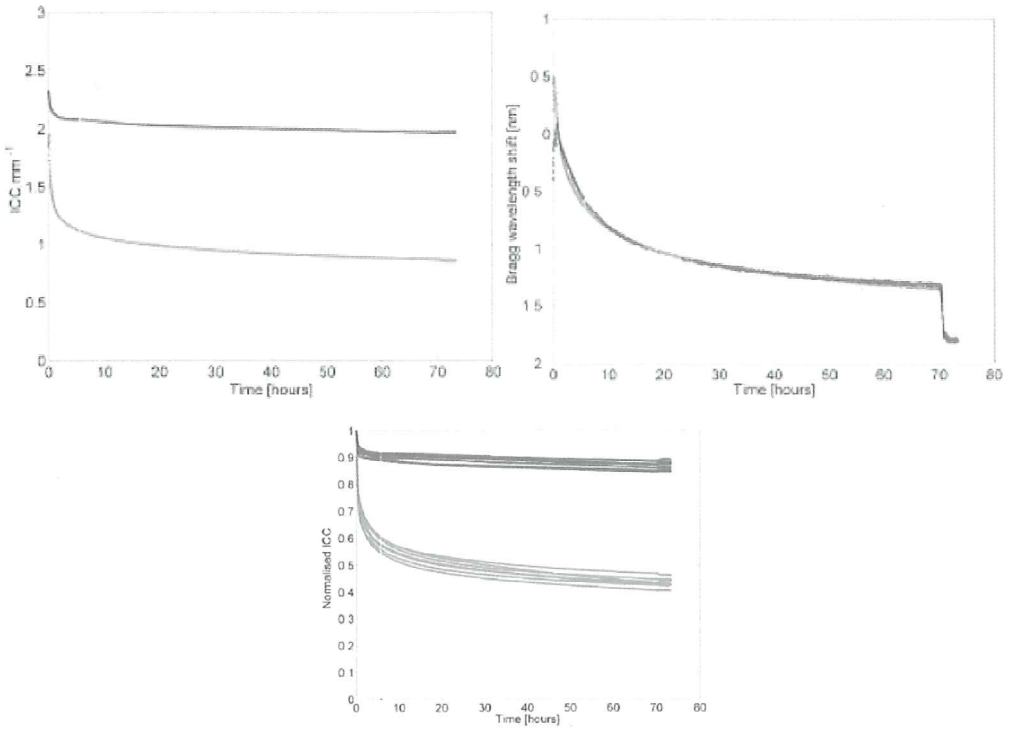

Figure 4. (a) (left-upper) The 80°C annealing curves for Type I (black-UPPER) and Type IA (grey-LOWER) gratings for sample reference FBG4 shown in terms of the ICC per unit length. (b) (right-upper) The annealing curves shown in terms of the Bragg wavelength shift during annealing. (c) (bottom-centre) The 80°C annealing curves for Type I (black-UPPER) and Type IA (grey-LOWER) gratings for 8 samples shown in terms of the normalised ICC.

decay of the fibre Bragg grating is a special case of this decay process. Fitting to this data indicates an excellent fit with a second order exponential decay, Figure 5. This is in keeping with the broader distribution of trap states for gratings in hydrogen loaded fibre, which extend to low energy states that are subject to faster decay at the annealing temperature. The data was fitted with a function of the form,

$$y = y_0 + A_1 e^{-x/t_1} + A_2 e^{-x/t_2} \qquad (7)$$

which is a standard dual exponential decay function representing relaxation mechanisms with two characteristic decay times, Table 1.

Table 1 Characteristic decay times for the Type I and IA gratings, based on data fitting using equation (7).

	Type I Grating	Type IA Grating
1st decay time (hr)	0.547	0.457
2nd decay time (hr)	47.85	15.37

4.3 High temperature stability

In order to evaluate the temperature stability of Type IA gratings an experiment was designed to make a direct comparison between Types I, IA and IIA. The test looked at six Type I, six Type IA and two Type IIA gratings. The fibre used in this trial was Fibercore PS1250/1500 B/Ge co-doped single mode fibre (serial number 30246B/A-00A). The Type I and IA gratings were fabricated in fibre hydrogenated at 200bar at 80°C for 64hours. The IA gratings were manufactured according to the blank beam exposure method detailed earlier; a 3mm section of fibre was pre-exposed by 244nm radiation at 1mms^{-1} until the 1400nm absorption band had reached a maximum value. A 2mm FBG was then written using a scanning phase mask technique at 0.1mms^{-1}. A 2mm Type I grating was then inscribed with a 1mm separation from the IA grating at 2mms^{-1}. The Type IIA gratings were fabricated by the shuttered scanning phase mask method in non-hydrogenated fibre (from the same PS1250/1500 batch) with a scan speed of 1mms-1 and a shutter width of 2mm. A typical spectrum of each grating is shown in Figure 6 for gratings manufactured to have the same strength but different length, hence the different grating bandwidths. All gratings were manufactured in the middle of a 1m section of fibre. The gratings were placed inside a high temperature Carbolite tubular furnace in place of the Sanyo environmental chamber. The gratings were held at 100°C, 200°C, 300°C, 400°C and 500°C, although we present data for the first two temperatures only, as these are pertinent to the results of this study.

In order to ascertain the thermal stability of the gratings the mean and modulated index changes of the samples were calculated. This was done by means of a software program designed to sift through the 8000 or so individual spectral traces and produce tables of the central reflecting wavelengths and peak insertion losses for each grating as a function of time. This information was then converted to mean and modulated index change as follows:

Mean index change

The mean index change was calculated according to the following rearrangement:

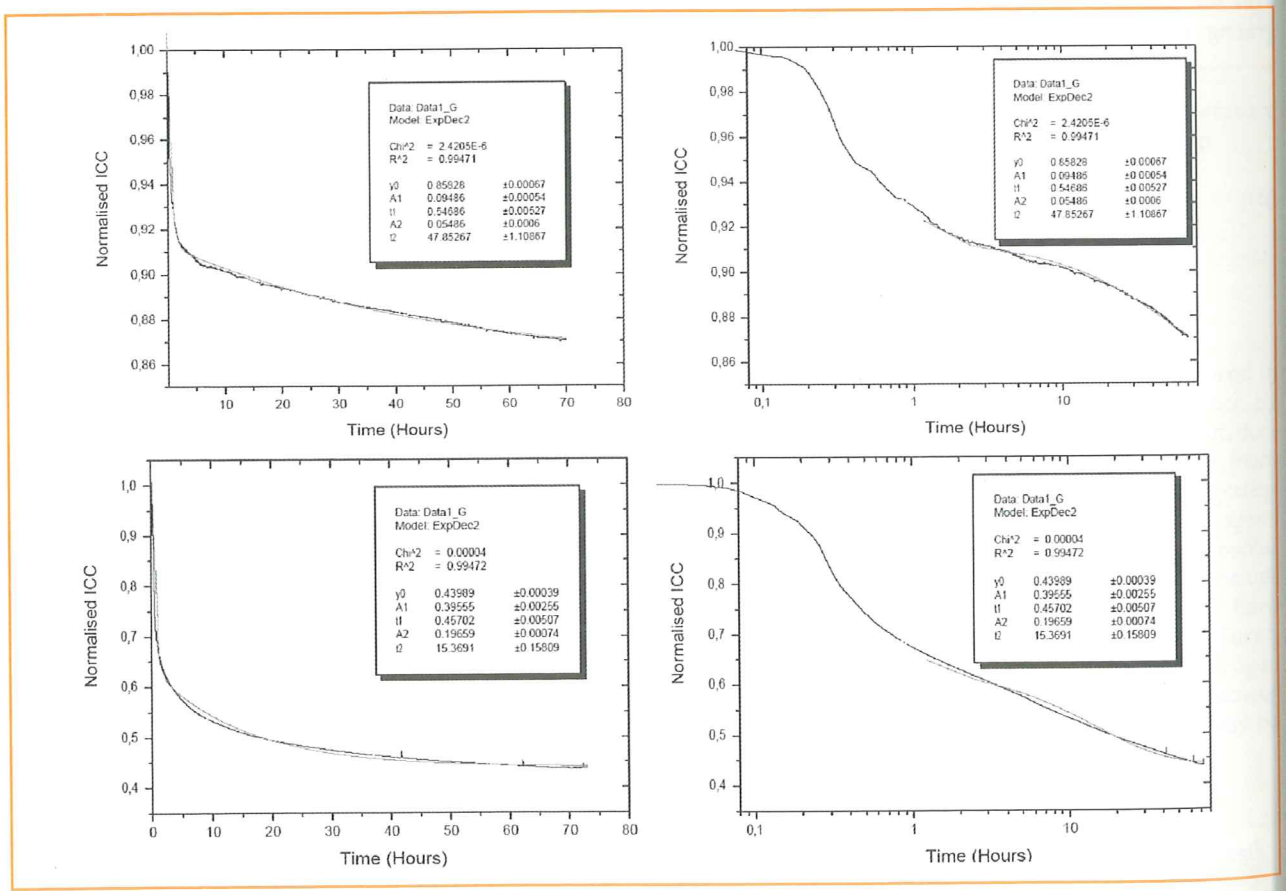

Figure 5. The 80°C annealing curves for Type I gratings with a linear time scale (upper left) and log time scale (upper right) and IA gratings with a linear time scale (lower left) and log time scale (lower right) shown with a representative fit to the normalised coupling coefficient with time.

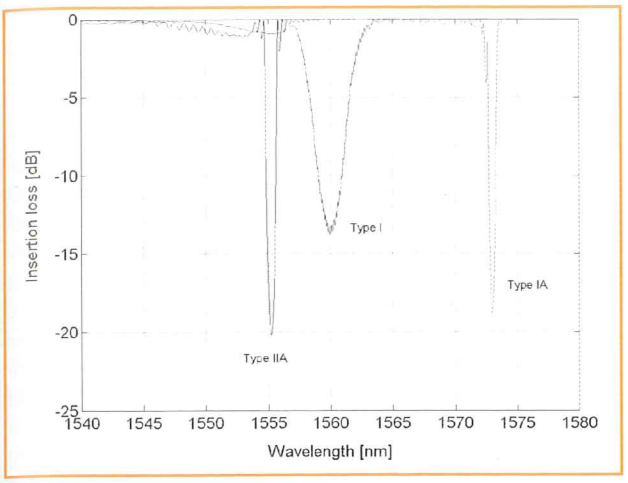

Figure 6. Spectra of Type I, IA, and IIA gratings prior to annealing written in B/Ge fibre. Each grating has the same period, but dissimilar lengths, and demonstrates the differences in the mean index of the three gratings.

$$\lambda_{BR} = 2 n_{eff} \Lambda \tag{8}$$

$$\Delta n_{eff}(t) = \frac{\lambda_{BR(t)}}{2\Lambda} - n_{initial} \tag{9}$$

where Δn_{eff} is the effective refractive index at time t, λ_{BR} is the Bragg wavelength at time t, $n_{initial}$ is the initial refractive index of the fibre core (supplied by the fibre manufacturer as 1.4441) and Λ is the grating period. Λ may be accurately approximated as follows:

$$2\Lambda = \frac{\lambda_{initial}}{n_{initial}} \tag{10}$$

where $\lambda_{initial}$ is found by inscribing a Type I grating in non-hydrogenated fibre. Care should be taken so that the grating is sufficiently immature that it has not exhibited a significant level of the red shift seen during the earliest stages of grating manufacture. This is shown in Figure 7, which yields a value of 1077.515nm for twice the period of the gratings when applied to Equation 10.

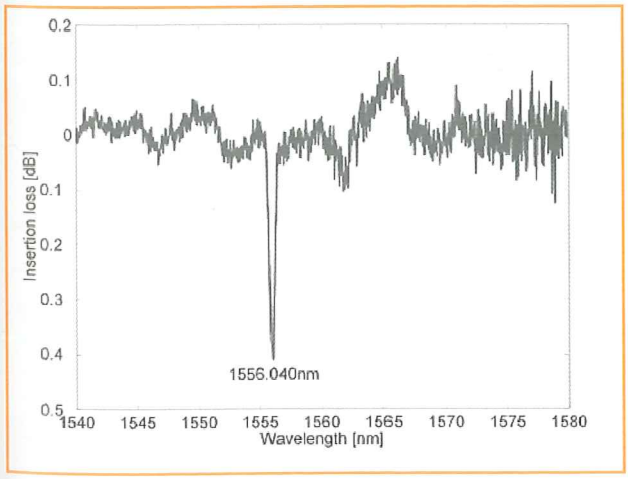

Figure 7. λ_{BR} of a Type I grating in non-hydrogenated Fibercore PS1250/1500 with n_{eff} = 1.4441 as used to calculate the period of the inscribed gratings during the annealing experiment.

It is also desirable to normalise the recorded values of central reflectance for the effects of thermal shift in the Bragg resonance. This is most simply done by applying $\lambda_{BR}(t) = T(t)\lambda'_{BR}(T)$, where $T(t)$ is the temperature at time t, and $\lambda'_{BR}(T)$ is the thermal coefficient of the individual gratings. The average values shown in Table 2 were used, since it was not possible to measure the thermal coefficients of these particular samples, as the high final temperatures used in this experiment carbonised the fibre beyond use.

Table 2 Summary of average thermal coefficients used to calculate the shift in the Bragg resonances during annealing.

Grating type	Thermal coefficient (pm/°C)
I	8.0
IA	6.0
IIA	11.0

This data represents an approximation used to normalise the mean index change under different temperatures.
The result of Equation 10 was substituted back into Equation 9 and normalised to $t=0$ for successive values of λ_{BR} thus producing a dataset containing the mean index change against time for the gratings at increasing ambient temperature. This data is shown in Figure 8 below

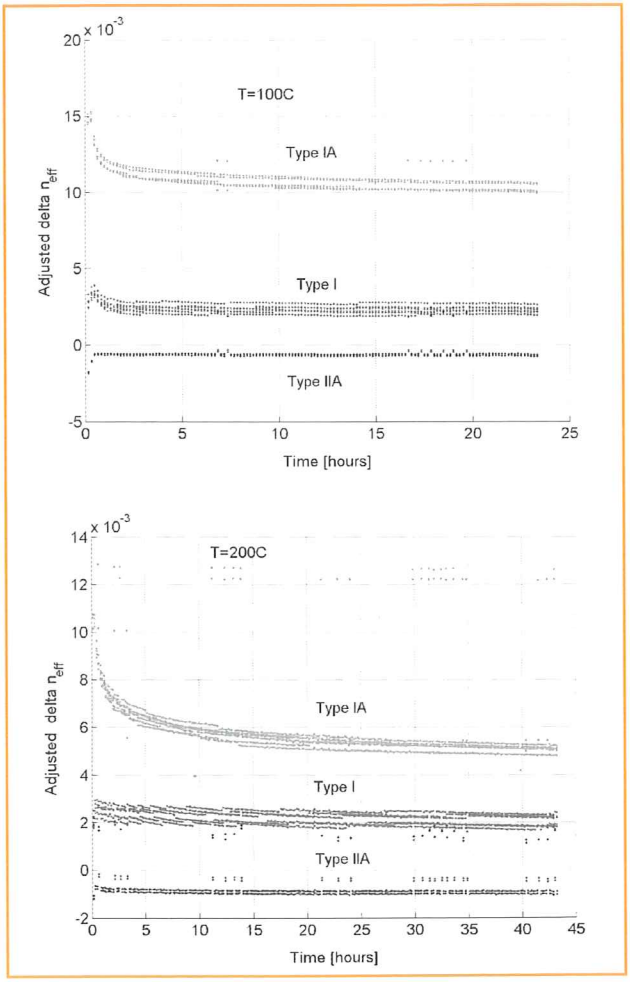

Figure 8. The decay in the mean index experienced by Type IA (top), Type I (middle) and Type IIA (bottom) gratings during heating at 100°C (left), 200°C (right). This figure is the first evidence that the mean index change of IA gratings also decays under moderate temperatures.

Figure 8 shows that the mean index change is severely

reduced at a temperature of 100°C. However, the results also indicate that the modulated index change of IA gratings remains stable at lower annealing temperatures of 80°C, and the mean index change decays at a comparable rate to Type I gratings at 80°C, as indicated in Figure 4. These results show that the maximum temperature IA gratings may be reliably used is less than 80°C.

Modulated index change

The modulated index change was shown in terms of the normalised ICC, and is shown below in Figure 9.

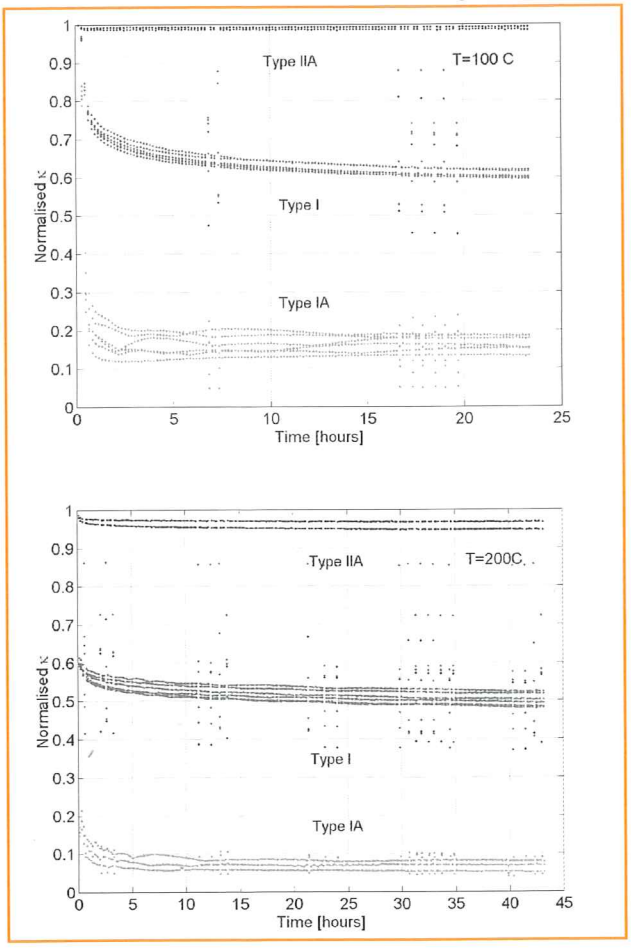

Figure. 9. The decay in the normalised integrated coupling constant by Type IIA (top), Type I (middle) and Type IA (bottom) gratings during heating at 100°C (left) and 200°C (right). This figure shows that the Type IA gratings present the lowest thermal stability, being erased at only modest temperatures. This has profound implications on the potential uses of IA gratings.

This data shows a vital result concerning the high temperature stability of Type IA gratings, indicating that IA gratings undergo a drastic initial decay at 100°C which implies that they are thermally unstable at this temperature. Figure 9 also confirms well known reports as to the stability of different types of Bragg grating showing that IIA gratings are more stable than Type I gratings.

5. EFFECT OF STRAIN ON TEMPERATURE STABILITY

As an extension to our previous studies we inscribed Type IA Bragg gratings under strain, as it has been well documented that strain can affect the growth dynamics of Bragg gratings during manufacture [17], and it was considered that strain would particularly impact the Type IA grating as it is characterised by a broad and shallow trap distribution. We used batches of highly hydrogenated Fibrecore PS1250/1500 fibre and recorded three grating Types into the same fibre section. In this way the fibre position relative to the phase mask and focussed inscription laser beam remained constant, thereby ensuring that the inscription procedure was repeatable. A Type IA grating was written without strain using the characteristic UV blank beam exposure method, as outlined earlier in this paper. A second (Type I) grating was written adjacent to the first, followed by a third Type IA grating inscribed under a constant strain of 1mε that was applied throughout the inscription procedure. This procedure was repeated for a second time and the fibres underwent thermal annealing for extended time periods. Relevant data is shown in Figure 10, confirming that the Type IA grating written under strain survived annealing to 180°C, whereas the unstrained Type IA grating was completely erased at close to 100°C. The figure shows data shifted along the wavelength axis to compensate for temperature induced wavelength shifts, to more clearly show the improved high temperature stability of the strained Type IA grating.

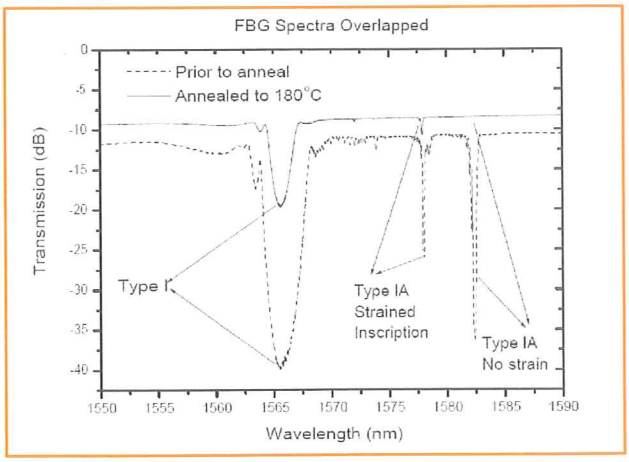

Figure 10. The transmission spectra of Type I, IA (inscribed without strain), IA (inscribed with strain) gratings prior to and after annealing to 180°C. The data shows the improved temperature stability of the Type IA grating. Note the data is shifted along the wavelength and transmission axes to separate the curves and compensate for temperature induced wavelength shifts, for the sake of clarity.

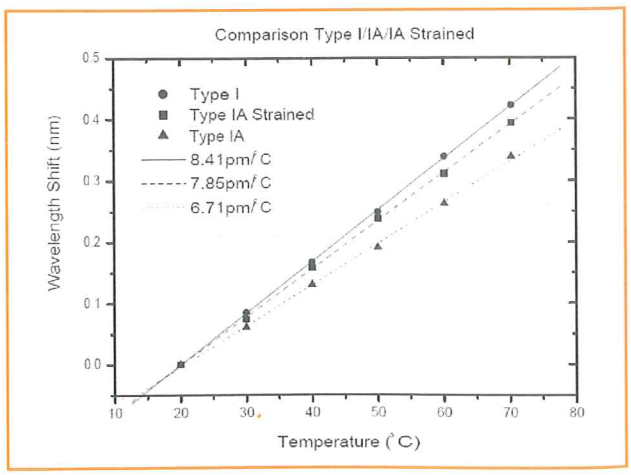

Figure 11. The difference in wavelength to temperature responsivity of Type I, IA, IA (inscribed with strain) gratings. It is observed that the strain increases the temperature coefficient of the Type IA grating and it behaves more like a Type I grating.

Furthermore, Figure 11 shows that straining the Type IA grating during inscription increases the wavelength to temperature responsivity, therefore there is the possibility of using strain to tailor the temperature coefficient of the Type IA grating for temperature compensated strain sensing applications. The effect of strain also hints at the role of defects on the grating stability with temperature and indicates an element of densification during inscription. This is under further investigation.

6. CONCLUSIONS

We have presented data that shows a fundamental result concerning the high temperature stability of Type IA gratings, which undergo a drastic initial decay at 100°C, implying that they are thermally unstable at this temperature. However, the modulated index change of IA gratings remains stable at lower annealing temperatures of 80°C, and the mean index change decays at a comparable rate to Type I gratings at 80°C, this sets a maximum temperature for which IA gratings may be reliably used as less than 80°C. Furthermore, we confirm the stability of different types of Bragg gratings showing that Type IIA gratings are more stable than Type I gratings. However, further studies show that straining the fibre throughout the inscription process leads to a robust Type IA grating surviving temperatures exceeding 180°C. Therefore, the combination of Type I and IA (strained) gratings make it possible to decouple temperature and strain over larger temperature excursions.

ACKNOWLEDGEMENTS

The authors acknowledge the COST270 action "Reliability of optical components and devices in communications networks and systems" for support of this work through the funding of a Short Term Scientific Mission.

REFERENCES

[1] A.G. Simpson, K. Kalli, K. Zhou, L. Zhang and I. Bennion, "Formation of type IA fibre Bragg gratings in germanosilicate optical fibre," Electronics Letters, Vol. 40, p 163-164, 2004.

[2] A.G. Simpson, K. Kalli, L. Zhang, K. Zhou and I. Bennion, "Abnormal photosensitivity effects and the formation of type IA FBGs," BGPP, Monterey, California, MD31, 2003.

[3] A.G. Simpson, K. Kalli, K. Zhou, L. Zhang and I. Bennion, "An idealised method for the fabrication of temperature invariant IA-I strain sensors," postdeadline session, OFS16 Nara, Japan, PD4, 2003.

[4] P. Lemaire, "Reliability of optical fibres exposed to hydrogen: prediction of long-term loss increases," Optical Engineering, Vol. 30, p 780-781, 1991.

[5] D. L. Williams and R. P. Smith, "Accelerated lifetime tests on UV written intracore gratings in boron germania codoped silica fibre," Electronics Letters, vol. 31, pp. 2120-2121, 1995.

[6] S. Kannan, J. Z. Y. Guo, and P. J. Lemaire, "Thermal stability analysis of UV-induced fibre Bragg gratings," Journal of Lightwave Technology, Vol. 15, pp. 1478-1483, 1997.

[7] S. Ishikawa, A. Inoue, M. Harumoto, T. Enomoto, and H. Kanamori, "Adequate aging condition for fibre Bragg grating based on simple power low model," presented at Optical Fibre Sensors (OFS1998), 1998.

[8] H. Patrick, S. L. Gilbert, A. Lidgard, and M. D. Gallagher, "Annealing of Bragg gratings in hydrogen-loaded optical-fibre," Journal of Applied Physics, Vol. 78, pp. 2940-2945, 1995.

[9] M. Aslund and J. Canning, "Annealing properties of gratings written into UV-presensitized hydrogen-out-diffused optical fibre," Optics Letters, Vol. 25, pp. 692-694, 2000.

[10] P. Niay, P. Bernage, S. Legoubin, M. Douay, W. X. Xie, J. F. Bayon, T. Georges, M. Monerie, and B. Poumellec, "Behavior of Spectral Transmissions of Bragg Gratings Written in Germania-Doped Fibres - Writing and Erasing Experiments Using Pulsed or Cw Uv Exposure," Optics Communications, Vol. 113, pp. 176 -192, 1994.

[11] T. Erdogan, V Mirzahi, P. Lemaire, and D. Monroe, "Decay of ultraviolet-induced fibre Bragg gratings," Journal of Applied Physics, Vol. 76, pp. 73-80, 1994.

[12] S. R. Baker, H. N. Rourke, V. Baker, and D. Goodchild, "Thermal decay of fibre Bragg gratings written in boron and germanium codoped silica fibre ," Journal of Lightwave Technology, Vol. 15, pp. 1470-1477, 1997.

[13] Y. Masuda and et. al, "Wavelength evolution of fibre Bragg gratings fabricated from hydrogen loaded optical fibre during annealing," Journal of Lightwave Technology, Vol. 22, pp. 934-941, 2004.

[14] K. E. Chisholm, K. Sugden, and I. Bennion, "Effects of thermal annealing on Bragg fibre gratings in boron/germania co-doped fibre," Journal of Physics D-Applied Physics, Vol. 31, pp. 61-64, 1998.

[15] S. Pal, J. Mandal, T. Sun, and K. T. V. Grattan, "Analysis of thermal decay and prediction of operational lifetime for a type I boron-germanium codoped fibre Bragg grating," Applied Optics, Vol. 42, pp. 2188-2197, 2003.

[16] J. Rathje, M. Kristensen and J. E. Pedersen, "Continuous anneal method for characterizing the thermal stability of ultraviolet Bragg gratings," Journal of Applied Physics Vol. 88, pp. 1050-1055, 2000.

[17] A. Othonos and K. Kalli "Fiber Bragg Gratings: Fundamentals and Applications in Telecommunications and Sensing", Artech House, Boston, London, 1999. Chapter 2, section 2.5.1.2.

* kkalli@cytanet.com.cy; phone 35722406537; fax 35722406545

ELECTRICALLY TUNABLE BRAGG GRATINGS IN SINGLE MODE POLYMER OPTICAL FIBER

K. Kalli[a], H. Dobb[b], D. J. Webb[b], K. Carroll[b], M. Komodromos[c], C. Themistos[c]; G. D. Peng[d], Q. Fang[f], I. W. Boyd[f]
[a]Photonics Research Laboratory, Higher Technical Institute, Cyprus, kkalli@cytanet.com.cy
[b]Photonics Research Group, Aston University, Birmingham, United Kingdom d.j.webb@aston.ac.uk
[c]Frederick Institute of Technology, Cyprus
[d]University of New South Wales, Australia
[f]University College London, United Kingdom

Abstract: We present the first demonstration of a tunable fiber Bragg grating device in polymer optical fiber that utilizes a thin-film resistive heater deposited on the surface of the fiber. The device underwent a wavelength shift of 2nm for a moderate input power of 160mW, a wavelength to input power coefficient of −13.4pm/mW and time constant of $1.7s^{-1}$.

1. Introduction

There are many important applications for tunable fiber devices in optical sensing and lightwave communication systems. The use of fiber Bragg gratings as tunable filtering candidates have been demonstrated in glass fibers with wavelength and bandwidth tunability demonstrated using strain [1] and temperature [2,3]. Fiber Bragg grating (FBG) filters coated with thin film heaters on the surface have been promoted as wavelength tunable devices because of their compact nature, fast response and high efficiency. It has been noted recently that polymer optical fiber Bragg gratings (POFBG) have a high temperature sensitivity [4], and hence may be suitable candidates for producing a widely tunable filter by heating the fiber. In this paper we demonstrate the first wavelength tunable POFBG filtering device that relies on thin-film resistive load heating to produce wavelength changes.

2. FBG inscription and metallic coating development

FBGs were inscribed into step-index single- and few-moded POF (PMMA - polymethylmethacrylate) using the inscription arrangement in figure 1, undertaken with a 30-mW Kimmon IK series HeCd laser emitting at 325 nm by means of the standard phase mask technique. The phase mask had a pitch of 1060.85 nm, and was designed to produce a FBG at 1568nm in the POF, in contrast to 1536 nm design wavelength for silica fiber. For successful fiber Bragg grating fabrication in polymer optical fiber, the fiber must be supported along its entire length in order to minimize the effects of air currents and laser-induced heating on the fiber position. Consequently, the fiber was rested on three v-grooves mounted on three-axis translation stages. Two plano-convex cylindrical lenses with 10 cm focal lengths were incorporated in the system, one before the phase mask, which served to focus the light down into the core, and a second lens that was used to expand the 1 mm diameter laser beam to cover approximately 1 cm of the POF. Without the second lens incorporated in the arrangement, FBGs of approximately 1 mm in length, the size of the laser beam, could be fabricated. Thus, the second lens provided some flexibly over the grating design.
The surface region around the grating was subsequently coated with a palladium/copper metallic layer, the former of which aided adhesion to the PMMA and the latter acted as the thin-film heater element. Metal deposition was initiated by the use of a vacuum UV (VUV) light source operating at 172 nm and at low (room) temperature using the arrangement of figure 2. At this wavelength the penetration depth of the light source is on the order of a micron and therefore there is no damage to the grating device, but the surface of the sample undergoes a chemical roughening, as the light initiates bond scission. The VUV exposure time ranged from 1 to 10 minutes. The dangling polymer bonds then bond both physically and chemically to metallic particles. This is of great advantage as there are very few approaches for coating polymers with metal at room temperature and much higher temperatures would have an adverse impact on the performance and spectral characteristics of the grating. Furthermore, the coating took place in a low vacuum of 10^{-2} mbar, which again is not enough to affect the basic fiber and grating properties. This approach of decomposing metal organic films with incoherent VUV excimer lamps at low temperature is ideal for the manufacture of thin film microcircuits and devices, proving to be an efficient technique for the preparation of uniform thin films. The film thickness is controlled by variation of the reaction parameters – the concentration of precursor and the UV-irradiation time.

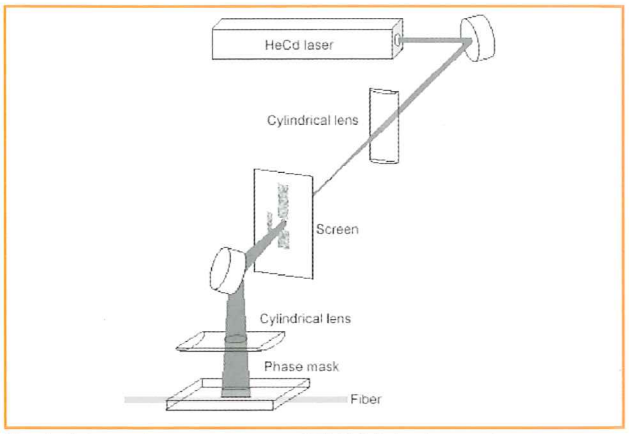

Fig. 1. Schematic arrangement of FBG fabrication equipment.

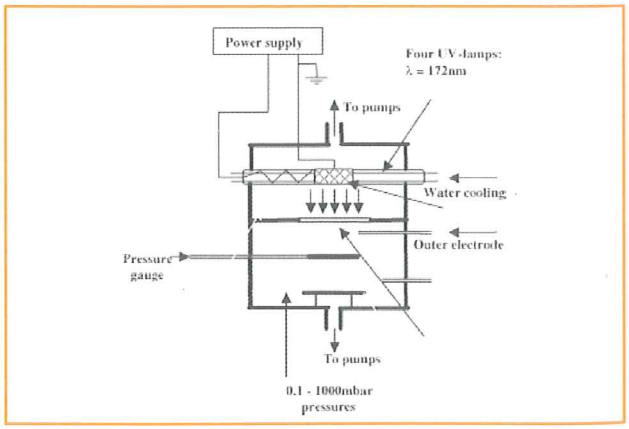

Fig. 2. Schematic diagram of the coating procedure

3. Modeling thermal response characteristics

The response of a thin film heated Bragg grating for a glass optical fiber has been characterized, but this is the first such demonstration for a polymer-based fiber Bragg grating. Here we anticipate some differences between the thermal properties of the glass and polymer based devices, principally the thermal diffusion and radiation dissipation,

given the different thermal conductivities and emissivities of glass and polymer materials. We consider a differential equation that describes the temperature distribution and thermal flow in the fiber, making the assumption that the coating is sufficiently uniform and greater in length than the grating to give a uniform temperature distribution across the grating length, so only the radial distribution and thermal flow along the grating length are of importance. The device can now be modeled as a polymer cylinder with a thin-film thermal source on the surface enclosed by air. In this way the heat diffuses into the fiber core and the surrounding air, in addition to radiation. Considering energy conservation within the fiber [5],

$$\frac{\partial T(x,t)}{\partial t} = \kappa \frac{\partial^2 T(x,t)}{\partial x^2} + \frac{P_{in}(x,t) - P_{out}(x,t)}{\rho c_p \pi R_{fiber}^2} \qquad (1)$$

where x is the distance along the fiber, $T(x,t)$ is the fiber temperature, κ, ρ and c_p are the thermal diffusivity, density and constant pressure heat capacity of the polymer (PMMA), R_{fiber} is the fiber radius. $P_{in}(x,t)$ is the heating generated by the thin film heater, and $P_{out}(x,t)$ is the rate of heat loss from the fiber to the air. In general $P_{in}(x,t) = I^2(t)R(x)$, where $R(x)$ is the local resistance per unit length of the coating and $I(t)$ is the electrical current. Furthermore, if we assume that the rate of heat loss is proportional to the change in temperature then $P_{out}(x,t) = a\,|T(x,t) - T_{air}|$, where is a constant that may be temperature dependent and represents a lumped heat transfer coefficient due to heat transfer from the surface of the device. The rate of heat loss is linearly proportional to the change in temperature,

$$P_{out}(x,t) = 2\pi R_{fiber}\, hT(x,t) \qquad (2)$$

where h is the surface conductance of the fiber, which characterizes the heat flow out of the fiber; additionally,

$$\frac{P_{out}(x,t)}{\rho c_p \pi R_{fiber}^2} = aT(x,t) \qquad (3)$$

hence a is related to h by

$$a = \frac{2h}{\rho c_p R_{fiber}} \qquad (4)$$

In addition to the above terms there are radial heat flow terms that may have to be considered,

$$2\pi R_{fiber}\, \kappa \frac{\partial T}{\partial r}_{r=Rfiber} \text{ and } 2\pi R_{fiber}\, \kappa_{air} \frac{\partial T_{air}}{\partial r}_{r=Rfiber} \qquad (5)$$

Specifically the difference

$$2\pi R_{fiber} \left[\kappa \frac{\partial T}{\partial r}_{r=Rfiber} - \kappa_{air} \frac{\partial T_{air}}{\partial r}_{r=Rfiber} \right] \qquad (6)$$

where κ_{air} and T_{air} are the thermal diffusivity of air and the air temperature, respectively. This term is important as it accounts for temperature gradients that may exist *radially* across the grating. Given that the thermal conductivity of PMMA (0.17W/mK) is only 7 times that of air (0.025W/mK), compared with 55 times for silica glass (1.38W/mK) one should consider the validity of ignoring radial gradients and consider only heat flow along the length of the fiber. The heat flow through and along the surface of the fiber is characterized by the Biot number, $Bi = h R_{fiber}/\kappa$. If the Biot number is sufficiently small (<0.1), meaning that the thermal conductance over the length R_{fiber} is far greater than the surface conductance then radial thermal gradients become negligible. Hence a measurement of a leads to an estimate of h and Bi, and determines whether the fiber can be treated as a 1-D system. a constitutes a system time constant, therefore we must measure the filter's wavelength shift in response to a sudden current input.

4 Wavelength shift and time response of the filter

In order to characterize the tunable filter, current was passed through the thin-film metal coating by using silver loaded paint and fine copper wires, resulting in joule heating that increased the temperature of the fiber and the grating. The copper wires had a separation of 12mm thereby encompassing the grating length (<1cm). For this device cooling is passive and occurs through convective and conductive flow of heat to the surrounding air. The spectral reflectivity, and its changes in response to current flowing through the thin copper film, was measured using a broadband light source and optical spectrum analyzer. The total resistance of the film encompassing the grating, and the connection via the copper wires and silver-loaded paint, was measured to be 3.2Ω. Figure 3 shows the wavelength shift induced by joule heating. It is noted that the wavelength to input power coefficient is negative, as expected, −13.4pm/mW. Figure 4 shows the spectrum of the grating for several values of input power. We note that throughout the wavelength tuning the grating spectrum remained unchanged, and this observation is consistent with a spatially uniform heating of the grating. The spectrum is dual-peaked, but this is a result of a dual-exposure inscription procedure.

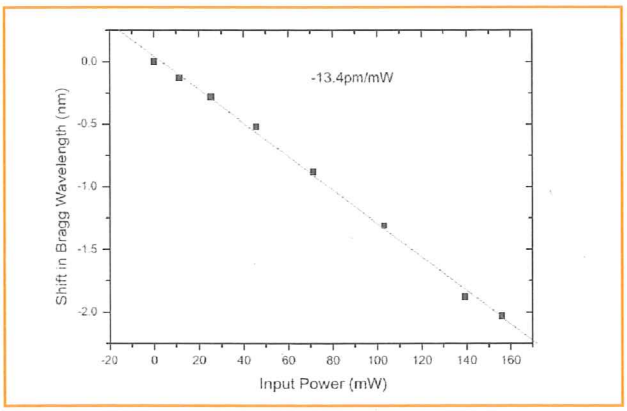

Fig. 3. Wavelength shift induced by joule heating with a wavelength to input power coefficient of −13.4pm/mW.

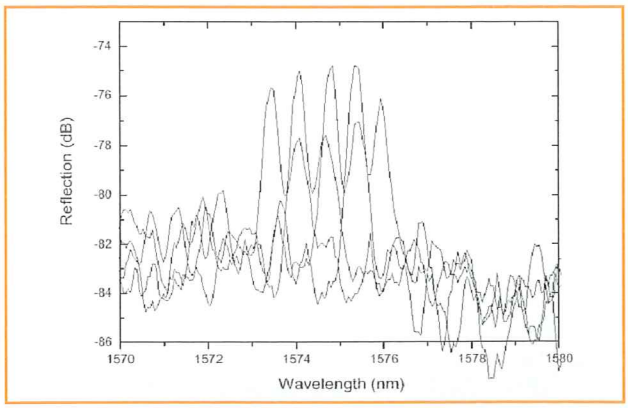

Fig. 4. Wavelength spectrum showing four typical traces for powers varying from 150, 100, 50, 0mW, respectively from right to left

When the input power is uniform the temperature variation as a function of time is

$$T(t) = \frac{P_{in}'}{a}\left[1 - \exp(-at)\right] \qquad (7)$$

where P_{in}' is related to the input power, but depends on the thermal capacity of the PMMA and the metal film. As noted earlier, a measurement of a yields information regarding the rate of heat flow out of the fiber. Figure 5 shows the rise time of a thermally tuned fiber Bragg grating, with data collected for three different heating powers applied suddenly at t=0s, 45.8, 71.5, and 103.2mW. The curves correspond to fits that use a single exponential form, from which we have determined the time constant, $a = 1.7s^{-1}$. There is no apparent or systematic dependence on the applied power.

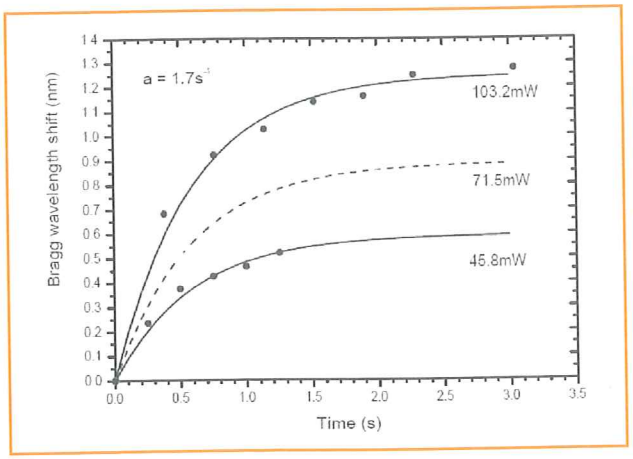

Fig. 5. Rise time of a thermally tuned fiber Bragg grating, for three different heating powers applied suddenly at t=0s: 45.8, 71.5, and 103.2mW. The time constant a =1.7s⁻¹.

Having determined a we can now evaluate h and Bi. Using the geometric and material properties of the fiber (ρ = 1190kg/m^3, c_p = 1450J/kgK, R_{fiber} = 120μm, κ = 0.17W/mK), h is found to be 175W/m^{2}K, and Bi is ~ 0.1; this is compatible with a treatment of the polymer fiber as a 1-D system.

5. Conclusions

We have successfully demonstrated the first wavelength tunable fiber Bragg grating filter in polymer optical fiber based on thin-film resistive load heating. The device underwent a wavelength shift of 2nm for a moderate input power of 160mW, a wavelength to input power coefficient of –13.4pm/mW and time constant of 1.7s^{-1}. A basic study has verified that for this fiber type one can treat the device as a one dimensional system. However, as fiber thickness increases one may have to account for radial gradients across POF based FBG devices.

6. Acknowledgements

The authors wish to acknowledge the financial support of the Eureka Project "POLYFILTRO" and the UK EPSRC.

7. References

[1] A. Iocco et al., "Bragg grating fast tunable filter for wavelength division multiplexing," J. Lightwave Technol., **17**, 1217–1221 (1999).

[2] J. A. Rogers, B. J. Eggleton, J. R. Pedrazzani, and T. A. Strasser, "Distributed on-Fiber thin film heaters for Bragg gratings with adjustable chirp," Appl. Phys. Lett., **74**, 3131–3133 (1999).

[3] B. J. Eggleton et al., "Integrated tunable Fiber gratings for dispersion management in high-bit rate systems," J. Lightwave Technol., **18**, 1418–1432 (2000).

[4] H. Dobb, K. Carroll, D. J. Webb, K. Kalli, M. Komodromos, C. Themistos, G. D. Peng, A. Argyros, M. C. Large, M. A. van Eijkelenborg, Q. Fang, I. W. Boyd, "Grating based devices in polymer optical fibre" in Optical Sensing II; Brian Culshaw, Anna G. Mignani, Hartmut Bartelt, Leszek R. Jaroszewicz; Eds., Proc. SPIE Vol. 6189, 2006, 1-12

[5] J. A. Rogers et al., "Characteristics of heat flow in optical fiber devices that use integrated thin-film heaters," Appl. Opt., **39**, 5109–5116 (2000).

MODELING OF AN ICS SOLAR WATER HEATER USING TRNSYS AND ARTIFICIAL NEURAL NETWORKS

Soteris Kalogirou[1], M. Souliotis[2], Y. Tripanagnostopoulos[2]
[1]Higher Technical Institute, P. O. Box 20423, Nicosia 2152, Cyprus
[2]Physics Department, University of Patras, Patra 26504, Greece

ABSTRACT

In this paper a study in which a suitable Artificial Neural Network (ANN) and TRNSYS are combined in order to predict the performance of an Integrated Collector Storage (ICS) prototype is presented. Experimental data that have been collected from outdoor tests of an ICS solar water heater with cylindrical water storage tank inside a CPC reflector trough are used to train the ANN. The ANN is then used though the Excel interface (Type 62) in TRNSYS to model the annual performance of the system by running the model with the values of a typical meteorological year for Athens, Greece. In this way the specific capabilities of both approaches are combined, i.e., use of the radiation processing and modelling power of TRNSYS together with the "black box" modelling approach of ANNs. From the results presented it is shown that this new method can be used effectively for such predictions for any system the TRNSYS model of which is not readily available.

1. INTRODUCTION

Integrated Collector Storage (ICS) systems are solar water heaters that cover domestic needs for hot water in the range of 100–200 litres per day and are considered as alternative solar devices to the well known thermosiphonic systems with flat plate or evacuated tube collectors. The storage tank of an ICS system has a dual function, i.e., to collect solar radiation and preserve the heat of the stored water. An effective thermal protection of the ICS storage tanks is difficult enough, as a significant part of their surface is exposed for the absorption of solar radiation. Double glazing, selective absorbing surface coatings and transparent insulating materials have been used for the thermal protection of the storage tank. Opaque thermal insulation however can only be placed on the non-illuminated parts of the tank surface and vacuum thermal protection is considered effective, mainly for ICS systems that consist of cylindrical tanks with small diameters. Cylindrical storage tanks are employed in most commercial ICS systems, as they resist the pressure of the water mains. The use of reflectors is considered necessary for ICS systems with cylindrical storage tank and depending on their orientation, reflector troughs of compound parabolic concentrator (CPC) or involute are used for the effective illumination of the storage tank surface.

Extensive study on ICS solar systems has been performed at the University of Patras in Greece, where models of different designs have been tested and analysed [1–6]. On the other hand, at the Higher Technical Institute in Cyprus several solar energy systems (including ICS systems) have been studied using TRNSYS methodology and artificial neural networks (ANNs) [7-13]. Artificial neural networks differ from the traditional modelling approaches in that they are trained to learn solutions rather than being programmed to model a specific problem in the normal way. Neural networks are widely accepted as a technology offering an alternative way to tackle complex and ill-defined problems. They can learn from examples, are fault tolerant in the sense that they are able to handle noisy and incomplete data, are able to deal with non-linear problems, and once trained can perform predictions at very high speed. ANNs have been used in many engineering applications such as in control systems, in classification and in modelling complex process transformations.

The objective of this paper is to present a model which combines the capabilities of both methods. This is necessary because there is no readymade model of the particular ICS unit in TRNSYS and the suggested methodology is an alternative to the creation of a new TRNSYS component. This method can also be used in cases where systems or parts of them cannot be described analytically.

2. DESCRIPTION OF THE ICS UNIT

The design of the studied ICS unit is mainly based on the effective use of the non–uniform distribution of solar radiation on absorber surface, which is the result of using CPC reflector geometry. This principal design along with the partially thermal insulation (non-illuminated part) of the storage tank aim at achieving effective water heating combined with sufficient temperature stratification during daily operation and improving water temperature preservation during night. In the specific ICS model the solar radiation acceptance angle a has been chosen to be 90° to allow a significant part of diffused solar radiation to be collected. By this choice the total volume of the device can be significantly decreased. Finally, the suggested ICS system have lower cost and height compared to that of the usual flat plate collector system that has the same ratio of storage water volume per aperture area and hence, ICS system can be better harmonized to the surrounding architecture.

In Fig. 1 the cross section of the experimental model ICS is presented, which consists of truncated symmetric CPC reflectors with parabolic parts (AB), (DA') and involute parts (BC), (C'D). The intersection point between the corresponding parabolas' axis BB' and DD' lies on the aperture surface (glazing) and determines the truncation level for the constructed experimental model. In Fig. 1 R_T is the radius of the cylindrical storage tank, ω and ω' are the angles that are used to form the two involute reflector parts (BC) and (C'D) correspondingly, and ψ, ψ' are the angles of the two parabolic reflector parts (AB) and (DA') respectively. The maximum angles ω and ω' are taken, i.e., $\omega_m = \omega'_m = 90°$, the maximum angles ψ and ψ' (rim angles) are $\psi = \psi' = 63.91°$ and the focal lengths are f_1 = [BE] = πR_T /2 and f_2 = [DE'] = πR_T / 2, respectively. The analytical mathematical equations of the reflector geometry and also

the materials used for the construction of the ICS unit can be found in [6].

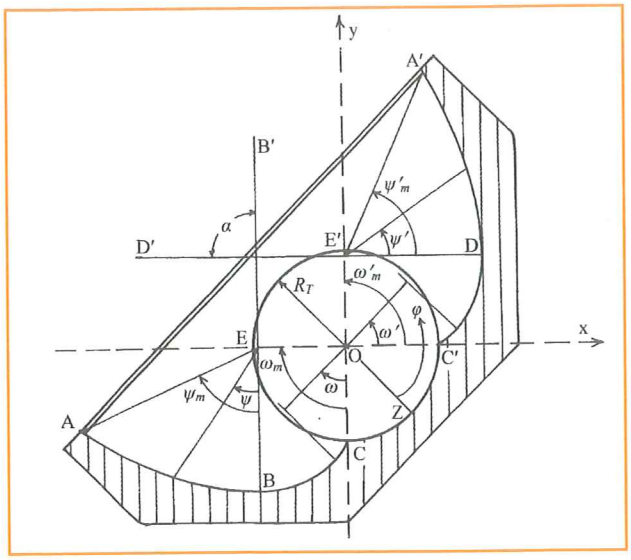

Fig. 1 Cross section of the ICS unit

By experimentally testing the unit for more than a year a number of patterns were collected, every 30 minutes. These are separated into two files a training file comprising 5232 data sets and a validation file comprising 960 data sets. These files will be used for the training and validation of the artificial neural network. Both datasets comprise data during the day (heating) and during the night (cool down). It should be noted that all testing of the ICS unit was performed without draw off.

3. ARTIFICIAL NEURAL NETWORKS

Artificial neural networks (ANNs) mimic somewhat the learning process of a human brain. Instead of complex rules and mathematical routines, ANNs are able to learn the key information patterns within a multidimensional information domain. In addition, the inherently noisy data does not seem to present a problem. According to Haykin [14], a neural network is a massively parallel distributed processor that has a natural propensity for storing experiential knowledge and making it available for use. It resembles the human brain in two respects: (a) the knowledge is acquired by the network through a learning process, and (b) inter-neuron connection strengths, known as synaptic weights, are used to store the knowledge.

ANN models represent a new method in energy prediction. ANNs operate like a "black box" model, requiring no detailed information about the system. Instead, they learn the relationship between the input parameters and the controlled and uncontrolled variables, by studying previously recorded data, similar to the way a non-linear regression might perform. Another advantage of using ANNs is their ability to handle large and complex systems with many interrelated parameters. They seem to simply ignore excess input data that are of minimal significance and concentrate instead on the more important inputs.

A training set is a group of matched input and output patterns used for training the network, usually by suitable adaptation of the synaptic weights. The outputs are the dependent variables that the network produces for the corresponding input. It is important that all the information needed by the network in order to learn, is supplied to it as a dataset. When each pattern is read, the network uses the input data to produce an output, which is then compared to the training pattern, i.e., the correct or desired output. If there is a difference, the connection weights are usually altered in such a direction that reduces the error. After the network has run through all the input patterns, and if the error is still greater than the maximum desired tolerance, the ANN runs again through all the input patterns repeatedly, until all the errors are within the required tolerance. When the training reaches a satisfactory level, the network holds the weights constant. The trained network can then be used to make decisions, identify patterns or define associations in new input data sets not used to train it.

3.1 Group Method Data Handling (GMDH) Neural Network (NN)

There are various methods that can be used to model the data. These could be based on simple regression analysis, multiple regression analysis, neural networks and many others. In this work, the neural network method is selected because of its accuracy. One type of neural networks, which is very suitable for the present application, is the group method of data handling (GMDH) neural network, which was used to model the data. GMDH works by building successive layers with links that are simple polynomial terms. These polynomial terms are created by using linear and non-linear regression. The initial layer is simply the input layer. The first layer created is made by computing regressions of the input variables and then choosing the best ones. The second layer is created by computing regressions of the values in the first layer along with the input variables. Again, only the best are chosen by the algorithm called survivors. This process continues until the network stops getting better (according to a pre-specified selection criterion).

The resulting network can be represented as a complex polynomial description of the model. The complexity of the resulting polynomial depends on the variability of the training data. In some respects GMDH, it is very much like using regression analysis, but it is far more powerful than the latter. GMDH can build very complex models while avoiding overfitting problems. A by-product of GMDH is that it recognizes the best variables as it trains.

The GMDH network is implemented with polynomial terms in the links and a genetic component to decide how many layers are built. The result of training at the output layer can be represented as a polynomial function of the inputs. The layer building GMDH procedure continues as long as the evaluation criteria continue to diminish. GMDH algorithm then checks if this is so and continues or stops training. There may also be other conditions, which determine when training is stopped.

The input data used in the network are the month (1-12), incidence angle, ambient temperature, total radiation on the collector aperture and wind velocity (most of these parameters are included in the meteorological file or are estimated by the solar radiation processor of TRNSYS).

The predicted parameter is the useful energy stored in the storage tank. From this energy the mean storage tank temperature can be determined during simulations. Additionally the incidence angle, used as input, inherently includes the day number and the time of the day, as it depends on these two parameters together with the particular inclination of the collector which is fixed.

The experimental data that have been collected from outdoor tests of an ICS solar water heater as described above have been used to train the GMDH ANN. The training dataset was learned by the ANN with good accuracy (R^2-value equal to 0.9392; the closer this value is to unity the better the training accuracy). Subsequently the validation data set was used, which is completely unknown to the network. This is used to test the ability of the network to produce accurate results. The R^2 value obtained in this case is 0.9383 and representative patterns are shown in Fig. 2 (top diagram).

A sample of actual and ANN predicted storage tank temperature for the day 224 (August 12) is shown in Fig. 2 (bottom diagram). As can be seen the actual and ANN data are very close and the two lines are almost indistinguishable. It should be noted that the initial temperature at the beginning of the day is set equal to the actual storage tank temperature so as the two series have the same starting point.

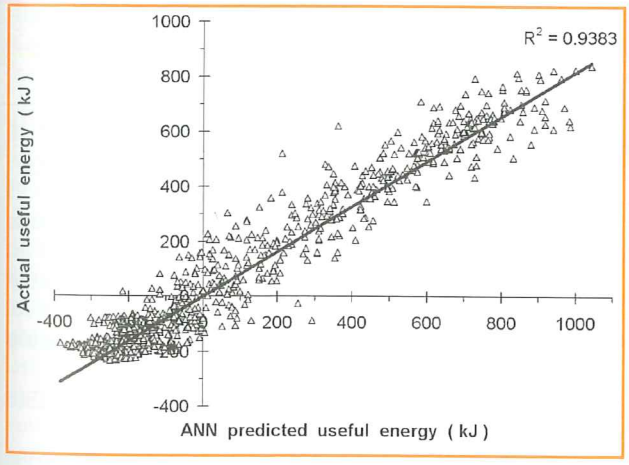

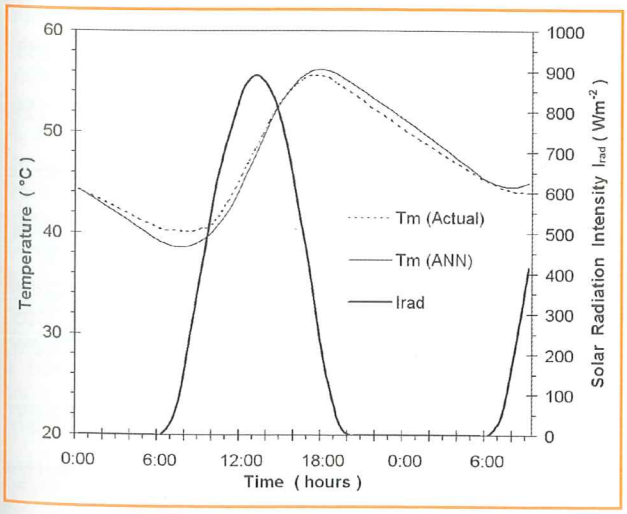

Fig. 2 Comparison between the actual and ANN predicted useful energy (top graph) and water tank temperature (bottom graph).

The final equation obtained from GMDH is quite complex:

$$
\begin{aligned}
Y = {} & 0.36*X_3+0.08*X2-0.032*X1+0.1*X5- \\
& 0.55-0.084*X_4+0.13*X_1^2+0.11*X_3^2+ \\
& 0.054*X_1^3+0.094*X_3^3+0.014*X_1*X_2- \\
& 0.018*X_2*X_3- \\
& 0.013*X_1*X_2*X_3+0.023*X_5^2 + \\
& 0.056*X_4^3-0.12*X_5^3-0.02*X_1*X_4- \\
& 0.0061*X_2*X_4-0.04*X_3*X_4- \\
& 0.0098*X_1^2*X_4-0.0071*X_3^2*X_4- \\
& 0.0033*X_1^3*X_4-0.0079*X3^3*X_4- \\
& 0.0012*X_1*X_2*X_4+0.00077*X_2*X_3*X_4+ \\
& 0.0011*X_1*X_2*X_3*X_4+0.0011*X_1*X_5- \\
& 0.0085*X_2*X_5-0.034*X_3*X_5- \\
& 0.0086*X_1^2*X_5-0.0062*X_3^2*X_5- \\
& 0.0029*X_1^3*X_5-0.0069*X_3^3*X_5- \\
& 0.001*X_1*X_2*X_5+ 0.00067*X_2*X_3*X_5+ \\
& 0.00097*X_1*X_2*X_3*X_5+0.0037*X_4^2- \\
& 0.0092*X_4*X_5-0.012*X_3*X_4*X_5- \\
& 0.026*X_2^3
\end{aligned}
\qquad (1)
$$

All the data required by the GMDH need to be scaled from –1 to 1. Therefore, parameters X1 to X5 as well as useful energy, obtained from Y (Eq. 1) needs to be scaled in the same interval. This is done with:

$$Y_i = \frac{2(X_i - X_{min})}{X_{max} - X_{min}} - 1 \qquad (2)$$

In Eq. (1) the parameter X_1 stands for the month, X_2 for ambient temperature, X_3 for the total radiation on the collector aperture, X_4 for wind velocity and X_5 for the incidence angle. The latter (incidence angle) can easily be estimated from the solar radiation processor of TRNSYS.

4. SIMULATIONS

The ANN is then used though the Excel interface (Type 62) in TRNSYS [15] to model the annual performance of the system by running the model with the values of a typical meteorological year (TMY) of Athens, Greece. In this way the specific capabilities of both approaches are combined, i.e., use of the radiation processing and modelling power of TRNSYS together with the "black box" modelling approach of ANNs. The time step used in TRNSYS was 30 minutes, i.e., it is similar to the data used in the training of the ANN.

The results of the simulations for April 14 and August 12 and 13 are shown in Figs. 3 and 4 respectively. Both these figures are for no draw-off. Of course here the accuracy depends on how close the actual weather data during testing are to the weather data included in the TMY file. The small deviation recorded in mean storage tank temperature in the above figures is considered acceptable. As can be seen in both cases the maximum mean storage tank temperature reaches 50°C in April and 60°C in August whereas the lowest temperature

which is the effect of tank cool down due to night time losses is 32°C in April and 40°C in August.

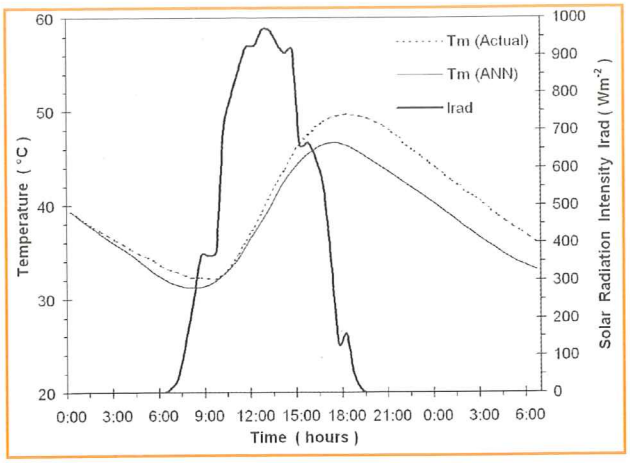

Fig. 3 Actual and ANN predicted storage tank temperature for April 14

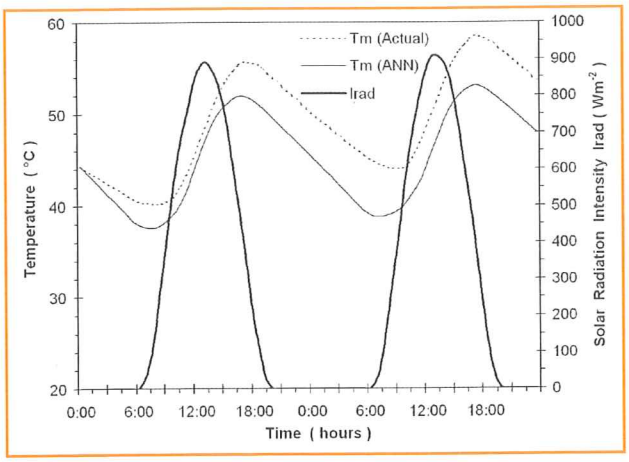

Fig. 4 Actual and ANN predicted storage tank temperature for August 12 and 13

Another test performed is to use certain patterns of draw off without the possibility of validation. Two such patterns were tested; a draw off pattern of 20 lt/hr from 19:00 till 22:00 (60 litters in total) and a pattern with 15 lt/hr draw off at 13:00, 15:00, 17:00 and 19:00. The results for August 12 are shown in Fig. 5. As can be seen the second pattern has more severe effect on the storage temperature because the temperature of the stored water has lower values at the time that the draw off pattern starts, although the solar radiation intensity has the maximum value at 12:30. In this point we should note that generally the time which the mean water tank temperature is maximized depends on a significant parameter used in the design of ICS systems. This parameter is the ratio of the stored water volume per aperture area, V_T/Aa (lt/m^2), which describes the sufficiency of the solar device for heating specific water volume and affects the time delay of the maximization of the mean water temperature to the corresponding maximization of the solar radiation intensity. In the specific device V_T/Aa equals to 100.28 lt/m^2.

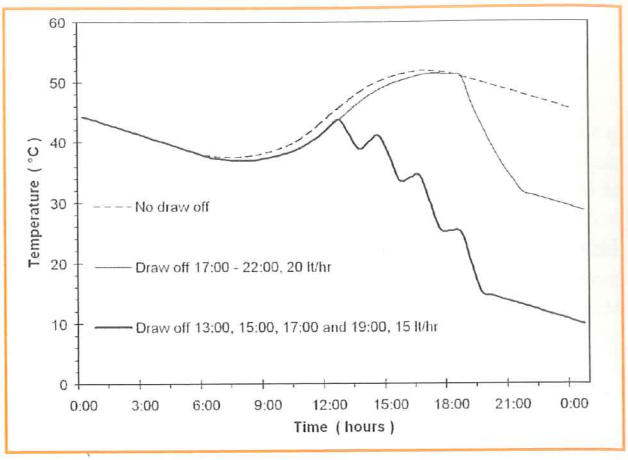

Fig. 5 Effect of draw off pattern on mean storage tank temperature

5. CONCLUSIONS

In this paper the details of the simulation of an integrated collector storage system with ANNs and TRNSYS is presented. This is the only way to simulate such a system as no ready made routine is available in TRNSYS to model this type of systems. It is proved by the results that this new method can be used effectively for such predictions.

The suggested methodology of combining ANNs and TRNSYS can be used to model other systems which are difficult to model analytically or their model is not available.

REFERENCES

[1] Y. Tripanagnostopoulos, P. Yianoulis, Solar Energy, Vol. 48, pp. 31-43, 1992.

[2] Y. Tripanagnostopoulos, M. Souliotis, Th. Nousia, Solar Energy, Vol. 72, pp. 327-350, 2002.

[3] Y. Tripanagnostopoulos, M. Souliotis, Renewable Energy, Vol. 29, pp. 13-38, 2004.

[4] Y. Tripanagnostopoulos, M. Souliotis, Renewable Energy, Vol. 29, pp. 73-96, 2004.

[5] Y. Tripanagnostopoulos, M. Souliotis, Renewable Energy, Vol. 29, pp. 223-248, 2004.

[6] M. Souliotis, Y. Tripanagnostopoulos, Solar Energy, Vol. 76, pp. 389-408, 2004.

[7] S.A. Kalogirou, Renewable Energy, Vol. 16, pp. 652-655, 1999.

[8] S.A. Kalogirou, Solar Energy, Vol. 90, pp. 248-259, 2006.

[9] A. Sencan, K.A. Yakut, S.A. Kalogirou, Renewable Energy, Vol. 31, pp. 29-43, 2006.

[10] S. Kalogirou, Y. Tripanagnostopoulos, M. Souliotis, Energy and Buildings, Vol. 37, pp. 824-835, 2005.

[11] S.A. Kalogirou, International Journal of Computer Application in Technology, Vol. 22, pp. 90-103, 2005.

[12] S.A. Kalogirou, Energy Conversion and Management, Vol. 45, pp. 3075-3092, 2004.

[13] S.A. Kalogirou, Progress in Energy and Computer Science, Vol. 29, pp 515–566, 2003.

[14] Haykin S. Neural Networks: A Comprehensive Foundation, Macmillan, New York, 1994.

[15] TRNSYS program Manual, Solar Energy Laboratory, University of Wisconsin, Madison, USA, 2005.

IN-SITU DETERMINATION OF THE THERMAL PERFORMANCE OF A U-TUBE BOREHOLE HEAT EXCHANGER

Georgios Florides and Soteris Kalogirou
Higher Technical Institute, P. O. Box 20423, Nicosia 2152, Cyprus.
Emails: Gflorides@hti.ac.cy, Skalogirou@hti.ac.cy

ABSTRACT

A borehole heat exchanger can be used for the injection or extraction of thermal energy into/from the ground. One of the methods that can be used to determine the characteristics of a borehole U-tube heat exchanger is the line source method which is simple and does not need expensive equipment. This method is explained and a test is performed in order to determine a borehole's characteristics in layers consisting of clay, silt and sand at various analogies. For the borehole under test the ground thermal conductivity (λ) was found to be 2.7 W/(m K) and the effective borehole thermal resistance (Rb) to be 0.10 K/(W/m). The results of the test are very sensitive to the amount of initial data that are discarded. The test is also sensitive to the daily flux penetration through the ground which gradually increases the temperature of the top layers in summer and to the variation of the heating coil injection rate which affect the temperature of the fluid of the heat exchanger at some later time.

Keywords: Borehole, earth heat exchanger, thermal performance

1. INTRODUCTION

Borehole heat exchangers are used to exploit effectively the heat capacity of the soil and commonly they are coupled to heat pumps for increasing their efficiency. In a vertical U-tube borehole heat exchanger a water pump circulates fluid through pipes inserted into a borehole in the ground. The borehole, after the insertion of the U-tube is usually backfilled with grout in order to ensure good thermal contact with the ground. The grout is often a bentonite clay mixture, with the possibility of having thermally enhanced additives in order to present a thermal conductivity significantly lower than the surrounding ground. The circulating fluid is usually water or a water-antifreeze mixture.

A borehole heat exchanger is usually drilled to a depth between 20 to 300 m with a diameter of 10 to15 cm. A borehole system can be composed of a large number of individual boreholes. For a typical residential house in Switzerland, a borehole heat exchanger of 100 to 200 m is used, depending on the energy demand and the ground conditions. For typical ground conditions and a single borehole heat exchanger, the borehole length is sized for a heat extraction rate per meter borehole of about 50 W/m [1]. For sizing the borehole heat exchanger its thermal properties should be estimated.

Several models for calculating the thermal properties of a borehole heat exchanger are available. These models are based on Fourier's law of heat conduction and include the analytical line source model [2], the cylindrical source model [3] and several numerical models [4, 5].

2. LINE SOURCE MODEL

In this paper, the line source model, which is the most widely used method at this time is employed. The data analysis is based on the theory describing the response of an infinite line source model [6, 7]. Although this model is a simplification of the actual experiment, accurate data for the design of borehole heat exchangers can be obtained on site [8].

The change in ground temperature at a distance (r) from the line source after a time duration (t) of constant heat injection rate per active length of borehole(qc (W/m)) may be used as an approximation of the heat injection from the borehole heat exchanger [6]:

$$T_{(r,t)} - T_{(t=0)} = \frac{q_c}{4\pi\lambda}\int_{\frac{r^2}{4\alpha t}}^{\infty}\frac{e^{-u}}{u}du = \frac{q_c}{4\pi\lambda}E_1\left(\frac{r^2}{4\alpha t}\right) \qquad (1)$$

Where u is an independent variable and E1 is the so-called exponential integral. For large values of the parameter αt/r2, E1 can be approximated with the following relation:

$$E_1\left(\frac{r^2}{4\alpha t}\right) = \ln\left[\frac{4\alpha t}{r^2}\right] - \gamma \qquad (2)$$

For the above expression the maximum error is 2.5% when αt/r2 ≥ 20 and 10% when αt/r2 ≥ 5.

The above condition indicates that the accuracy increases as the thermal front reaches further beyond the borehole wall and the velocity of the thermal front is dependent on the ratio between thermal conductivity and heat capacity of the ground i.e. the ground thermal diffusivity [9].

The thermal characteristics of a borehole heat exchanger are determined by its effective borehole thermal resistance Rb, which defines the proportional relationship between the temperature difference of the fluid (Tf) and the borehole wall (Tb) and the heat rate exchanged by the borehole so:

$$R_b = (T_f - T_b)/q_c \qquad (3)$$

As the temperatures and heat rate are time-dependent, this relation disregards the heat capacitive effects of the borehole itself. The effective borehole thermal resistance takes into account both the geometrical parameters of the borehole heat exchanger (pipe spacing, diameter, number of pipes, depth) and the physical parameters (thermal conductivity of the materials, flow rate in the borehole, fluid properties, etc.) [1].

The fluid temperature is evaluated by taking the line source temperature at the borehole radius (r=rb) and adding the effect of the borehole thermal resistance (Rb) between the fluid and the borehole wall. Thus the quality of the borehole heat exchanger is higher with a lower bore-

hole thermal resistance and the fluid temperature (T_f) as a function of time is:

$$T_{f(t)} = \frac{q_c}{4\pi\lambda} * \left[\ln\left(\frac{4\alpha t}{r_b^2}\right) - \gamma \right] + q_c R_b + T_{(t=0)} \qquad (4)$$

where, Tf(t) denotes the arithmetic mean of the inlet fluid temperature ($T_{f\text{-}in}$) and outlet fluid temperature ($T_{f\text{-}out}$) of the borehole heat exchanger at time t [$Tf(t)=1/2(T_{f\text{-}in}+T_{f\text{-}out})$].

Equation (4) can be rearranged in a linear form as:

$$T_{f(t)} = \frac{q_c}{4\pi\lambda} \ln(t) + q_c \left[R_b + \frac{1}{4\pi\lambda} \left(\ln\left(\frac{4\alpha}{r_b^2}\right) - \gamma \right) \right] + T_{(t=0)} \qquad (5)$$

Hence the thermal conductivity can be determined from the slope of the line resulting from the plotting of the fluid temperature against ln (t).

Solving Eq. (3) in respect to Rb we get:

$$R_b = \frac{T_{f(t)} - T_{(t=0)}}{q_c} - \frac{1}{4\pi\lambda} * \left[\ln\left(\frac{4\alpha t}{r_b^2}\right) - \gamma \right] \qquad (6)$$

Therefore, using the value of the thermal conductivity determined above, leads to a number of borehole thermal resistances, one for every pair of fluid temperature and time and consequently a mean value can be calculated. This procedure also requires knowledge of the ground volumetric heat capacity, which can normally be deduced with adequate precision from the geological data of the site.

The effective borehole thermal resistance may also be determined on the basis of Eq. (5) by using a software that can deduce the equation of against ln(t). Such a program may fit a straight line, using the method of least squares, to the arrays known y's and x's and produce the appropriate formula.

The undisturbed ground temperature can be obtained before the beginning of the test by circulating the fluid in the borehole heat exchanger and measuring its temperature.

For the in situ test for estimating ground thermal conductivity a pulse of fixed energy flux is imposed on the borehole and the resulting temperature response is measured. The response test for the u-tube in the borehole was carried out by heating the circulation medium in the tube with an electric heater supplying a constant heat output of 2.7 kW. Flow, temperature, and several other test parameters were recorded during the experiment at specific time intervals.

4. GEOLOGICAL DATA OF BOREHOLE

The lithology prevailing over the site of the borehole is the Nicosia-Athalassa formation and is represented by the calcareous sandstone and the in situ mari. Yellowish-creamy, fine to coarse-grained weak to moderately cemented, calcareous sandstone is present in the top 15 meters. Khaki, sandy marl (fine sand, clay and silt) follows for the next 15 meters and from 30 to 50 meters the soil consists of Grayish marl (fine sand 5-10%, clay 30-40%, silt 50-65%). The water table in the borehole is at about 15 meters. The layers above the water table contain about 30% of water and layers under it contain about 50% water. The discharge rate is estimated between 2 to 3 m^3/h. An analysis of the geological data gives a mean density ρ of the undisturbed soil of about 1900 kg/m^3 and a mean specific heat (c_p) of about 1400 J/(kg K). Consequently the ground volumetric specific heat capacity is C =2.66x10^6J/(m^3K).

5. U-TUBE BOREHOLE HEAT EXCHANGER CHARACTERISTICS AND EQUIPMENT SPECIFICATION

In Cyprus, there are no studies undertaken so far related to the efficiency and cost estimation of borehole heat exchanger systems and it is of interest to examine such systems in this environment. For this purpose, we have installed a 50 m deep U-tube heat exchanger, made from polyethylene pipe with 32mm external and 25mm internal diameter. We have also installed 20 thermocouples at various depths, for recording the ground temperature and exploit the possibilities of using this type of systems. In order to carry out the test an electrical heater was installed in line with the pipes. A circulation pump, expansion valve, an air separator, a feeding line and well-insulated pipes were also fitted. The circuit was also provided with sensors and a data acquisition system for electronically recording the flow and the power provided to the heating coil. Temperatures at the inlet and outlet of the heat exchanger and at various depths of the borehole as well as the flow rate and power input to the heating coil were recorded at 15 minutes intervals with a data logger type Omega OMB-DAQ-55/56 USB data acquisition module.

6. EXPERIMENTAL RESULTS

Before the beginning of the test, the borehole heat exchanger fluid was circulated and in this way the undisturbed ground temperature was recorded. Figure 1 indicates the recorded temperatures of the fluid. Therefore, the mean temperature was measured to be 23.85 °C.

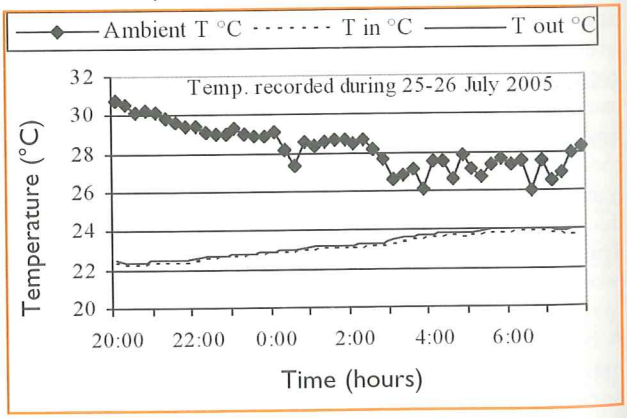

Fig. 1 Recorded inlet and outlet temperatures of the circulated fluid during 25 and 26 July 2005, before test.

After the establishment of the fluid mean temperature the heater was switched on and the test was carried out for 240 hours (ten days). During the test, the flow of the pump remained nearly constant at about 6.2 l/min. The recorded mean fluid temperature, ambient temperature and power input to the system are indicated in Fig. 2. As it is seen, the mean fluid temperature increased continuously for the first 120 hours (5 days) and then a steady state was reached.

The steady state can better be seen in Fig. 3 where the

mean fluid temperature is plotted for various days against the hours of the day (for 8:00 in the morning to 8:00 in the morning of the next day). As can be seen from this figure the mean fluid temperature profile follows the same path for the last 120 hours of the test which indicates that a steady state is reached. Therefore the test data of the first 120 hours are taken into consideration for deriving the geothermal properties by using the line source model which specifically requires the absence of steady state. The experimental values recorded in this period are indicated in Fig. 4.

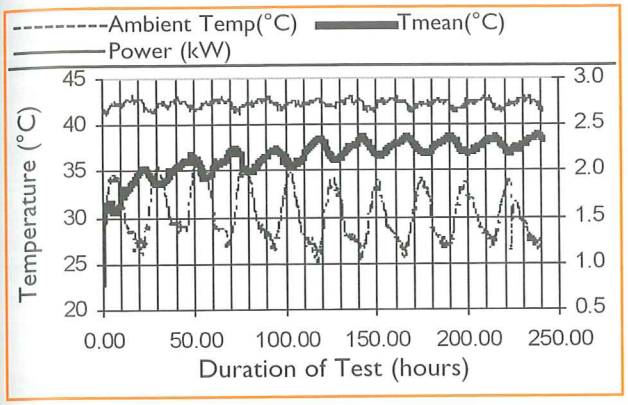

Fig. 2 Mean fluid temperature, ambient temperature and power input to the system during the test.

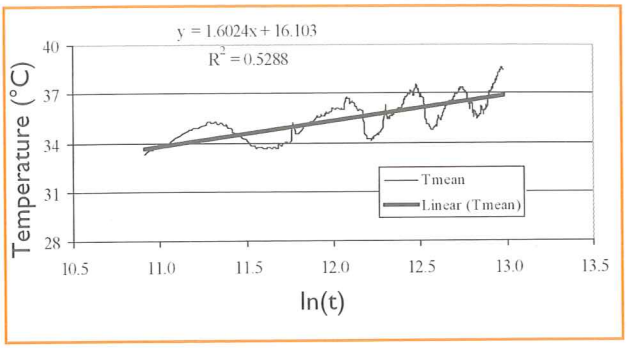

Fig. 5 Data satisfying the criterion at/r2 ≥ 5

The analysis of the theory presented in section 2, requires that a certain amount of data at the beginning of the test be discarded so that the approximate solution used in deriving the method, approaches the exact solution. For the characteristics of the borehole under study discarding the first 15 h of data is necessary so that the requirement $\alpha t/r2 \geq 5$ is fulfilled. Figure 5 presents the mean fluid temperature and the trend line as well as the equation of the trend line for the actual data eventually used.

The trend line equation makes possible the calculation of the ground thermal conductivity (λ) and the effective borehole thermal resistance (Rb) as indicated in Table 1.

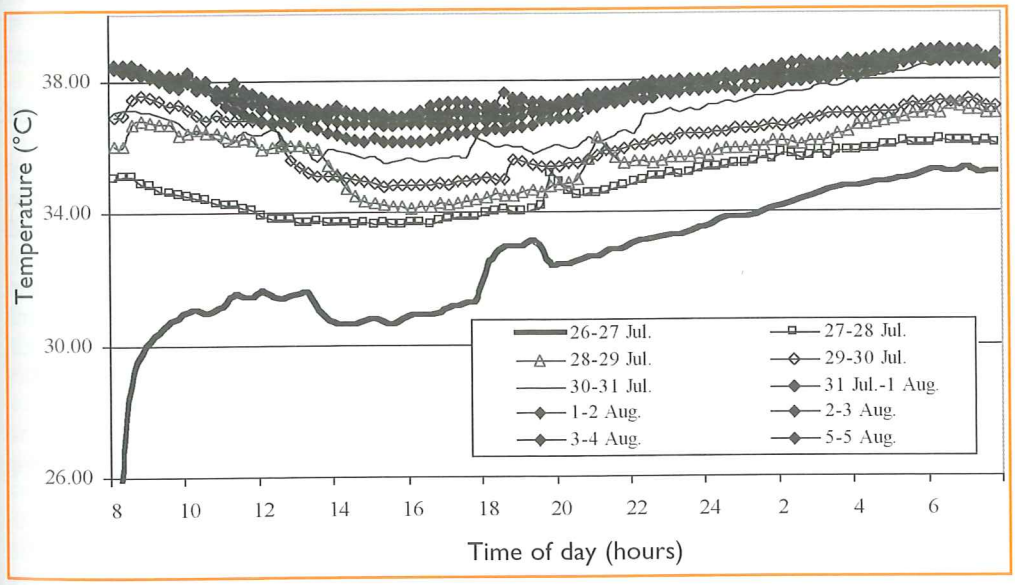

Fig. 3 Mean fluid temperature against time of day (for 8:00 in the morning to 8:00 in the morning of the next day)

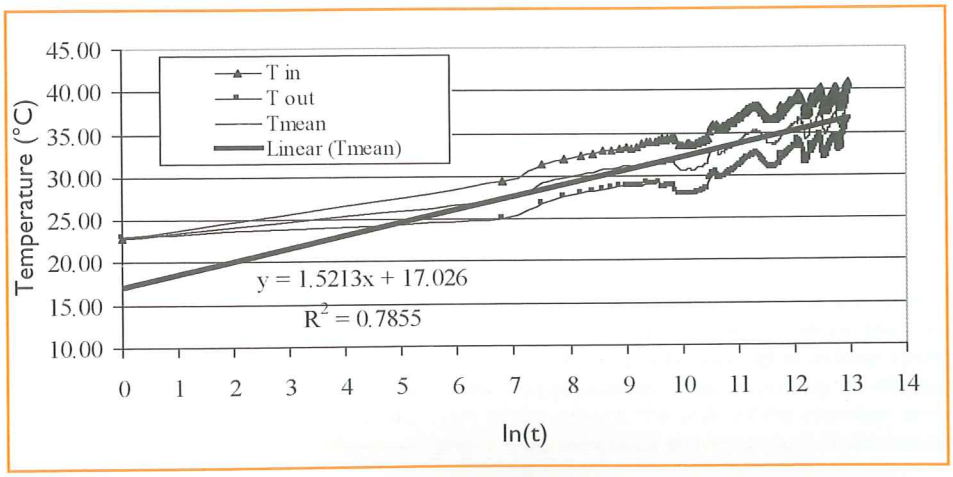

Fig. 4 Mean fluid temperature for the first 120 hours plotted against the time logarithm, ln(t), with time in seconds.

As it is observed, ignoring more initial data makes the trend line fitting factor (R^2) increasingly worse. This is due to the fact that the collected data were affected by mainly two factors.

The first factor is the daily flux penetration through the ground which gradually increases the temperature of the top layers and therefore the temperature of the fluid of the heat exchanger at some later time. The second factor is a variation of the heating coil injection rate per active length of borehole of about 3 W/m (about 5%) as seen in Fig. 2. This combined effect has a time shift of about 8 hours from the maximum ambient temperature and about 2-3 hours from the maximum heat injection causing a gradual rise in the mean fluid temperature of about 2°C.

Number of hours discarded	gradient	Intercept on temp. axis	R^2	λ *W/(m K)*	R_b *K/(W/m)*
0	1.5213	17.026	0.7855	2.845	0.1077
10	1.6747	15.201	0.6252	2.584	0.1001
15	**1.6024**	**16.103**	**0.5288**	**2.701**	**0.1047**
20	1.6753	15.190	0.4809	2.583	0.1005
30	1.9622	11.589	0.4490	2.206	0.0845

Table 1. Ground thermal conductivity (λ) and the effective borehole thermal resistance (Rb) as calculated when ignoring a certain amount of initial data (hours off).

CONCLUSIONS

The line source model is an easy method of evaluating the characteristics of the borehole and does not need expensive equipment. It is observed though that it is very sensitive to the amount of initial results that are discarded. For the borehole under test the ground thermal conductivity (λ) is found to be about 2.7 W/(m K) and the effective borehole thermal resistance (Rb) to be about 0.10 (m K) /W. This is in accordance with values concerning similar types of ground layers [8]. The test is also sensitive to the daily flux penetration through the ground which gradually increases the temperature of the top layers in summer and to the variation of the heating coil injection rate which affect the temperature of the fluid of the heat exchanger at some later time.

NOMENCLATURE

t	time (s)
r	radius (m)
q_c	constant heat injection rate per active length of borehole =Q/H (W/m)
γ	Euler's constant = 0.5772
λ	ground thermal conductivity (W/(m K))
a	ground thermal diffusivity (m^2/s), $a = \lambda/C$
C	ground volumetric specific heat capacity ($J/(m^3K)$) $C = \rho * cp$
P	ground density (kg/m^3)
c_p	specific heat of ground (J/(kg K))
u	independent variable
E_1	exponential integral
R_b	borehole thermal resistance (K/(W/m))
T_f	mean fluid temperature (°C)
$T_{(t=0)}$	undisturbed ground temperature before heat injection (°C)
$T_{f(t)}$	arithmetic mean of the inlet fluid temperature ($T_{f\text{-}in}$) and outlet fluid temperature ($T_{f\text{-}out}$) of the borehole heat exchanger at time t
H	active length of borehole (m),
Q	total heat rate transferred by the borehole (W)
D_{eq}	Equivalent diameter (m)
r_b	radius of the borehole (m)
D	diameter of the U-tube (m)
L^s	center to center distance between the two legs (m)
n	number of U-tube legs in a borehole

REFERENCES

[1] D. Pahud, B. Matthey Comparison of the thermal performance of double U-pipe borehole heat exchangers measured in situ. Energy and Buildings 2001, Vol. 33 pp. 503-507.

[2] Ingersoll, L.R., O.J. Zobel, and A.C. Ingersoll. 1954. Heat conduction with engineering, geological and other applications. New York: McGraw-Hill.

[3] Carslaw H.S. and J.C. Jaeger, 1993. Conduction of heat in Solids, Second ed., Oxford: Clarendon Press.

[4] Shonder, J A., and J.V. Beck. 1999. Determining effective soil formation thermal properties from field data using a parameter estimation technique. ASHRAE Transactions 105(1): 458-466.

[5] Kavanaugh, S. P., and K. Rafferty 1997. Ground Source Heat Pumps: Design of Geothermal Systems for Commercial and Institutional Buildings, Atlanta: American Society of Heating, Refrigeration and Air-Conditioning Engineers.

[6] Ingersoll, R., and H. Plass, 1948. Theory of the Ground Pipe Heat Source for the Heat Pump. Heating Piping and Air Conditioning. July. pp. 119-122.

[7] Mogeson, P. 1983. Fluid to duct wall heat transfer in duct heat storages. In Proceedings of the International Conference on Subsurface Heat Storage in Theory and Practice. Swedish council for building research.

[8] In situ determination of underground thermal parameters. Erich Mands, Burkhard Sanner, IGD2001, 17.-22.09.2001. (International Summer School on Direct Application of Geothermal Energy. http://www.geothermie.de/ueb_seiten/ub_sanner.htm)

[9] Gehlin, S. 2002. Thermal response test, Method Development and Evaluation, Licentiate thesis.

DESIGN OF AN EXPLOSION CHAMBER

Lazaros Lazaris, Mechanical Engineering Department, HTI

The problem of using explosives inside a closed spherical pressure vessel of 1.83m (72") diameter with nozzle attachments is considered. Theoretical and experimental analyses of the response are used to examine the safe use of the vessel as an explosion chamber. Prior to conversion the vessel underwent extensive static analysis, both experimental and theoretical.

Explosive charges up to 150 g were detonated within the chamber and the blast pressure and shell response measured by transducers. A finite element analysis was performed and found to agree well with the experimental data including areas where the classical analysis was in disagreement. The procedure for determining the safe explosive mass is outlined.

INTRODUCTION

Operations such as explosive welding, forming, compaction, etc., involving small explosive charges, up to 10 g, can be carried out using ear defenders and a minimum of blast protection. If, however, large scale operations involving a few kilograms of explosive are to be carried out the choice of a site to accommodate such operations becomes a problem.

In the course of explosive welding research a simple, safe explosion chamber had to be designed. The main requirement was that it should safely contain repeated firing of explosive charges up to a few hundred grams. The chamber would be sited inside a laboratory about 20 m away from offices. It was obviously important that explosions in this chamber should not cause damage to the building fabric nor should they create excessive noise. Other features to be incorporated were the need for ease of positioning of charge and the extraction of explosion fumes before entry of personnel for recovering of the work-piece. Later on the requirement of the chamber was increased to accommodate work on explosive cutting of small scale structures. This has initiated the present study.

BACKGROUND

In several fields of engineering and science, there are requirements for safe gastight or near gastight structures which must withstand the effects of internally applied dynamic loads. Examples of such structures include:

(a) Blast chambers, within which the effects of explosives or propellants can be studied under controlled atmospheric conditions.

(b) Safety chambers, for proof testing of small pressure vessels.

(c) Nuclear-reactor containment structures designed to contain the effects of accidental runway from the reactors which they house.

Depending on the engineering application, these structures may have to withstand static as well as dynamic pressures, therefore, they are usually constructed in the form of large-sized, thin-walled pressure vessels, such as spherical or cylindrical shells with hemispherical or ellipsoidal end caps.

In designing such structures, it is necessary to consider their dynamic response to the expected transient pressure and to determine whether the static pressure design criteria are sufficient. The simplest analytical problem relating to the design of these structures is that of the response of a spherical shell to a spherically symmetric transient pressure on its inner surface. Baker and Allen (1) considered the elastic response of a spherical shell of any thickness to such a pressure pulse. They showed that the response of even relatively thick shells could be adequately described by an approximate "thin-shell" equation of motion. Baker (2) extended the analysis to include plastic deformation and the nonlinear effects of shell thinning and increase in radius, and obtained solutions to these problems.

The same equation for the dynamic pressure, resulting from an explosion in a spherical chamber filled with air used by Baker et al (1) was later adopted by Zhdan (3), together with a system of equations of one-dimensional gas dynamics in an attempt to determine the dynamic load and the impulse acting on the wall of the chamber. In order to do so, the effect of pressure macropulsation at the wall and the possibility of resonance of the chamber was examined. From experiments, it was concluded that resonance of the chamber will occur when the displacement of the chamber shell relative to the equilibrium position is larger than the displacement in the quarter of the first period of intrinsic oscillation, predicted by equation (1), see ref. (3) for details.

$$\delta \max = j_{ref} / \rho_w \, h_\omega \qquad (1)$$

Where, δ_{max} is the maximum shell displacement, j_{ref} is impulse per unit area, h is the shell thickness and ω is the frequency of vibration.

This effect must be taken into account in designing the chamber for maximum explosive charge weight. Quantitative analysis of the results obtained by Zhdan (3) shows that at resonance pressure macropulsation, the additional impulse acting on the spherical shell in course of its radial expansion may be as much as 50% of the original impulse.

Similar observations were made by Buzukov (4,5) who used the same approach to study the effect of internal blast loading of a cylindrical chamber. In examining the experimental strain amplitude results, it was noticed that the peak deformation of the chamber was higher in later cycles than that of the first oscillation. Approximately 20-40 μsec after the start of movement, the walls of the chamber were "set swinging". The excess of the maximum deformation

over the initial deformation reached 100-150% in the case of relatively small charges and was reduced to 30-40% for larger explosions. This is in close agreement with Zhdan's (3) findings if a 50% increase in the original impulse acting at the wall of a spherical shell at resonance.

The "swinging" observed by Buzukov (4,5) was found to originate 20-40 μsec after arrival of the shock wave at the side walls of the chamber. This appearance cannot be explained by the secondary shock of the reflected wave, since the transit time of the reflected wave in this chamber design was 3-5 msec. It is obvious that the phenomenon is associated with a complex oscillatory process of the whole structure and, in particular, with the fact that the natural frequencies of the radial and longitudinal oscillations of the wall are close. The same phenomenon was observed by Zhdan et al (3,6) and Adischev et al (7,8) who attributed the increase in the magnitude of spherical and cylindrical shell displacements to the possibility of a resonance effect of the chambers in question.

Ivanov et al (9) used destructive tests and statistical theory to evaluate the fracture strength of explosion chambers. The specimens were made of steel of ellipsoidal shape and variable wall thickness. The vessel models were filled with water and they were internally blast loaded to failure to check for a scale effect on the fracture strength of explosion chambers. They found that there is a marked scale effect in explosive loading of similarly loaded geometrically similar vessels filled with water. They concluded that this scale effect is of energy character and is in accordance with the findings of references (10-12).

An entirely different approach was employed by Ahrens et al (13) in an attempt to obtain an expression for the peak pressure generated by the expansion of detonation products in evacuated chambers. Using small charges (0.2 to 2 g) of HNS (Hexanitrostilbene) explosive in vacuums of 10^{-4} to 5×10^{-4} kPa they found that the resultant gas blast rapidly achieves a terminal velocity of 1.0 to 1.2 km/sec. From their experimental measurements they suggested that the reflected peak pressure may be represented by

$$P = 6.5\times10^{5}\, r^{-3.5} \quad (\text{bar}) \qquad (2)$$

where r is the ratio of the radius from the centre of the charge to the transducer to the radius of an equivalent charge. Similar results for the exponent of r were obtained by Lutzky (14) for the fall off of the gas blast at a distance of 10 charge radii from a 1-lb PETN sphere detonated in vacuum.

The pressures generated by an explosion in evacuated chambers was studied by Dawson et al (15) who carried out systematic explosive tests in cylindrical mild steel bell in order to obtain data for the design of an explosion chamber for high energy rate forming purposes. The chamber was evacuated to a pressure of less than 3 kPa and explosive charges (of Trimonite 1) of up to 550 g were detonated.

For charges up to and including 130 g the pressure in the vessel the quasi-static final overpressure was found to be approximately given by,

$$P = \frac{0.145\,W}{V} \qquad (3)$$

Where P is in kPa, W explosive charge input in gm and the volume of the vessel in m^3.

ANALYSIS

The chamber under consideration is a spherical steel pressure vessel of 1.83 m (72") outside diameter and 25.4mm (1") wall thickness. Three pad reinforced nozzles of diameters 0.22 mm, o.41 m and 0.61m were attached (See Fig.1). The steel used was BS1501-161 26A. Gill (16) performed tensile tests on a selection of materials and found values of 200 GPa for the Young's modulus, 0.275 for the Poisson's ratio, and 300 MPs for the lower yield stress. The vessel had been studied over several years and the design pressures, stresses and limitations were well known, see Gill (16), Paine (17) and Kannas (18).

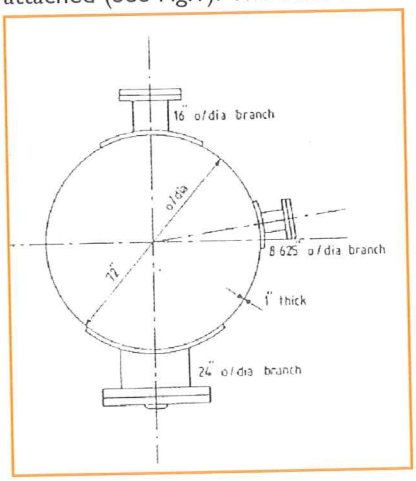

Figure 1 Explosive chamber under analysis (17)

The present paper highlights the analytical and experimental steps taken in deciding the safe limit of this vessel for explosive working.

Thin Shell formulation of the Problem

A closed-form thick shell, arbitrary loading solution would be extremely difficult to generate and unwieldy to use. By making some engineering assumptions a usable equation has been formed by Baker et al (1) for spheres. The major assumptions are:-

(i) only radial motion is considered
(ii) thin shell theory is applied
(iii) the internal pressure loading is of the form $P=P_p(1-t/T)$

Consider the shell element show in Fig. 2, subjected to an internal transient pressure P(t). From thin shell theory it may be assumed that the radial strain ε_r and the radial stress σ_r are negligible in comparison with tangential strains and stresses, and that the variation of the tangential strains and stresses through the thickness of the shell is small.

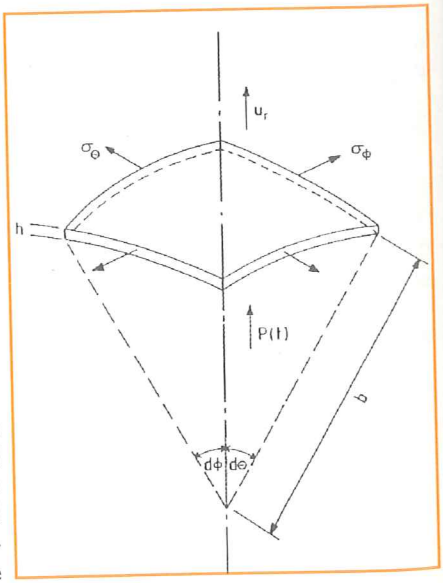

Figure 2 Element of a spherical shell under transient pressure

Then the equation of motion in the radial direction of the shell element shown in Fig. 2 is,

$$h(\sigma_\theta + \sigma_\phi) + \rho h b \frac{d^2 u_r}{dt^2} = bP(t) \qquad (4)$$

Using Hooke's law and since, $\varepsilon_\theta = \varepsilon_\varphi = \frac{ur}{b}$ equation (4) becomes

$$\rho \frac{d^2 u_r}{dt^2} + \frac{2E}{1-\upsilon} - \frac{u_r}{b^2} = \frac{1}{h} P(t) \qquad (5)$$

The solution of this equation, for the blast pulse

$$P(t) = P_p \left(1 - \frac{t}{T}\right), \quad 0 < t \le T$$
$$P(t) = 0 \qquad t > T \qquad (6)$$

is, see Baker et al (1)

$$u_r = K\left[1 - \frac{t}{T} - \cos\omega t + \frac{\sin\omega t}{\omega T}\right] \quad 0 < t \le T \qquad (7)$$

$$u_r = A\cos\omega(t-T) + B\sin\omega(t-T) \quad t > T$$

where

$$\omega^2 = \frac{2E}{\rho b^2(1-\upsilon)}, \quad K = \frac{P}{\omega^2 \rho h} \qquad (8)$$

and

$$A = K\left[\frac{\sin\omega T}{\omega T} - \cos\omega T\right] \qquad (9)$$
$$B = K\left[\sin\omega T + \frac{\cos\omega T}{\omega T} - \frac{1}{\omega T}\right]$$

According to this approximate theory, the shell vibrates in a single radial mode with a maximum radial displacement of

$u_{max} = (A^2 + B^2)^{\frac{1}{2}}$.

The maximum tangential strains are thus given by

$\varepsilon_{max} = u_{max}/b$ (10)

EXPERIMENTAL WORK

Charges of Trimonite No. 1 were detonated close to the centre of the chamber. Trimonite No. 1, manufactured by ICI Nobels in the UK, is a mixture of anodized aluminium, TNT and ammonium nitrate, and has a yield of 6280 jg-1 and a detonation velocity of about 2000ms-1, but the latter is known to vary with geometry and confinement.

Strain gauges were mounted on the outside the spherical surface of the chamber and connected via a suitable amplifier to a storage oscilloscope. Dynamic pressure measurements were made using a piezoelectric pressure gauge (Kistler type 607A SN, 0 - 250 bar, linearity 0.3%) on a suitable mounting in one of the nozzles close to the outside of the chamber. The transducer was positioned to minimize the effect of reflections from the chamber walls. Strain and pressure were recorded for 15 explosions in the mass range 15 -141 g.

Strain gauges records for the 56 g and 106 g shots are shown in Fig. 3. The first maximum in the strain amplitude was taken to correspond to the peak pressure.

Pressure records for the 42 g and 63 g shots are shown in fig. 4. (The second peak is due to reflection from a structure within the chamber and need not concern us here).

From these recordings the peak strain, peak pressure and

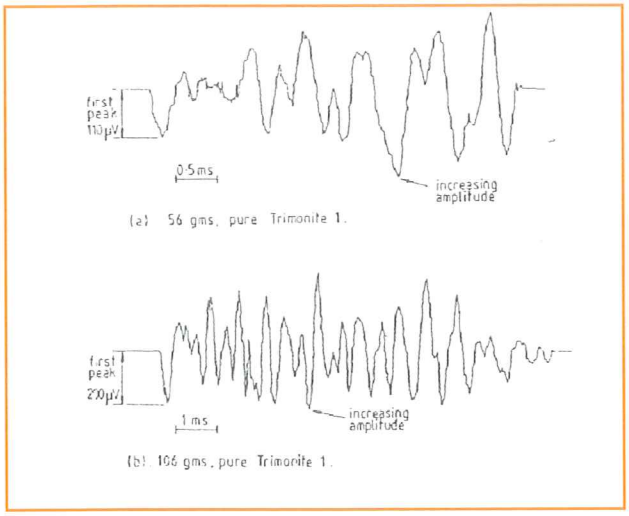

Figure 3 Typical oscillographs showing oscillations of spherical shell

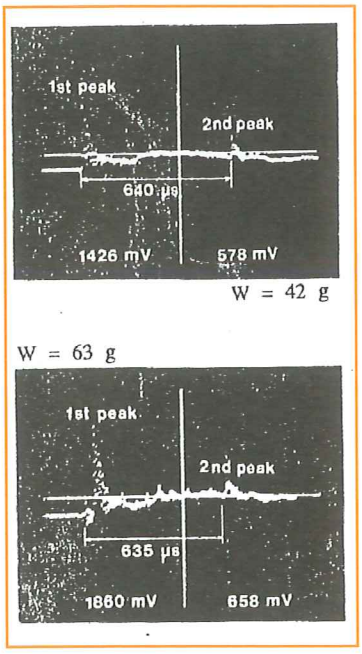

Figure 4 Typical pressure pulses (0.5 μs/sample, scale 2.5 V/MPa)

overpressure duration were determined. Using the experimentally found Pp and T the values of the constants K, A and B were calculated to give, using equations 7,8,9 and 10, a semi-theoretical value for the first peak strain I φ.

The values for each parameter are listed in Table 1. It can be seen that the agreement between the experimental and the semi-theoretical values are very good, see Fig. 5.

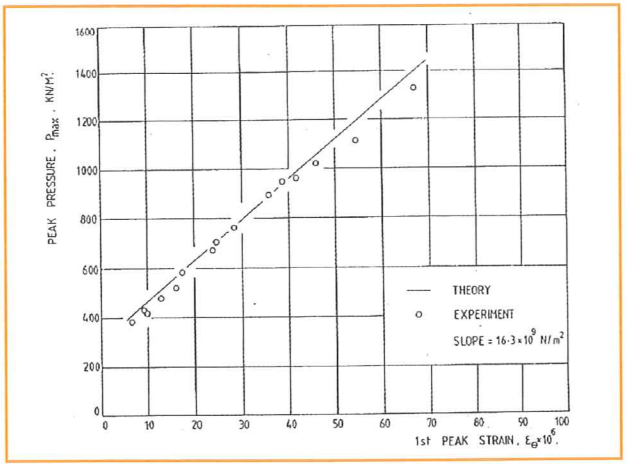

Figure 5 Peak pressure versus hoop strain for various charges

Determination of the maximum allowable explosive charge mass

If the mean lower yield stress of the vessel's material is 300 MPa then the corresponding strain at the threshold of yielding is

$\varepsilon_y = \sigma_y\sqrt{E(1+\upsilon)} = 1.25 \times 10^{-3}$. By extrapolating from the Pmax vs ε_θ relationship of Fig. 5 for $\varepsilon = 1.25 \times 10^{-3}$ the dynamic pressure required to cause yielding of the material is $P_{yd} \approx 24$ *MPa* From the static analysis of thin spherical pressure vessels the pressure required to cause yielding is given by

$$P_{ys} = \frac{2h\ \sigma_y}{a} = 17\ \ MPa \qquad (11)$$

where σ_y is the mean lower yield stress.

Thus the dynamic yield pressure is about 30% greater than the static yield pressure. At this point it must be emphasized that the measured dynamic pressure was a "free field" measurement taken about 300mm away from any structure. The actual dynamic load applied will, of course, be higher due to the reflection of the blast.

Gill et al (16) reported that the design stress of the spherical shell of this vessel is about 140 MPa. Using equations (11) the static design pressure is about 8 MPa and by extrapolating from Fig. 5 for the design strain of 5.6×10^{-4}, the dynamic design pressure will be about 11.4 MPa.

The experimental data for peak pressures obtained from the detonation of various charge weights is listed in Table 1. By plotting peak pressure, Pmax, against charge W, it was found that an approximate linear relationship could be fitted through the points as shown in Fig. 6. A similar relationship was reported by Dawson et al (15). This result however is not general and only applies to contained explosions of certain geometries.

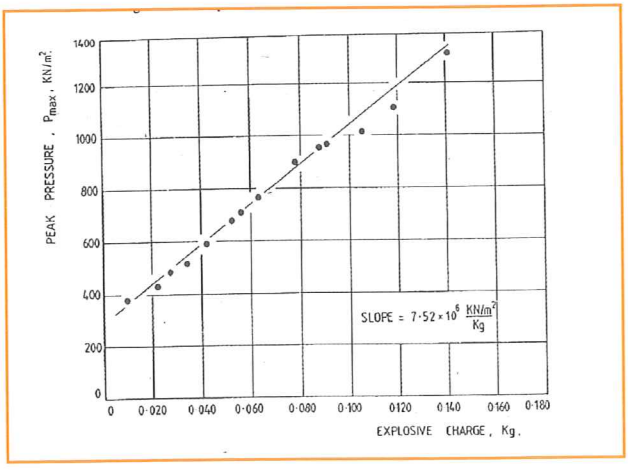

Figure 6 Peak pressure versus explosive charge

If for the sake of argument we assume that the Pmax vs W relationship of Fig. 6. is valid up to the dynamic design pressure then by extrapolating it was found that the charge required to cause a pressure rise in the chamber of 11.4 MPa is about 1.5 kg. These design pressures and charge weights would also satisfy the design requirements for the pad reinforced nozzles of the vessel since the static analysis (16) indicates that the thickness of the nozzles and that of the welded pads was chosen to fulfill the design pressure requirements. This obviously needs to be substantiated by a dynamic analysis. The explosive charge required to raise the pressure inside the chamber to the dynamic yield pressure of, $P_{yd} = 24$ MP_a, can in this case be estimated from Fig. 6 at $W \approx 3.2kg$ ($\approx 7.0lb$).

TABLE 1 – Experimental and theoretical results from the detonation of explosive charges at the centre of the chamber

EXPLOSIVE CHARGE, W, (g)	PEAK PRESSURE P_{max} MP_a	CONSTANT k*10-5	TIME T μs	ε_θ EXPERIMENTAL μ-strain	ε_θ EXPERIMENTAL μ-strain
15	0.380	2.15	50	6.9	5.7
22	0.428	2.43	60	9.4	8.2
22	0.428	2.43	62	9.6	8.5
27	0.483	2.74	62	12.7	10.9
34	0.518	2.94	90	15.8	15.2
42	0.593	3.36	100	17.4	17.3
52	0.676	3.83	113	24.0	22.5
56	0.704	3.99	116	25.0	23.6
63	0.759	4.30	123	28.5	26.9
78	0.897	5.08	138	36.0	35.3
88	0.952	5.39	144	39.9	38.9
91	0.966	5.47	146	42.2	40.0
106	1.021	5.79	156	46.0	44.9
119	1.104	6.26	164	54.0	50.8
141	1.325	7.51	175	67.0	64.0

FINITE ELEMENT MODELING

The above arguments did not warrant sufficient confidence and a safe limit of 150 g incorporating a generous safety margin was used over many explosions and found to be adequate. The analysis is, however, only strictly applicable to spherical shells, and whilst the strains at the "equator" of the vessel, well away from the nozzles have been accurately predicted, there was no information on the strains or stresses in the region of the shell/nozzle junctions, where raised stresses would be expected. It was decided to extend the analysis by the use of finite elements.

The chamber was modeled using a finite element package (ABAQUS) on an Apollo workstation (Model DN4000). Both static and dynamic analyses were performed.

It would be prohibitively expensive in computer time to fully model the chamber using three dimensional elements, so a decision was taken to concentrate on the largest (0.61m outside diameter) nozzle. An advantage of concentrating on this nozzle arises from the fact that this is the main entry/exit route for positioning work within the chamber. The flange is attached by up to 24 (50mm diameter) bolts and the effort required to insert and remove these bolts was such that rarely were more than six used for charges of 50g or so. The analysis should indicate the stress in the bolts and help in deciding safe practice.

To further reduce computer time ax symmetric elements were used. This has the effect of suppressing certain modes of vibration, for example where the cross section of the nozzle deforms into an ellipse.

A further disadvantage was that cross-coupling of the modes of vibration of each nozzle was not allowed for. This manifested itself as an incorrect prediction of the frequency of oscillation, see below. (CPU times were about 700 s for

a static analysis and about 140000 s for the dynamic).

The chamber has been the subject of extensive static analysis and experimental work by Gill (16), Paine (17) Kannas (18) and their data was used to check the model prior to dynamic analysis.

The results of a static analysis are shown alongside experimental data from Paine (17) in Figure 7a and 7b, showing circumferential and meridional stresses for the inside and outside of the branch. The agreement is excellent, and differences between the analysis and experiment seem to be mainly due to uncertainties in the position and extent of the welds joining the pad to the nozzle etc. Difficulty was reported by Paine (17) when plotting the experimental data and comparing to classical analysis. The excessive strain at the "toe" of the weld is due to the sharp inside corner, which is filleted on the chamber. The analysis of the pad gave results closer to those reported by Paine (17). Comparison with classical analysis (17) shows that the finite element method provides more accurate results. It is felt that if the dimensions of the pad, sphere and nozzles, and the extent of the weld was accurately known, the analysis could be improved.

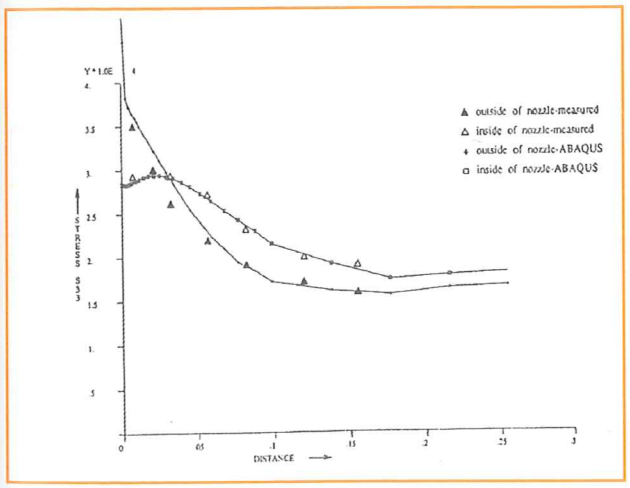

Figure 7a Experimental and finite element predictions of circumferential stresses along nozzle near sphere

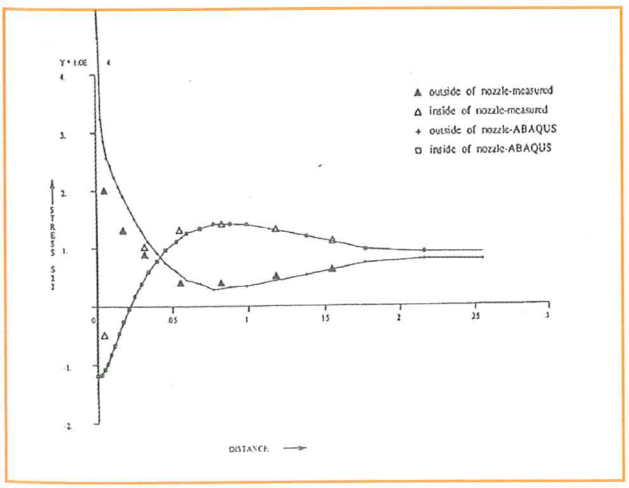

Figure 7b Experimental and finite element predictions of meridional stresses along nozzle near sphere

The finite element mesh used is shown in Figures 8 to 10 and consists of 228 two dimensional ax symmetric elements. It was found that a fine mesh was necessary in the sphere/nozzle weld region. As this area contains both the pad/sphere weld and the sphere/nozzle weld this is not surprising.

From the edge view (Fig. 8) it can be seen that the flange plate is a separate entity, coupled to the flange by a prestressed truss element. A single interface element separates the flange and the flange plates and represents the seal. Motion in the y-direction (see Fig. 8) was suppressed at the edge of the sphere and motion in the x-direction suppressed at the centre of the flange plate.

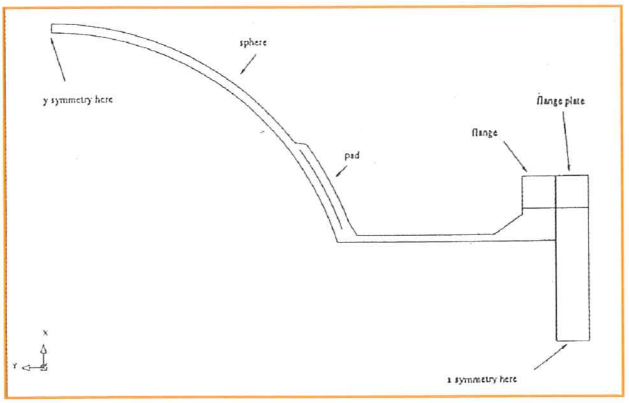

Figure 8 Outline of finite element model for 0.61m diameter nozzle

Several analyses were performed with the flange plate removed in which the position of the load due to the flange plate was applied at a single point or distributed over the flange. It was found that any variations in the stress distribution were local to the flange and did not propagate far down the nozzle. This was taken to indicate that the modeling of the bolts and seals was not critical.

Analyses were performed with interface elements between the pad and sphere (to stop the structures "passing through" each other) but it was found that the results were erroneous. This is in agreement with Kitching et al (16) who used an analysis contact at the welds only. The reason is that the movements are small, about 0.6 mm at the design pressure (8MPa) and the pad is not in intimate contact with the sphere.

Dynamic Loading of the FE model

Loading was via a subroutine in the ABAQUS input deck. The form of the loading is the modified Friedlander equation.

$$P = P_p \left(1 - t/T\right) e^{-\beta t/T}, \qquad (12)$$

the simplest form capable of retaining peak pressure, overpressure duration and total impulse. P_p, T and β vary with explosive type, explosive mass and range. Equation (13) can be integrated between t=0 and t=T, to yield the impulse

$$I = \frac{P_p T}{\beta^2}\left(e^{-\beta} - 1 + \beta\right) \qquad (13)$$

in terms of P_p, T and β. Baker (19) provides non-dimensional plots of reflected and side on pressure (as P/P_o), reflected and side on impulse as $(Ia_o/P_o^{2/3}E^{1/3})$, overpressure duration as $(Ta_oP_o^{1/3}/E^{1/3})$ and the Mach number for reduced distance $(R P_o^{1/3})/E^{1/3}$.
These plots represent summaries of a large number of experiment by many workers of all types of explosive and range.

The loading was split into three regions, the spherical part, the nozzle wall and the flange plate.

The sphere Only explosions at the centre of the chamber were considered, so the shock wave propagates normally to the surface and data on normal reflections were used.

The nozzle It can be be shown that a Mach stem must be present along the side of the inside of the nozzle.

The load was determined by calculating the Mach number of the Mach stem as, see (20)

$$M_{stem} = \frac{M_o}{\sin\theta} \qquad (14)$$

where θ is the angle between the ray at the shock front/nozzle wall interface and the normal at that point.

Using data in Baker (19) the loading required for this Mach number was calculated and inserted in equation (12) for side loading.
The flange plate Normal reflection from the flange plate was assumed, to avoid having to code in polar reflection curves, and as the deviation from normal is at most about 10°. This led to excessive loading and thus errors on the side of safety.

Limitations of the loading subroutine Only the initial shock is allowed for. Reflections are assumed to have little effect. The width of the Mach stem is not calculated so the outer region of the flange (by the nozzle) is not loaded correctly. This error is considered to be small.

RESULTS

The results of a dynamic analysis modeling the detonation of 106g of Trimonite at the centre of the chamber is shown in Figs 11 and 12 and can be compared directly with the strain gauge readings in Fig. 3.

Figure 11 shows strain ε_{θ} (ε_{zz} in Figure 9) mid way between the nozzles, on both the inside and the outside of the chamber.

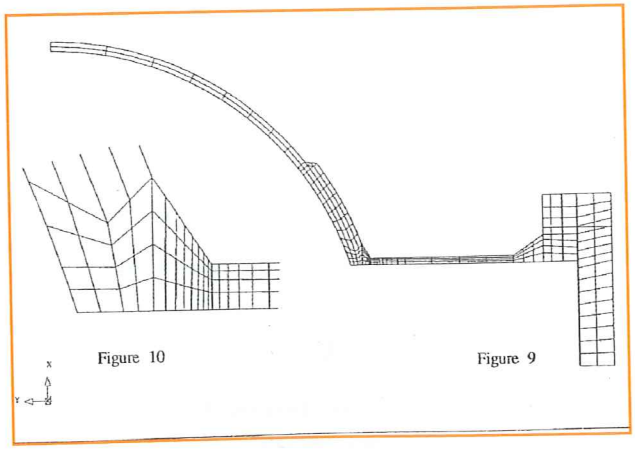

Figure 9 Finite element model and (inset Figure 10) detail of nozzle/sphere/pad weld

Figure 12 shows strain ε_{θ} (ε_{yy}) at the same positions. Given that the loading uses data for free air blasts, the agreement between the prediction of initial peak strain (about 50 micro strain) and experiment (46 micro strain) is remarkable.
Figure 11 shows that the initial peak does not correspond to the maximum strain reached, as found experimentally and shown in Figure 3.

There is a major quantitative difference between Figures 3 and 11 in that the frequency of oscillation in the strain in Figure 3 is about double that in Figure 11. Figure 12 provides the explanation. After a few milliseconds the strain on the inside and outside of the chamber are 1800 out of phase, indicating bending at this point. The chamber is not now oscillating as a sphere but rather (looking at Fig. 10) the nozzle and flange plate are oscillating in the y-direction.

Recalling that diametrically opposite to the 0.61m diameter nozzle is a 0.41m diameter nozzle, it is clear that each will oscillate at a slightly different frequency. Furthermore, as each flange plate is at a slightly different distance form the centre of the chamber, the phase of such oscillations will be different. The higher frequencies visible in Figure 3 are due to interference between these modes of oscillation.

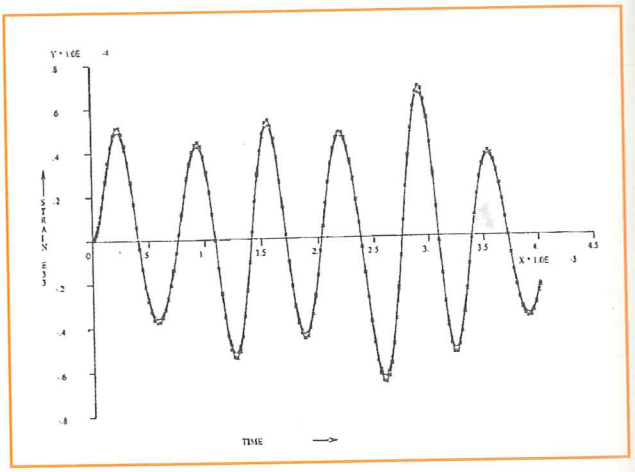

Figure 11 ABAQUS prediction of hoop strain e33 versus time

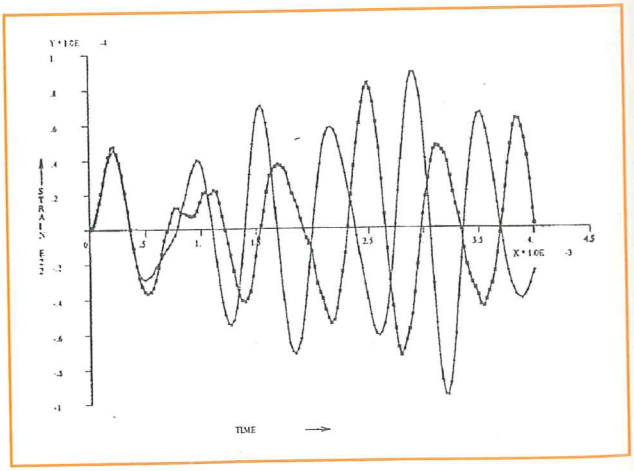

Figure 12 ABAQUS prediction of meridional strain e22 versus time at inside and outside of vessel

The maximum principal stress at the three modes closets to the "toe" of the pad/nozzle weld is shown against time in Figure 13. The stress does not exceed 25 MPa and is thus well below the design stress of the vessel (140 MPa).

From this it was concluded that the vessel was entirely safe for 106 g of explosive.

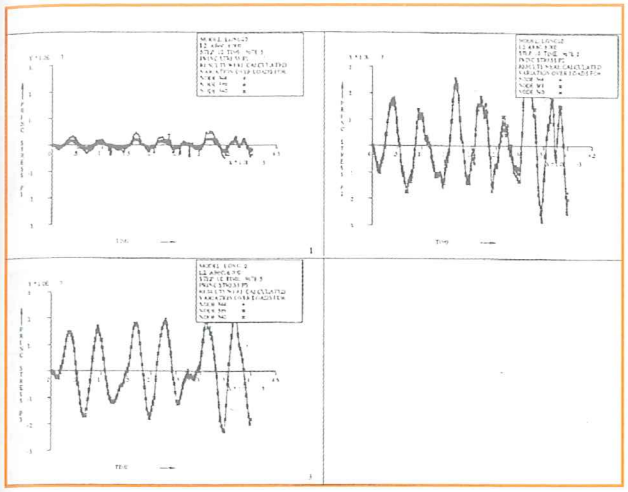

Figure 13 ABAQUS prediction of principal stresses at three points nearest to e of weld for a charge mass of 106g

The analysis was repeated for an explosive mass of 1 Kg. The principal stresses at the three modes nearest the "toe" of the weld are shown in Fig. 14. The stress approaches 300 MPa, the yield strength of the steel, and is well in excess of the design stress of 140 MPa. It was concluded that 1 Kg is the largest charge mass that be detonated without exceeding the static yield stress of the vessel.

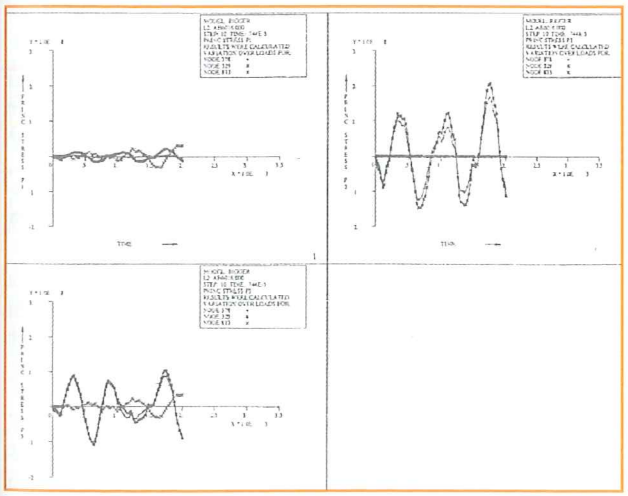

Figure 14 ABAQUS prediction of principal stresses at three points nearest to e of weld for a charge mass of 100g

Calculation of the strain rate indicates values of approximately 2 s-1, and using this value in the Cowper Symonds equation for strain effects,
$\sigma_y / \sigma_o = 1 + \varepsilon_o / D^{1/p}$ where σ_y is the yield strength σ_o is the static yield strength and D and p are material constants, (for mild steel p = 5 and D = 40) indicates an increase in the yield strength of about 50%.

Thus even allowing for strain rate effects in the design stress of a 50% increase 1 kg of explosive is too close to the safe limit of this chamber. In practice a generous safety margin has to be allowed.

However, 1 kg charge gives a first peak strain of 2.5×10^{-4}. This is five times that of the one produced experimentally and theoretically by the 106 g charge. The linear relation between the charge mass and the peak pressure (which is proportional to the strain) at low values, is not valid at higher charge masses. Larger charge masses produce relatively lower peak strains and consequently lower peak stresses. Further experimentation will be needed for more accurate definitions of the non-linear relationship. In the meantime, the charge limit is set to 300 g. A full analysis of the vessel needs to be carried out at this charge mass.

Results of Short Analyses of Several Charge Masses

Due to lack of computer and data interpretation time it has not been possible to undertake full analyses of other charge masses. However, the magnitude of the first peak strain has been obtained for eight other charge masses extending the range to 15 - 1000 g. The results are plotted, with the experimental data, in Figure 15. The experimental data are less than the predicted values for low charge masses, but asymptotically approach the predictions near to 60 g. The reasons for this discrepancy, with experimental data values only 70% of predicted cannot be determined without further investigation, but it is probable that incomplete detonation of the very small (less than 2 cm radius) charges is responsible. This hypothesis could be checked by using a plastic explosive charge of similar yield. A datum at about 300 g of explosive would be helpful.

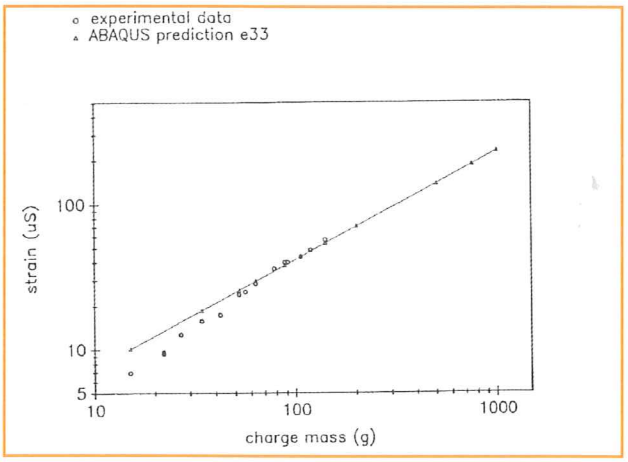

Figure 15 ABAQUS prediction of first peak strain and experimental data points

CONCLUSIONS

Experiments using small charges have been performed and have validated both closed form and numerical analyses.

A literature review showed that the phenomenon of "swinging" whereby large deformations evolve after several cycles, was well known and documented. The numerical analysis correctly predicted this, but the closed form analyses was not capable of extension.

The numerical analysis also showed that the vibration modes of the nozzles were important and tended to become the predominant oscillation.

The design limit was found by (i) extending experimental data fitted to a closed form analysis leading to a safe limit of 1.5 kg and (ii) finite element analyses concentrating on the stress raising properties of the sphere nozzle junction, leading to a safe limit of 1 kg.

Both theory and experiment indicated that the strain rate, at about 2 s^{-1}, was high enough for strain rate strengthening effects to take place, thus increasing margins.

FUTURE WORK

The work has shown that FE is invaluable in extending confident safe limits of real structures. Future work will involve a further modeling of the process to ensure that no major quantitative effects are ignored by the simple ax symmetric half model used. The analysis has been on stress-free models. A full plastic analysis, at say 2 kg of explosive, will indicate the extent of plastic deformation, and may indicate that shakedown effects will be beneficial.

The effect of non-central charges will be investigated with aid of strain gauges and pressure transducers at critical points within the vessel.

SYMBOLS USED

Note: The original notation has been retained in the literature review.

a_o = speed of sound in air (340.29 ms^{-1})
a = internal radius of vessel (m)
b = external radius of vessel (m)
E = Young's modulus (Nm^{-2}), total energy of blast source (J)
h = shell thickness (m)
I = impulse per unit area (Nsm^{-2})
m= Mach number
P = pressure (Nm^{-2})
P_o = atmospheric pressure (10^5 Nm^{-2})
P_p = peak blast overpressure (Nm^{-2})
R = distance form blast source (m)
T = blast overpressure duration (s)
u_r = radial displacement (m)
W = explosive charge mass (g)
β = parameter in modified Friedlander equation
ε = strain
σ = stress (Nm^{-2})
ω = radial frequency of oscillation ($rads^{-1}$)

REFERENCES

1 Baker W E and Allen F J, "The Response of Elastic Spherical Shells to Spherically Symmetric Internal Blast Loading", Proc. 3rd US Nat Congress Appl Mech, p 79-87, New York, 1958.

2 Baker W E, "The Elastic-Plastic Response of Thin Spherical Shells to Internal Blast Loading", Ballistic Research Laboratories, Aberdeen Proving Ground, Mem ASME J of Appl Mech, P 139-144, March 1960.

3 Zhdan S A, "Dynamic Load Acting on the Wall of an Explosion Chambers", Combustion, Explosion and Shock Waves, Vol 17, No 2, p 141-144, 1981.

4 Buzukov A A, "Characteristics of the Behaviour of the Walls of Explosion Chambers Under the Action of Pulsed Loading", Combustion, Explosion and Shock Waves, Vol 12, No, 4, p 549-554, 1976.

5 Buzukov A A, "Forces Produced in an Air-Filled Explosion Chamber", Combustion, Explosion and Shock Waves, Vol 16, No 5, p 555-559, 1980.

6 Vasil'ev A A and Zhdan S A, "Shock-Wave Parameters on Explosion of a Cylindrical Charge in Air", Combustion, Explosion and Shock Waves, Vol 17, No 6, p 669-673, 1981.

7 Adishchev V V And Komev V M, "Calculation of the Shell of Explosion Chambers" Combustion, Explosion and Shock Waves, Vol 17, No 6, p 780-784, 1979.

8 Komev V M, Adisheev V V, Mitrofavov A N and Grekhov V A, "Experimental Investigation and Analysis of the Vibrations of the Shell of an Explosion Chamber", Combustion, Explosion and Shock Waves, Vol 15, No 6, p 821-824, 1979.

9 Ivanov A G, Ryzhanskii V A, Tsypkin V I and Shitov A T, "Scale Effect in the Strength of a Pressure Vessel Under Internal Explosive Loading", Combustion, Explosion and Shock Waves, Vol 17, No 3, p 327-330, 1980.

10 Ivanov A G. Novikov S A and Sinitsyn V A, Fiz Geroniya Vzryva, 8, No 1, (1972) Dokl Akad Nauk SSSR 194, 1970.

11 Ivanov A G And Mineev V N, Dokl Akad Nauk SSSR, 220, 1975.

12 Ivanov A G And Mineev V N, Fiz. Geroniya Vzryva, 15, No 5, 1979.

13 Ahrens J T, Allen F C and Kovach L R, "Explosive Gas Blast: The Expansion of Detonation Products in Vacuum", J of Appl Phys, Vol 42, No 2, p 815-829, 1971.

14 Lutzky M, Naval Ordnance Laboratory, NOL-TR-62-19, 1962.

15 Dawson P H and Alexander K, "An Enclosure for Explosive Processes", Proc of 7th Int Conf on High Energy Rate Fabrication, Leeds, p39-47,1981.

16 Gill S S, Kitching R, Kannas A and Paine R T, "Experiments on Spherical Pressure Vessels with Pad-Reinforced Nozzles", Chapter 3, Applied Mechanics Division, UMIST, UK.

17 Paine R T, MSc Thesis, University of Manchester, 1976.

18 Kannas A, MSc Thesis, University of Manchester, 1975.

19 Baker W E, "Explosions in Air", University of Texas Press, 1974.

20 Baker W E, Cox P A, Westine P S, Kulesz J J, Strehlow R A, "Explosion Hazards and Evaluation", Elsevier Scientific Publishing Company, 1983.

TECHNOLOGY, LANGUAGE AND THE INEVITABLE CREATION OF NEW LITERACIES

Anastasia Mouskou-Peck
Lecturer of English and Report Writing
General Studies Department

PART I

The following article examines the relationship between technology and language – especially the English Language – in the fast growing world of technology and the consequent creation of new literacies which go beyond the traditional use of language.

Technology is not a simple scientific, static development of knowledge. It is a much wider concept, encompassing social and literacy aspects.
Michael Stubbs (in Fairclough 1996:219), argues that:

"Technology is not just a set of inert things. It is also a set of social practices. It is presented to consumers in highly symbolic ways which convey messages about power and prestige".

Undoubtedly all the technological advances – and among them the computer which constitutes one of the most highly ranked inventions – have created new educational demands.

"The evaluation of educational change due to the new technologies involves the analysis of changed cognitive and social relations in the classroom. We therefore need simple but powerful concepts to study the ***pedagogic*** *and* ***cognitive*** *logic of such situations." (Stubbs in Fairclough (Ed.,) 1996:220).*

Undeniably these new technological advancements inevitably have led to changing demands of literacy, nurturing new kinds of language awareness, and creating new educational implications. Furthermore, this leading-edge technology will need a kind of linguistic code, an appropriate language in which to express itself. The language that is extensively associated with technology, viz., computers, information technology, internet, is mainly English. As usual, nothing in society happens coincidentally, but developments occur because of certain undisputed and forceful determinants.
David Graddol (in Burns & Coffin (Eds.,) 2001:33) argues that this leading-edge technology is mainly based on the English language because, 1) Firstly its research and development originates in the US, although often through special collaboration with Japanese transnational companies (TNCs) , 2) Secondly, the literature and language of conferences where the results of research are reported is largely English. This is a very extensive area of language usage considering the amount of research being carried out worldwide, which aims at scientific advancement.

"The drive to make progress in science and technology fostered an international intellectual and research environment which gave scholarship and further education a high profile". (Crystal 2003:10).

3) Thirdly, communications, technology and document-handling software have also been developed around the English language. And 4) Fourthly, the US is the basis of all the installed user help lines concerning new technology i.e. support manuals, on-screen menu systems and others, providing all this assistance in the English language; of course, for a more balanced argument, nobody can vouch for the permanency of this situation. David Graddol argues that, with the development of newer, more sophisticated technology and software, other languages are capable of being promoted also. However, currently English continues to be at the leading edge of economic modernization and industrial development. The typical set-up of economic modernization requires technology and skill, transferred from the Big Three regions (North America, Europe and Japan), following investments by TNCs, which are often joint-venture companies. All these enterprises require some language commonality, which as already mentioned, again is none other than English. Again here, Graddol believes that this is a situation that is likely to change in the next decades, due to the development of local networks of small companies assisting the TNC enterprises. Nevertheless, this is speculation for the future which does not alter the reality of the present. Societies and institutions, upon deciding what accomplishments to offer to their citizens and youth, need to mainly provide for the existing situation and the immediate future. My personal view – with all its limitations – does not envisage any drastic changes with regards the English language; on the contrary, the expansion of the language will continue to the extent that people – if allowed – will become unavoidably bilingual, searching for further means of expression, rather than abolishing what they already possess.

A further major technological breakthrough was the development of the Internet. The Internet is the technology that has revolutionized the communication system and has bonded nations from opposite geographical poles.

"The Internet epitomizes the information society, allowing the transfer of services, expertise and intellectual capital across the world cheaply, rapidly and apparently without pollution or environmental damage". (Graddol in Burns & Coffin (Eds.,) 2001:34).

According to Graddol, 90 per cent of Internet hosts are based in English – speaking countries. This as a result leads to the majority of traffic and websites to be based in English, and the users who are placed in other countries and therefore users of other languages, have to communicate with other members of the cyberspace community, through the medium of English. In fact in an article in *"The New York Times"* (quoted by Specter

1996 in Crystal 2002:217), it was stressed that: *"If you want to take full advantage of the Internet there is only one real way to do it: learn English"*. This sentiment is not surprising if we consider the language distribution on the web which is predominantly English. (See TABLE 1) (Crystal 2002:217).

However, Graddol - as I have already mentioned - sees an Internet base community developing rapidly to non-English-speaking countries, which as a result will reduce the English computer-based communication in the following decades. The truth of the matter though is that no-one can predict the future accurately. We can only follow the indications and make our own hypotheses for the future.

What we do however need to do as educators is to fulfill and satisfy the needs of today and gradually plan for the needs of tomorrow through a well-drafted, rounded plan of education.

PART 2

In the next part of this article I will examine how the evolution of new technologies, has inevitably brought about crucial changes to literacy practices associated with their use, which has inevitably imposed new demands.

"Whether the technology is word processing, electronic mail, hypertext, or the internet, these technologies alter how language, both written and visual, is produced, processed and used". (Snyder, 1998 :xx).

These new technologies have not impaired the use of traditional languages, but on the contrary they have enriched them with more options and choices. Just as printing did not replace writing, neither will 'Netspeak'[1] replace language. Plainly, new methods of usage will have to be designed.

The majority of citizens nowadays are in daily contact with these new technologies encountered. According to Brod (1984) (quoted by Murray in Burns & Coffin (Eds.,) 2001:38) people are familiarized with computers in two distinct zones: first the private, for conducting their own personal tasks (banking, mail ordering, etc), and second the production area, where they perform their professional duties and often their very livelihood depends on that.

What we are faced with presently is "*newness*", which unavoidably creates re-thought and re-evaluated situations.
Unquestionably, the 'web' has decreed new stipulations and prerequisites, both in terms of language usage and linguistic design as well as social conception.

There is little question that the internet has brought dramatic changes to the very essence of language, for both now and the future.

"...the sheer scale of the present internet, let alone its future telecosmic incarnations has convinced me that we are on the brink of the biggest language revolution ever". (Crystal, 2002:241).

Traditionally, according to Crystal (2002:7), written language fostered five main stylistic approaches: 1) *Graphic features* (including page design, illustrations, colour, columns), 2) *Orthographic or graphological features* (alphabet, capital letters, spelling, punctuation, italics), 3) *Grammatical features* (the syntax, word order, pronouns), 4) *Lexical features* (vocabulary, set of words, idioms), 5) *Discourse features* (coherence, relevance, paragraph, structure, etc). Additionally spoken language can use: a) *phonetic features* (voice quality, vocal register), and b) *phonological features* (the sound system, intonation stress and pause).

All the above features can be used in the internet also, since the internet culture is still very much a text-based affair.
What is different though now, is the flexibility of its usage, the plasticity of its form, the transition of its state.

"The internet world is an extremely fluid one, with users exploring its possibilities of expression, introducing fresh combinations of elements and reacting to technological developments". (Crystal, 2002:14).

It seems to be in a permanent state of progression, lacking precedent, struggling for standards and searching for direction.
Additionally it is a social construction, through which citizens are expected to mingle, explore and communicate.

"The web is more a social creation than a technical one... And as the internet comes increasingly to be viewed from a social perspective, so the role of the language becomes central. Indeed, notwithstanding the remarkable technological achievements and the visual panache of screen presentation, what is immediately obvious when engaging in any of the internet's functions is its linguistic character. If the internet is a revolution therefore, it is likely to be a linguistic revolution". (Crystal, 2002 vii-viii).

Consequently, how can we as educators provide assistance and guidance to our students with regards the new technological demands? As already mentioned earlier, the mastering of the English language is a necessary, unquestionable prerequisite, if one is to gain full benefit from this technological diversity.
Additionally, assistance should be offered in areas such as writing, reading and talking to enable users of technology to take full advantage of what the new diversified world of technology has to offer, as well as, be able to successfully cope and deal with all this "newness" and technological development. However, these are huge

---

1 'Netspeak' = the term "netspeak" is an alternative to "netlish", "weblish", "internet language", "cyberspeak", "electronic language", "Interactive written discourse", "computer mediated communication" (CMC), and other terms. Each term has a different implication;"netlish", for example is plainly derived from English. (Crystal, 2002:17)

areas of discussion that need to be examined on their own merit in possible future publications. For the time being, what we need to do is to be awave of the new facts and to realize that we are on the threshold of a linquistic revolution by which we are inevitably affected directly both in our personal as well as professional capacity.

TABLE 1 – Language distribution on the web

(Crystal 2002:217).

Ranking	Language	Number of pages	Corrected percentage
1	English	2722	82.3
2	German	147	4.0
3	Japanese	101	1.6
4	French	59	1.5
5	Spanish	38	1.1
6	Swedish	35	0.6
7	Italian	31	0.8
8	Portuguese	21	0.7
9	Dutch	20	0.4
10	Norwegian	19	0.3
11	Finnish	14	0.3
12	Czech	11	0.3
13	Danish	9	0.3
14	Russian	8	0.1
15	Malay	4	0.1
	None or unknown (correction)		5.6
	TOTAL	3239	100

BIBLIOGRAPHY

Crystal, D. (2002) *Language and the Internet*, Cambridge University Press

Crystal, D. (2003) *English as a Global Language*, 2nd Edition, Cambridge University Press

Graddol, D. (2001) "English in the Future" chapter 2 in Burns, A. and Coffin, C. *Analysing English in a Global Context: A reader*,Routledge

Murray, D.E. (2001) "New Technology: New Language at Work?" chapter 3 in Burns, A. and Coffin, C. (eds.,) *Analysing English in a Global Context: A Reader*, Routledge

Snyder, I. (1998) *Page to Screen: Taking Literacy into the Electronic Era*, Snyder ILana (ed.,), Routledge

Stubbs, M. (1996) "English teaching, Information Technology and Language Awareness" chapter 8 in Fairclough, N. *Critical Language Awareness*, Longman

RETROFIT OF A CHURCH WITH LINEAR VISCOUS DAMPERS

Christis Z. Chrysostomou[1], Themos Demetriou[2], Michael Pittas[3] and Andreas Stassis[4]
[1] *Department of Civil Engineering, Higher Technical Institute, Nicosia, Cyprus*
[2] *Themos Demetriou and Associates, Nicosia, Cyprus*
[3] *Michael Pittas and Associates, Nicosia, Cyprus*
[4] *Department of Mechanical Engineering, Higher Technical Institute, Nicosia, Cyprus*

SUMMARY
The church of Agios Ioannis Prodromos in the village of Askas, Cyprus, contains a vast cycle of important and rare Byzantine wall paintings dating from the 15th and 16th centuries. Because of its importance to the cultural heritage of Cyprus, the church has been selected as one of the monuments to be studied in an INCO-MED project for the Conservation of Historical Mediterranean sites by innovative seismic-protection techniques (CHIME). The computational model developed for the church is presented, as well as the measurements obtained using hammer-impact excitation. The fine-tuning of the selected computational model to match the dynamic characteristics obtained from the site-measurements is also discussed. The model was used to test analytically the cost effectiveness of damping devices in providing the best earthquake-protection to the church without spoiling its monumental value.

1. INTRODUCTION

The Mediterranean region is an area of the world where many civilizations have flourished throughout the centuries. These civilizations left behind many monuments as evidence of their technological know-how and expertise. All countries that have the privilege to own such structures are interested in preserving and protecting them from natural disasters such as earthquakes. Unfortunately, the Mediterranean region is affected by earthquakes and many monuments have been destroyed because of them.
The conservation of ancient monuments presents many difficulties. Any intervention in their structural system should be such that it neither violates their form nor changes drastically their structural behavior. In addition, the materials to be used must be compatible with the ones the monument is constructed. Traditional seismic retrofitting techniques, such as reinforced concrete shear-walls and steel rigid frames, have the disadvantage that violate the above conditions. An alternative to the above is the use of innovative seismic-protection techniques, such as passive or semi-active energy dissipation systems. Such systems can be very inconspicuous and therefore not violating the form of the monuments and at the same time can be very effective in dissipating the energy generated by earthquakes and hence protect the monuments.
Several researchers have studied the behavior of viscous dampers ([1] to [7]) and shape memory alloy damping devices ([8] to [11]). Most of the applications that appear in the literature concern modern structures and only a few are applied to monuments ([12] and [13]).
Such techniques were evaluated within the INCO-MED project, "Conservation of Historical Mediterranean Sites by Innovative Seismic-Protection Techniques," CHIME. The partners in this project come from Italy, Greece, Cyprus, Egypt and Tunisia. In this paper the monument selected in Cyprus is presented along with a system identification study, which includes measurements and a computational model. The model was used as the basis to investigate the effectiveness of linear viscous dampers in protecting the monument from future catastrophic earthquakes.

2. DESCRIPTION OF THE MONUMENT

The church of Agios Ioannis Prodromos in the village of Askas, Cyprus, contains a vast cycle of important and rare Byzantine wall paintings dating from the 15th and 16th centuries.
Robert Gowing et al. from the Courtauld Institute Conservation of Wall Painting Department performed an exploration to clarify the various construction phases of the church. According to Gowing's report [14], the earliest building phase appears to consist primarily of a large semi-domed apse and the surrounding east wall. Dating of this section of the church is not assisted by any specific architectural features. In this instance, the painted decoration provides the only clue with a proposed date, based on stylistic examination, of around the middle of the 16th century.
Gowing reports that extensive rebuilding appears to have occurred, around the beginning of the 17th century, involving the complete enlargement of the body of the church. Constructed as a three-aisled basilica plan church, the design accommodated the original apse and east wall, retaining their painted decoration.
The third phase that was noted by Gowing is dated to 1952. This involved the raising of the outer walls to increase the height of the aisles. The exterior changes are visible on the south and east walls with a noticeable change in the construction type. The new roof is noticeably lower in pitch as a result of maintaining the old peak height and the increased outer walls.
The main reasons for selecting this monument are:

- the church is a relatively small structure and therefore the innovative methods that will be developed in this project can be more easily applied,
- this is a church that both the Department of Antiquities and the Archbishopric of Cyprus have already spent a great amount of resources in trying to preserve the paintings, which are considered to be rare late Byzantine,
- the Department of Antiquities of Cyprus will continue the preservation of the church in the following years, based on the suggestions of the Gowing report, and therefore the protective devices that will be installed within the present project, will be part of the preservation, and
- despite the fact that the village of Askas is in the mountainous earthquake zone, which is considered to be of low seismicity according to the present zoning, recent earthquakes have caused considerable damage to build-

ings in this zone. The previous belief was based on historic earthquake data and the absence of historic earthquakes in the region may be due to the fact that this area was uninhabited.

3. METHODOLOGY

The retrofitting of structures, and in particular monuments, requires a careful planning of all the steps that will be followed. Such a methodology is proposed below and it is then applied to the case study building:

- First the earthquake hazard in the area of the monument should be identified. Unless the hazard for the region is well documented, there will be a requirement for on site measurements to establish the dynamic characteristics of the soil and the expected site-specific ground accelerations.
- A system identification should be performed in order to establish the dynamic characteristics of the structure. This should include on-site measurements to obtain the frequencies, mode shapes and damping of the structure, followed by the development of a computational model, which should be updated using the measurements, so as to have an as close to reality model as possible.
- Alternative retrofit schemes should then be selected and evaluated, having in mind the safety of the monument and in particular being sensitive in proposing non-intrusive, reversible solutions.
- Finally, the cost-effectiveness of the selected retrofit scheme should be established.

In the following sections the above methodology was applied to the Church of Agios Ioannis Prodromos. It should be noted that one of the main goals of this research was to examine the cost effectiveness of the proposed retrofit scheme, therefore a considerable effort was put in this direction, which is described in detail in the last part of this section.

3.1 Collection of historical and instrumental data on the seismicity of Cyprus

In order to be able to perform a vulnerability and hazard analysis, a number of data has to be collected. The first step in such an analysis is to identify the sources of earthquakes that affect the area under study and obtain their expected magnitudes and recurrence period.

To achieve the above, a literature review was performed to obtain both historic and instrumental data, which are listed below:

- The first list consists of the historic earthquakes (26 BC to 1900 AD) and the ones obtained by instrument recordings (1900 AD to date). The historic earthquakes were obtained from the paper by Ambraseys N.N. [15]. The list from 13 Jan 1894 to 21 Feb 1991 was again obtained from a report by Ambraseys N.N. [16]. The data from 5 Jun 1991 to 7 Aug 1993 were obtained from ISS/ISC reports.
- The second list consists of 145 records of shallow depth earthquakes and the third one includes 50 records of intermediate depth earthquakes. Both lists of earthquakes are reported by Papazachos et al [17].
- The fourth list of 279 records for the period 1 Apr 1997 to 6 Sep 2000 was obtained from the Geological Survey Department of Cyprus.
- Finally, the fifth list of 449 records for the period 28 Apr 1974 to 3 Sep 2000 was obtained from the NEIC of the US geological survey department for a radius of 200 km with center 34o 56' N and 33o 05' E, which corresponds to the location of Askas Village. The search page of NEIC from which the catalogue was formed is http://wwwneic.cr.usgs.gov/neis/epic/epic_circ.html.

3.2 System identification

3.2.1 Measurements

In order to obtain the periods of vibration of the church so as to be able to update the computational model, the Kinemetrics Model VSS-3000 Vibration Survey System was used, together with a triaxial EpiSensor force balance accelerometer (model FBA ES-T). The EpiSensor has user-selectable full-scale recording ranges of ±4g, ±2g, ±1g, ±1/2g or ±1/4g and a bandwidth of DC to 200 Hz. For this research the scale was set to ±1/4g and a sampling rate of 1000 points per second was used.

The EpiSensor was positioned at four different locations on the church indicated with numbers 1 to 4 (see Figure 1), and a rubber impact hammer was used to induce vibrations in the church. Six different impact locations were used indicated in Figure 1 with letters A to F.

The results of the measurements are shown in Table1. The frequencies of vibration obtained from a Fast Fourier Transform (FFT) analysis of the acceleration records for the various positions of the EpiSensor and the different directions of excitation are summarized in the table. Figures 2 and 3 show the FFT for cases 1XA and 1YB, respectively. It should be noted that each Figure represents a superposition of the blocks analyzed.

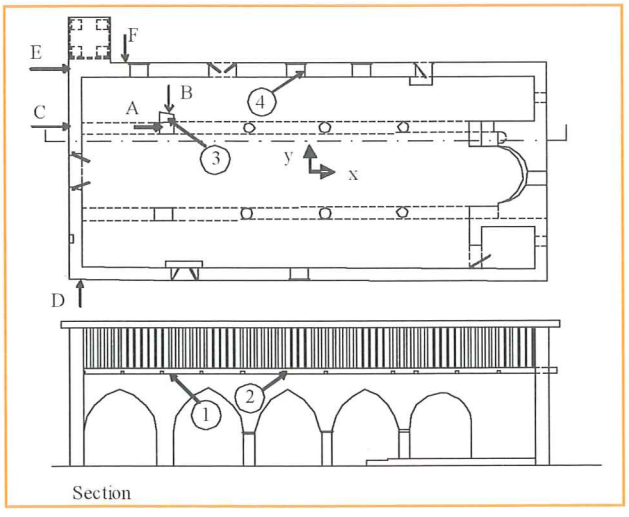

Figure 1. Location of instrument and excitation.

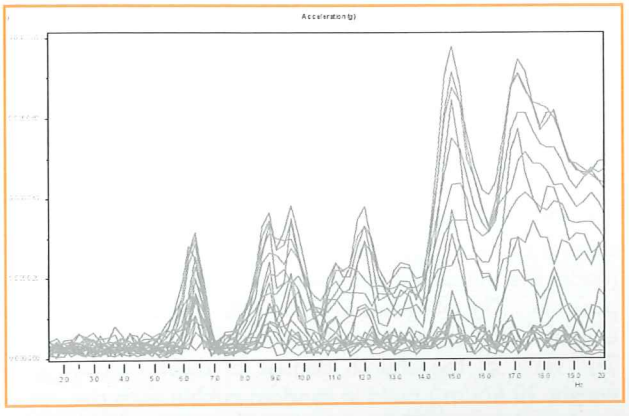

Figure 2. FFT for position 1XA

TABLE 1. Measured frequencies of vibration of church

		Frequency (Hz)					
Position	Direction	A	B	C	D	E	F
1	x	6.4, 8.8, 9.5, 11.0, 12.0	Inconcl.	6.4, 8.8, 9.5, 11.0, 12.0	6.1, 9.0 -		
	y	9, 14.5	4.4, 5.8, 7.6, 9.0, 11.8	7.6, 5.8, 9.0	4.4, 5.8, 7.6, 9.0, 11.0		
2	x	6.4, 8.8, 9.5, 12.0	12.0	6.4, 9.5, 11.0, 12.0	4.4, 6.4, 8.8, 9.5		
	y	4.4, 5.8, 7.6, 9.0, 12.0, 14.5	4.4, 7.6, 9.0, 11.8, 14.5	4.4, 7.6, 9.5, 13.0	4.4, 5.8, 7.6, 9.0, 11.0		
3	x			6.4, 9.5, 11.0, 12.0	9.5		
	y			Inconcl.	7.6, 9.0		
4	x	Inconcl.	Inconcl.	Inconcl.	Inconcl.	Inconcl.	Inconcl.
	y	Inconcl.	Inconcl.	Inconcl.	Inconcl.	Inconcl.	4.2, 7.5, 10.0, 12.1

Inconcl. means inconclusive results

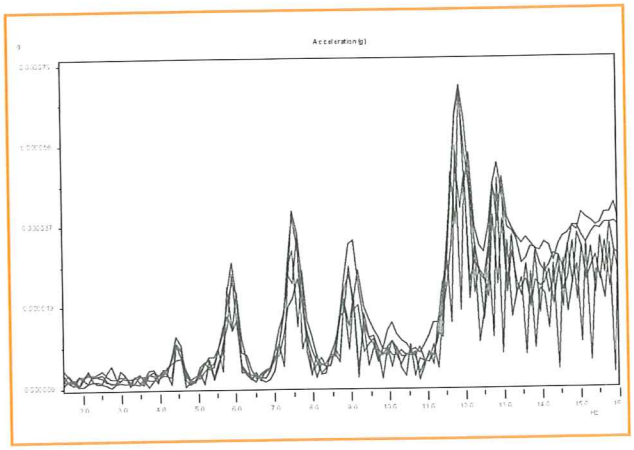

Figure 3. FFT for position 1YB

From the results it is clear that the first five dominant frequencies arranged in increasing order of magnitude are: 4.4 Hz, 5.8 Hz, 6.4 Hz, 7.6 Hz, and 8.8 Hz. The corresponding periods in decreasing order of magnitude are: 0.23 sec, 0.17 sec, 0.16 sec, 0.13 sec, and 0.11 sec. It should be noted that, as expected, these values appear consistently irrespective of the location of the instrument or the direction and position of the excitation.

3.2.2 Computational model

Following the measurements on the church and the establishment of the first few periods of the structure, several computational models where developed so as to model the measured behavior of the church as closely as possible. The program SAP2000NL was used with shell elements and beam-column elements.

The walls of the church consist of diabase stone (unit weight 30 kN/m^3) build in random rubble with the use of mud, and brick gallets, which are used to fill the gaps between the large stones and to complete the horizontal string line of each bed joint (see Figure 4). The modeling of such a construction presents many problems especially in establishing the modulus of elasticity of the matrix. The methodology used in this research was to vary the modulus of elasticity of the shell elements representing the wall until the periods calculated by the eigenvalue analysis matched, as closely as possible, the measured ones. An original modulus of elasticity of 2 kN/mm^2 was used for a trial analysis and the final modulus of the updated finite element model was 1.84 kN/mm^2.

The church has two roofs, as explained in section 2, made out of wood and covered with clay tiles. A modulus of elasticity of 5.8 kN/mm^2 and a unit weight of 3.6 kN/m3 were used for the elements representing the wooden sections. The weight of the clay tiles was considered to be 0.75 kN/m^2.

Two models were developed for the church. The difference between the two models was the modeling of the roof. In the first one the roof was modeled by shell elements while in the second by beam elements. On examining the modes of vibration of the first model, it was observed that most of the modes were concentrating on the roof and there was very little movement of the walls of the church. This was mainly due to the large difference in the flexibility of the roof relative to that of the walls. This was considered to be an invalid model and a second one was developed.

In the second model all the beams, rafters and purlins of the roof where modeled using beam elements. Strong-axis moment releases were applied on the ends of the beams since this was considered to represent more accurately the actual connection of the beams to the main rafter, the external walls, and the arches within the church. The eigenvalue analysis of this model resulted in the mode shapes shown in Figure 5 and the following periods of vibration: 0.21 sec, 0.17 sec, 0.15 sec, 0.13 sec and 0.11 sec.

Figure 4. Rubble stone construction of the wall of the church.

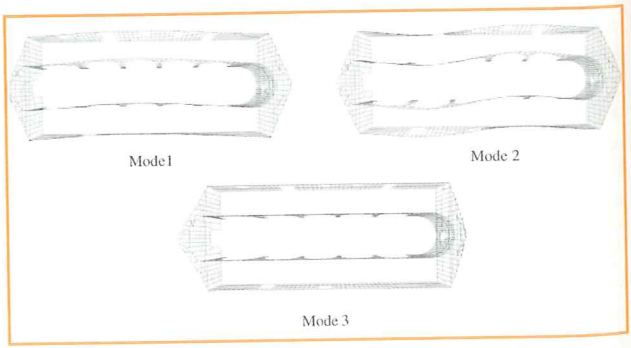

Figure 5. First three modes of vibration of the church.

The first and second modes are translational modes in the transverse direction of the church, and the third one a translational mode in its longitudinal direction. This is confirmed by the experimental results in which the first two frequencies of vibration are in the transverse direction and the third one in the longitudinal direction. The measured and computed periods obtained are compared in Figure 6. The close agreement between the calculated and the measured periods of vibration should be noted.

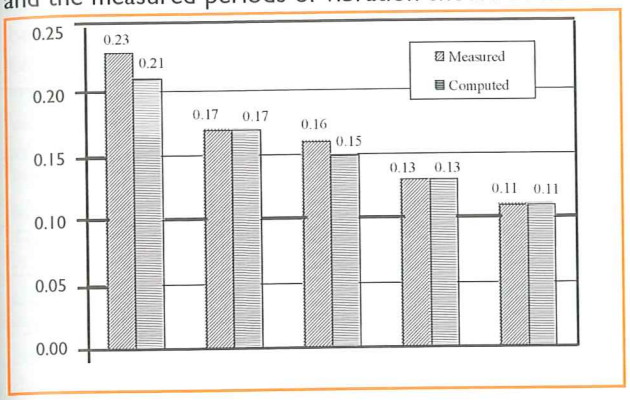

Figure 6. Comparison between computed and measured natural periods

3.3. Damping devices

3.3.1 Modeling of dampers

In order to study the effects of dampers on the response of the church, it was decided to use time history analysis, and to monitor the interstorey drift of crucial locations. Since this is a monument with very sensitive paintings it was decided to use an interstorey drift of 0.1% as the limit of acceptability of the results. The question was then raised as to whether this limit should be applied to the Design Basis Earthquake (DBE) or to the Maximum Considered Earthquake (MCE, which is obtained by multiplying the ground acceleration of DBE by 1.5). It was decided to study both cases and make the final decision by comparing the results of the two cases. In the absence of an earthquake record in Cyprus, it was decided to use a record from the 1999 Athens earthquake (Metro, 90Φ) which was scaled to a peak ground acceleration of 0.15g (for the DBE). The same record was used in both horizontal directions in the analysis.

The location of the dampers was a second parameter that had to be studied. In SAP2000 linear and nonlinear dampers can be modeled. It was decided to try linear dampers the behavior of which is governed by the equation

$$f = c\dot{d} \qquad (1)$$

where f is the damper force, c the damping coefficient and $\dot{d}$ the deformation rate across the damper. Based on the above equation the effectiveness of the damper is a function of the deformation rate. Therefore, the dampers should be located between points which will provide the largest possible deformation rates.

In order to find these locations and the ones at which the maximum displacements occurred, the church without any damping devices was analyzed for both the DBE and MCE case. This is CASE1 and it formed the basis for the comparison with the analyses when dampers were introduced. From the results it was observed that nodes 147 and 291 produced the largest displacements in the x (longitudinal) and y (transverse) directions of the church, respectively, therefore it was decided that these two nodes were going to be monitored for all the analyses and checked against the interstorey drift limit of 0.1% (Figure 7). In addition, the base shear in the x and y directions as well as the damper force was noted.

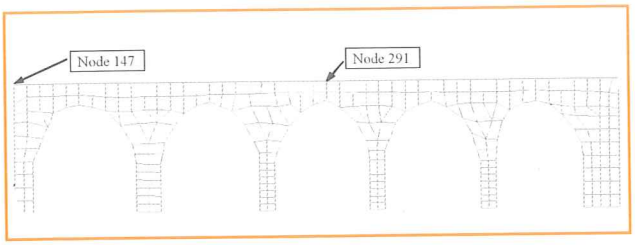

Figure 7. Position of control nodes and dampers for CASES 2 and 3

Two alternative positions of the dampers were checked. In the first, the dampers were placed on the top of the arches in such a way that the total horizontal displacement and velocity of the top of the arch relative to the bottom of the arch, which is the maximum possible, caused the response of the dampers (CASES 2 and 3, Figure 7). Since this methodology requires some engineering ingenuity to be achieved without intruding into the monument, a second one was also examined, which required a much larger number of dampers. In the second one, the inner and outer walls were connected with dampers, which will be out of sight and hidden into the roof of the monument (CASES 4 and 5, Figure 8). In the first alternative 20 dampers with the same properties were used, while in the second 96, of which 46 had properties named NLLINK1 and the rest 50 had properties named NLLINK2 (Fig. 8, Table 2).

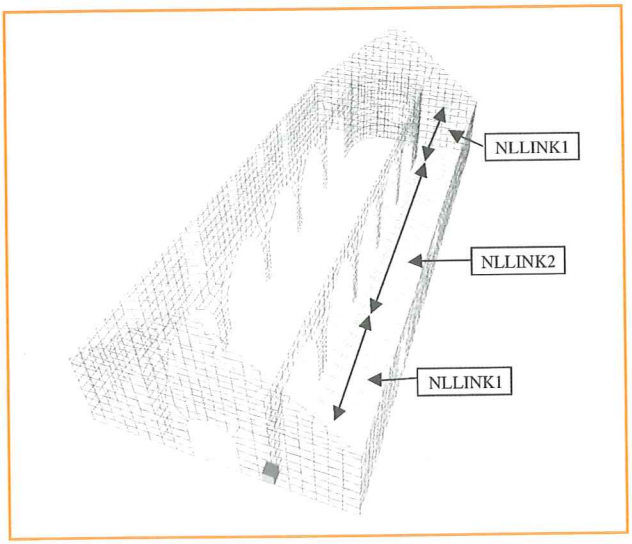

Figure 8. Position of control nodes and dampers for CASES 4 and 5

Table 2. Damper properties

Case	Effective damping (kN s/mm)
CASE2	0.060
CASE3	0.115
CASE4	
NLLINK1	0.060
NLLINK2	0.130
CASE5	
NLLINK1	0.150
NLLINK2	0.200

3.3.2 Results

Two analyses were performed for each alternative. In the first one the damper properties were varied until the inter-storey drift of the control node was below the 0.1% limit for the DBE earthquake (CASE2 and CASE4), while in the second the damper properties were changed until the imposed limit was satisfied for the MCE earthquake (CASE3 and CASE5). It should be noted that no stiffness was used for the damper, so as to behave as a damping device only. This was checked in the model and indeed there was no additional stiffness introduced since the periods of vibration of the structure remained the same as in CASE1.

The results of CASE1 have shown that the displacements in the x-direction were below the required limit for both the DBE and the MCE excitation, therefore no dampers were introduced in the longitudinal direction.

The results for the DBE and the MCE analyses are shown in Tables 3 and 4, along with the calculated interstorey drift. The height of the arches is 3970 mm and it was used to calculate the interstorey drifts.

Table 3. Maximum absolute values of selected for the DBE analysis

Case	Base shear x(kN)	Base shear y(kN)	Displac. x(mm)	Displac. y (mm)	Damping Force (kN)	Interst Drift (%)
CASE1	603	866	1.65	8.85	-	0.22
CASE2	603	498	1.65	4.02	5.2	0.10
CASE3	603	396	1.64	2.68	6.7	0.07
CASE4	593	456	1.59	4.04	2.2	0.10
CASE5	581	372	1.55	2.72	2.3	0.07

Table 4. Maximum absolute values of selected for the MCE analysis

Case	Base shear x (kN)	Base shear y (kN)	Displac. x (mm)	Displac. y (mm)	Damping Force (kN)	Interst Drift (%)
CASE1	904	1299	2.47	13.27	-	0.33
CASE2	904	747	2.47	6.03	7.8	0.15
CASE3	904	548	2.46	4.02	10.0	0.10
CASE4	889	684	2.39	6.07	3.3	0.15
CASE5	872	557	2.32	4.07	3.4	0.10

On examining the results in Tables 3 and 4 the following observations can be made:

- The base shear in the x-direction remains the same in all the analyses since there are no dampers introduced in that direction. On the other hand the introduction of dampers in the y-direction has as an effect the reduction of the DBE base shear in the range of 42% to 54% for the first alternative and in the range of 47% to 57% for the second alternative. For the MCE analysis the ranges of reduction are 42% to 57% and 47% to 57% for the first and second alternatives respectively.
- As it was mentioned before the displacement in the x-direction does not exceed the interstorey drift limit and therefore there is no need for the introduction of dampers.
- It is interesting to note that all the values of Table 4 can be obtained by multiplying the values of Table 3 by 1.5 which is the scaling between DBE and MCE.
- The response of the dampers for CASES 2 and 3 are shown in Figures 9 to 12.

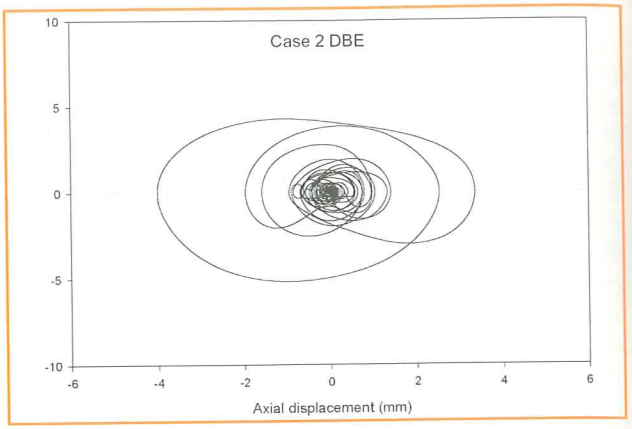

Figure 9 Force-displacement for a damper CASE 2 DBE

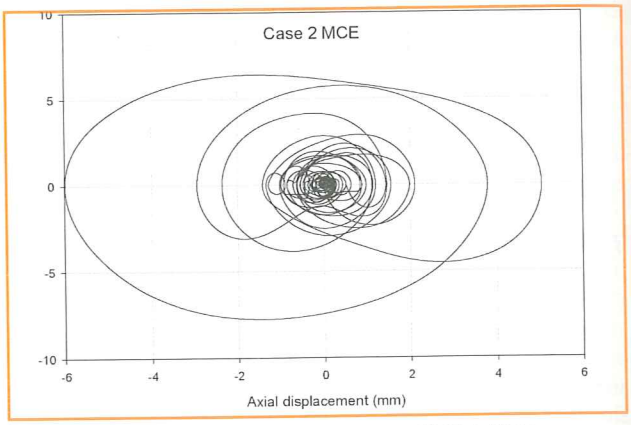

Figure 10 Force-displacement for a damper CASE 2 MCE

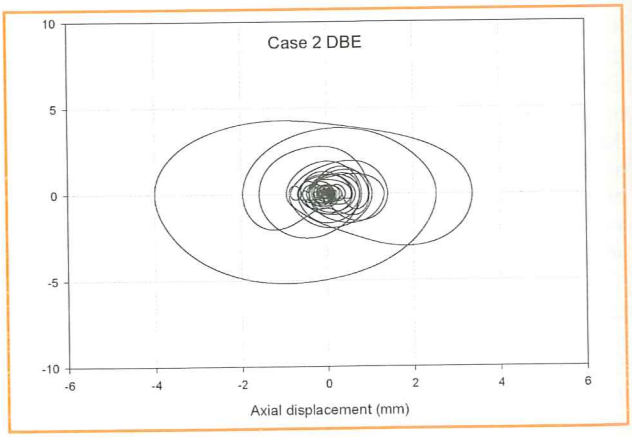

Figure 11 Force-displacement for a damper CASE 3 DBE

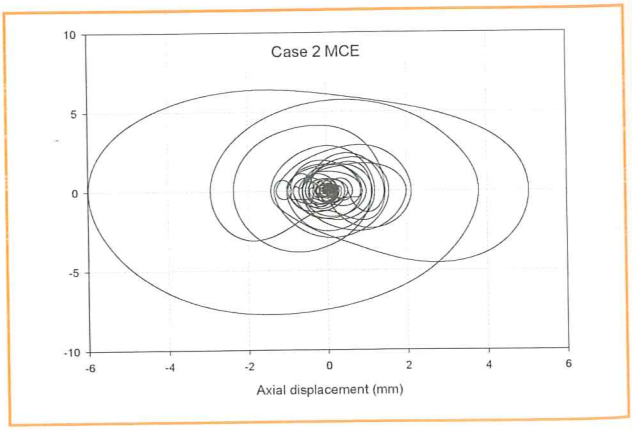

Figure 12 Force-displacement for a damper CASE 3 MCE

3.4 Cost-benefit analysis

The effectiveness of the two damper arrangements can now be examined. The first, which uses considerably fewer dampers with smaller damping coefficients, is more efficient provided a method is found to support the dampers in such a way that the relative movement of their end-points will be equal to the movement of the top of the arches relative to the ground. Such a solution could be a horizontal member, which will be supported on the two ends of the arches (where the lateral motion is small), or to vertical members positioned to places that would not interfere with the monument, and will be used as the reaction to the dampers. Since the forces from the dampers are relatively small such a solution might be feasible.
The second arrangement connects the inner walls with the outer walls. Since the outer wall is much stiffer and shorter than the inner walls, the dampers will lessen the forces transferred from the latter to the former with considerable dissipation of energy. The larger number of dampers involved can provide the extra effectiveness required. At the same time the incorporation of the dampers into the structure is much easier than the first case and the interference with the aesthetics of the monument. Since this arrangement is much more likely to be acceptable to the Antiquities Department, it was used in the cost effectiveness assessment.
It is most useful for a monument to make the analysis for the case of Maximum Considered Earthquake, with a 0.1% limit for the inter-storey drift. Thus the comparisons are made for Cases 1 and 5. For these cases the results show base shear values in the two directions:

V_{x1}=904kN V_{x5}=872kN (a reduction of 3.5%)
V_{y1}=1299kN V_{y5}=557kN (a reduction of 57%)

The displacement results are:

d_{x1}=1.65mm d_{x5}=1.55mm (a reduction of 6%)
d_{y1}=13.27mm d_{y5}=4.07mm (a reduction of 69%)

Since the x-direction results were satisfactory without any dampers, no provision for dampers in that direction was made. Thus the small reductions in base shear and displacement are only a by-product of the introduction of dumpers in the y-direction and were expected to be modest.
In the y-direction the reductions are considerable. Both the wall strength required and the movement of the arches are less than half of the original configuration. This more than doubles the resistance of the monument to earthquake forces.

3.4.1 Damper cost
Off-the-shelf damping devices were selected that could be easily attached to the rafters of the roof. Their cost is of the order of $100 or less, thus making feasible their use in the large number required for their application as considered above.
The total cost for the 96 dampers required will thus be of the order of $10 000 or less. This cost is not prohibitive. However, if the attempt is made to retrofit the monument, considerable expense will be required to modify the rafter supports in order to incorporate the dampers. This could prove to be as expensive as the purchase of the dampers if not more. Although $20 000 or even more is probably worth spending in order to protect a structure of such historic value, it would be necessary to prove that the risk of serious damage due to earthquakes is considerable before such an expense is justified. Further, the intrusion into the monument itself would be justified only if the danger is high enough. In the case of the church at Askas, this is probably not the case.
However, in the case of a more extensive restoration the opportunity will arise to incorporate the damper protection into the restoration works. In such a situation, the additional cost of innovative protection would be solely the cost of the dampers, since all other expenses will be incurred in any case.
The cost of such a traditional restoration is expected to be of the order of $100 000. Comparing the cost of the dampers to the total cost of restoration, the extra expense seems justified. In fact, at less than 10% of the total cost the extra protection is considerable. Thus, while retrofitting by itself may not be a cost effective operation, if combined with a more general restoration it is worth applying.

3.4.2 Possible refinements of protection techniques
In the above example a simple linear viscous damper device was chosen. This device has the advantage of being off-the-shelf thus minimizing the expense for a one-off job. It is also easy to model since it offers only linear damping without stiffness. Nevertheless, there is no reason why these characteristics should limit possible device choices. A much simpler yield-device could also provide similar protection and, provided enough demand could make mass production possible, be much cheaper. Reliable devices of this sort could slash the cost to just a fraction of the devices considered above. More exotic shape-memory alloys could also provide enhanced protection. Research in these directions seems promising.

4. CONCLUSIONS

In this research project the possibility of applying innovative protection techniques, such as linear viscous dampers, to monuments was investigated. The monument chosen as a testing ground for these techniques in Cyprus was the church of Ayios Ioannis Prodromos at Askas village.
A methodology is proposed for the retrofit of monuments. Based on the first phase of this methodology general data about the seismic hazard of the area were collected and an estimate of the seismic forces was made. These estimates were used to select the seismic input used in the analysis. Building characteristics were then collected. A survey of the building was made and drawings were produced showing the geometric characteristics. A detailed measurement of its dynamic characteristics was made using a Kinemetrics VSS-3000 vibration survey system.
The measurements were used to update a finite element computer model to analyze the building response to earthquake forces. Excessive deflections and high base shears were estimated to occur in the transverse direction necessitating the introduction of protective measures. Linear viscous dampers were introduced into the model which resulted in significant reductions in both seismic forces and deflections.
The cost of the dampers is estimated at less than $10 000

for the 96 devices used in the analysis. If a simple retrofit is carried out on the building, the cost of the operation could easily rise to double that amount to include the modification on the rafters needed to fix the dampers. This seems excessive and can only be justified in areas of very high seismic hazard.

However, in the case of an extensive restoration of the church, which involves a number of major operations including the removal of the upper roof and restoration of the lower, this gives the opportunity to introduce the dampers with virtually no additional cost except the actual cost of the dampers. As the estimated cost of restoration is of the order of $100 000, the additional protection cost will be approximately 10%. This is a reasonable cost for the added protection.

Off-the-shelf dampers were used but custom-made cheaper devices could slash the cost to a fraction of the one quoted above. If produced on a mass scale, such devices could provide a very cost effective way of protecting monuments of this type. Research in this area could concentrate on simple yield-type devices and more exotic shape-memory alloys.

ACKNOWLEDGEMENTS

The authors acknowledge the financial contribution of the European Commission through the project CHIME (Conservation of HIstorical MEditerranean Sites by Innovative Seimic-Protection Techniques). The authors are also thankful to Professor Fabio Casciati, coordinator of the project.

REFERENCES

1. Constantinou, M.C. and Sigaher, N.. Energy Dissipation System Configurations for Improved Performance, Proceedings of the 2000 Structures Congress & Exposition, ASCE, Philadelphia, PA, 2000.
2. Constantinou, M.C. and Symans, M.D. Experimental and Analytical Investigation of Structures with Supplemental Fluid Viscous Dampers, Technical Report NCEER-92-0032, National Center for Earthquake Engineering Research, University at Buffalo, State University of New York, Buffalo, N.Y., 1992.
3. Constantinou, M.C., Soong, T.T. and Dargush, G.F. Passive Energy Dissipation Systems for Structural Design and Retrofit, Monograph Series No.1, Multidisciplinary Center for Earthquake Engineering Research, University at Buffalo, State University of New York at Buffalo, Buffalo, N.Y., 1998.
4. Pekhan, G., Mander J.B., and Chen S.S. Design and Retrofit Methodology for Buildings Structures with Supplemental Energy Dissipating Systems, Technical Report MCEER-99-0021, Multidisciplinary Center for Earthquake Engineering Research, University at Buffalo, State University of New York, Buffalo, N.Y., 1999.
5. Reinhorn, A.M., Li, C., and Constantinou, M.C. Experimental and Analytical Investigation of Seismic Retrofit of Structures with Supplemental Damping Part I: Fluid Viscous Damping Devices, Technical Report NCEER-95-0001, National Center for Earthquake Engineering Research, University at Buffalo, State University of New York, Buffalo, N.Y., 1995.
6. Seleemah, A.A., and Constantinou, M.C. Investigation of Seismic Response of Buildings with Linear and Nonlinear Fluid Viscous Dampers, Technical Report NCEER-97-004, National Center for Earthquake Engineering Research, University at Buffalo, State University of New York, Buffalo, N.Y., 1997.
7. Soong, T.T. and Dargush, G.F. Passive Energy Dissipation Systems in Structural Engineering, John Wiley & Sons Ltd., London (UK) and New York (USA), 1997.
8. Faravelli L. and Casciati S.. Dynamic Behavior of Shape Memory Alloy Structural Devices: Numerical and Experimental Investigation, Proc. IUTAM Symposium, Yonezawa, Japan, 2002.
9. Faravelli, L. Experimental Approach to the Dynamic Behavior of SMA in Their Martensitic Phase, F. Casciati (ed.), Proceedings 3rd World Conference on Structural Control, vol.2, 163 -168, John Wiley & Sons, Chichester, UK, 2003.
10. McKelvey A.C. and Ritchie R.O. On the Temperature Dependence of the Superelastic Strength and the Prediction of the Theoretical Uniaxial Transformation Strain in Nitinol, Philosophical Magazine A, Vol. 80 (8), 1759-1768, 2000.
11. Castellano, M.G.. Development and experimental characterisation of shape memory alloy devices, Proc. Final Workshop of ISTECH Project – Shape Memory Alloy Devices for Seismic Protection of Cultural Heritage Structures, 23 June, Joint Research Centre, Ispra, Italy, 11-19, 2000.
12. Biritognolo, M., Bonci, A., and Viskovic, A., Numerical models of masonry façade walls with and without SMADs, Proc. Final Workshop of ISTECH Project – Shape Memory Alloy Devices for Seismic Protection of Cultural Heritage Structures, 23 June, Joint Research Centre, Ispra, Italy, 117-140, 2000.
13. Croci, G., General methodology for the structural restoration of historic buildings: the cases of the Tower of Pisa and the Basilica of Assisi, Journal of Cultural Heritage, 1, 7–18, 2000.
14. Gowing R. et al. The church of Ayios Ioannis Prodromos, Askas, Cyprus, Report, Conservation of Wall Painting Department, Courtauld Institute of Art, University of London.
15. Ambraseys NN. The seismic history of Cyprus, Revenue Union Intern. Secours, Geneva; 3: 25-48, 1965.
16. Ambraseys NN. The seismicity of Cyprus. ESEE Research Report, Engineering Seismology No. 92/9, 1992.
17. Papazachos BC and Papaioannou ChA. Lithospheric boundaries and plate motions in the Cyprus area. Tectonophysics, 308: 193-204, 1999.

MARTE PROJECT : TELE-ECHOGRAPHY BETWEEN KYPEROUNTA AND NICOSIA (CYPRUS)

Sotos Voskarides[1,4], Sotiris Avgousti[1], Marios Kassinopoulos[1], George Florides[1], Costas Pattichis[2], Chrysa Tziakouri[3] & Marios Hadjinicolaou[4]
[1] Higher Technical Institute, P.O.B. 20423, Nicosia, 2152, Cyprus, [2] University of Cyprus, Kallipoleos 75, 1071, Nicosia, Cyprus, [3] Nicosia General Hospital, Nechrou Ave. 1102, Nicosia, Cyprus, [4] Brunel University, Uxbridge, Middlesex UB8 3PH, London, UK
{svoskarides, savgousti, mkassinopoulos, gflorides} @hti.ac.cy, pattichi@cs.ucy.ac.cy, kythreas@cytanet.com.cy, marios.hadjinicolaou@brunel.ac.uk
Arnaud Capri[5], Pierre Vieyres[5], Gerard Poisson[5], Arbeille Philippe[6], Natalie Smith-Guerin[5], Aïcha Fonte[5], Gilles Mourioux[5], Laurence Josserand[5] & Cyril Novales[5]
[5] Laboratoire Vision & Robotique, 63 av. de Lattre de Tassigny, F-18020 Bourges, [6] Dpt Méd. Nucléaire et Ultrasons, CHU Hopital Trousseau, F-37044 Tours
{Firstname.Name}@bourges.univ-orleans.fr

Abstract: Ultrasound experts, who are few and not always on hand when needed, have now the tool and the possibility to examine patients from a distance, and thus perform a complete diagnosis without being in the same geographical position with the patient. This is possible thanks to a telemedicine system aiming to provide the possibility to examine a remote patient using a tele-operated controlled robot. In the frame of this project, different validations have been performed to show the technical performances of the teleoperated chain and the repercussions on the clinical aspect. The clinical validation is the crucial part for the validation of the overall concept of tele-echography. Thus, various specialities were investigated all throughout the project life, with the participation of different medical experts from several countries, namely France, Spain and Cyprus.

Keywords: robot, teleoperation, telecontrol, telerobotics, ISDN, ethernet, satellite.

1. INTRODUCTION

Ultrasound examinations are only performed by well-trained specialists in main clinical centres such as public hospitals, private centres, etc. Studies have demonstrated the potential use of echography or ultrasound scan to perform a quick and efficient diagnosis for many types of pathologies. Unfortunately, ultrasound experts are few and not always on hand when needed.

For the last decade many small hospitals are closing and thus the need for patients to move long distances to reach the nearest regional hospital is increasing. In front of this need, the Laboratory of Vision and Robotics – LVR – works on the proposal of having a complete device to be available to ultrasound medical experts, so as to perform an examination on patients in another hospital situated far away from the expert site. Specific tele-echography projects have been realised since 1995 in LVR as described in Figure 1. The first prototype of a probe holder robot was designed and constructed in 1998. Two years later the second prototype – TERESA – (Vieyres, et al., 2003) evolved in collaboration with the European Space Agency – ESA– (Vilchis, et al., 2001) and from 2002 to 2004 two models of the most recent prototype were designed and realized, under the EU - funded project OTELO (OTELO Consortium, 2002). In order to validate the usefulness of the whole system in the case of patients situated in isolated areas, certain technical and clinical experiments were designed and performed.

The MARTE project is a new research collaboration between several Cypriot and French Institutions on robotized tele-echography: Tours University Hospital, SINTERS Group, University of Orleans, Nicosia General Hospital, Higher Technical Institute, University of Cyprus and the Cyprus Telecommunications Authority (CYTA).

Fig.1. Tele-echography projects in LVR

Three objectives have been set within the MARTE project:

a- Performance of clinical tests within Cyprus between two sites, which were identified by the local medical experts: Nicosia General Hospital, which is situated in the central valley of the country, and a small rural hospital on the Troodos mountains, in the village of Kyperounta, 75 km away.
b- Validation tests within a moving vehicle for emergency purpose (ambulance, Emergency unit vehicle).
c- Validation tests within a moving vessel for emergency purpose (cruise or military ship).

The communication links for a-test were designed to be ISDN and Ethernet Connection, UMTS for the b-test and satellite channels for c-test. This paper presents the Marte experiments performed between Nicosia and Kyperounta hospitals.

2. TELE-ECHOGRAPHY SYSTEM

The tele-echography chain developed in LVR consists of 3 parts, as shown in Figure 2. A medical expert moves a fictive ultrasound probe like he would do in a standard echographic examination, in his office. The instantaneous motion of the fictive probe is converted into an electronic signal which is sent, via a communication link, to the site where the patient is. The expert performs normally his examination by moving the fictive probe as if it was in conduct with the patient and performs a diagnosis thanks to the ultrasound images that he receives from the patient site (acquired by a real ultrasound probe). The patient site is equipped with an ultrasound device and a probe holder robot. The light weight robot is held in position by a paramedic. The robot reproduces the motions made by the distant expert (Pierrot, et al., 1999).

The ultrasound device acquires the images to be sent to the expert site. Different data are exchanged between the two sites via a communication link which can be a fixed connection (e.g. ISDN or Ethernet) or a wireless connection (e.g. satellite or UMTS channels).

With such a service, when the patient is at home or remote area, the paramedic or local doctor can be in

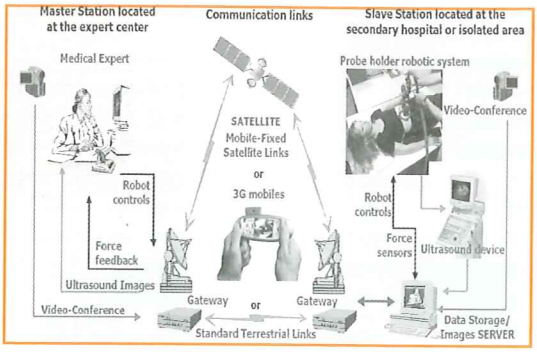

Fig. 2. Tele-echography chain

complete interaction with the expert and can request disease-specific information (Smith-Guerin, et al., 2003). The service is also important for a second opinion diagnosis that can be provided from another distant expert centre.

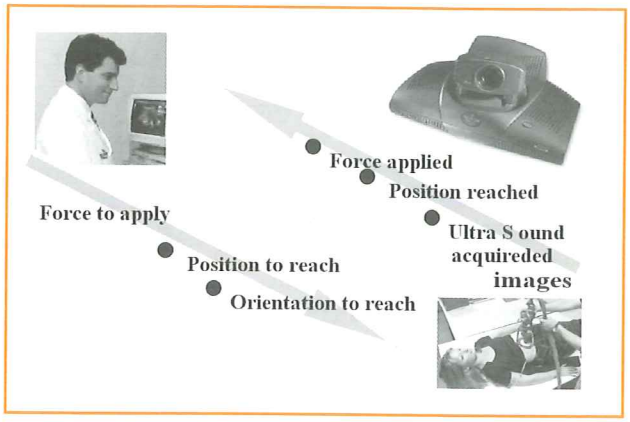

Fig. 3. Tele-echography communication links

The expert receives the patient's ultrasound image, the current robot position/orientation, the measured reaction force as well as the ambient image and sound from the patient site. On the other hand the probe holder robot receives the signal produced by the analogous motion of the fictive probe performed by the expert. This signal specifies the position and the orientation to be reached by the real probe and also the intended (by the expert) force to be applied on the patient. The paramedic or the doctor on the patient site also receives the ambient image and sound from the expert site. The tele-echography chain works as classical master-slave robotic system: the expert site, which controls the distant probe holder robot, is the master station and the patient site, where the robot is located, is the slave station (Poisson et. al 1999).

3. NICOSIA – KYPEROUNTA EXPERIMENT

The results of the clinical validation tests which were performed in Corporaci½ Sanitaria Clinic in Barcelona gave a good guidance and reference for the tests which followed in Cyprus. Tables 1 and 2 show these results (OTELO clinical validation, 2004).

3.1 Patient examination and methods

Table 1 Results of clinical tests performed in Corporació Sanitaria Clinic (Barcelona)

Complete Abdominal Exam of 32 Cases Categorisation of Channels		No of Cases
Volunteer/ Patient	- Volunteer	16
	- Patient	16
Connection	- ISDN(384 Kbs)	22
	- Satellite (284 kbs)	10
Echographic Device	- Tringa	14
	- Toshiba Just-vision	12
	- Toshiba SAL 140D	6
Other Findings	- Acute diverticulitis	1
	- Ascites	2
	- Intra Uterine Device	2
	- Portal tumoral trombosis	1
	- Portal fibrosis	1
Causes of Dis-agreement	- Lesions smaller than 0,4 cm (cholesterolosis,kidney lithiasis, gallbladder polyp)	7
	- Lesions around 1 cm (deep angiomiolipoma, kidney lithiasis, liver hemangioma at the dome of the liver)	8
	- Lesions between 1,5 and 3,8 cm (cysts, solid renal mass, multiple focal hyperechoic hepatic areas corresponding to focal steatosis	4

Tele-echography tests were performed after authorisation was obtained from patients. During the clinical validations tests performed using the OTELO tele-echography system, the leading experts involved were Dr Philippe Arbeille, in the University hospital of Tours, in France, Dr Conchita Bru, in Corporaci½ Sanitaria Clinic (Barcelona), and Dr Chrysa Tziakouri in Nicosia General Hospital. Abdominal examinations were performed by the experts which followed a study methodology that included:

a) Positioning of the robot in pre-defined anatomic areas that should allow to explore all the abdomen.

b) Evaluation of the organ visualisation, considering the complete exam of the organ, partial exam, absence of visualisation (not seen) or area not evaluated (not explored).

c) Pathology identification in each organ.

d) Ultrasound (US) exam performed by an expert Radiologist with an US state-of-the-art equipment.

e) The diagnosis obtained by the expert with the OTELO robot were compared with the final ultrasound diagnosis and follow-up. Continuous clinical tests took place in two different periods April–June 2003 and September–October 2004.

Punctual connectivity tests between Corporaci½ Sanitaria Clinic and Bourges Lab., Cyprus Hospital, Tours Hospital, and Ceuta Hospital took place between both periods. The clinical tests which were carried out between two fixed points in Cyprus were identified by the local medical experts. Nicosia General Hospital, which is situated in the central valley of the country, is the biggest hospital of the country. The radiology department has 7 expert doctors, who are not enough to cope with the high numbers of patients of the Radiology department. The common practice is that this department gives diagnosis also for X-rays for patients of another three

small rural hospitals of the country. These X-Rays must be sent from the rural hospitals to the central hospitals for diagnosis and then back to the rural hospital by courier.
This is because there are no experts in rural hospitals and thus the delay in having a diagnosis for a patient in a remote area is enormous (usually from 3 to 5 days).
The use of tele-echography will thus contribute to the increase of the level of the offered medical care ; Both the quality and the speed of diagnosis will be of much higher quality. On the other hand it will reduce the load to the expert doctors as well as the expenses of the state.

One such small rural hospital is situated on the Troodos mountains, in the village of Kyperounta, 75 km away from Nicosia, the capital of the country.
During the validation clinical experiments in Cyprus, under the MARTE project, the expert site equipment was installed in Nicosia hospital and the patient site equipment in Kyperounta hospital. The connection link was consisting of 4 x 128 ISDN lines. One line was needed for controlling the probe holder robot and the rest three lines for the teleconferencing system. The installation, the support and the covering of the expenses of operation of the telemedicine system were provided free by the Cyprus Telecommunications Authority (CYTA). The leader of the medical experts in Nicosia was Dr Crysa Tziakouri and in Kyperounta the leader of the medical team was Dr Michael Tryphonos. The installation and testing of the equipment was carried by the research teams of LVR (France) and the Higher Technical Institute (Cyprus).
The members of the French team trained the expert doctors of the central hospital. Consequently the leader of the doctors trained rural hospital medical staff involved in the validation tests. According to the medical protocol of the experiments, patients in the rural hospital had to be examined first by a non-expert doctor locally, following the normal ultrasound examination procedures and then by an expert doctor remotely, using the tele-echography MARTE system (Voskarides et. al. , 2004).

To make the examination easier and more comfortable for both the patient and the assistant who would hold and support the probe holder robot, a robotic arm was designed and constructed which was installed in Kyperounta hospital. This arm proved to be very useful since it improved the quality of the examination in the sense that the patient felt very relaxed and safe that the equipment would not exert any pressure on his or her body. On the other hand the assistant was free to concentrate on following the instructions and directives of the expert rather than being continuously alert for holding the robot properly.

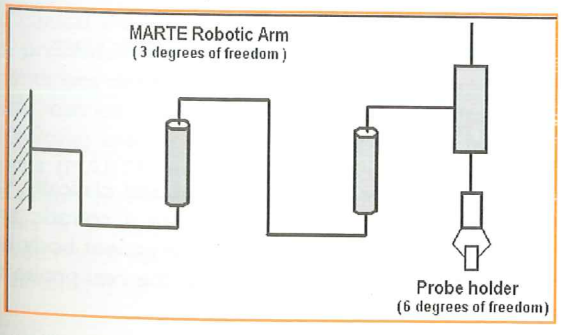

Fig. 4. MARTE Robotic Arm principle of operation

Table 2 Analysis of the capacity of tele-operated ultrasound study to identify pathology

ORGAN	Diagnosis Agreement	Decease	Cases	cm
LIVER STUDY Overall Accuracy 91%	Yes	Simple cyst	3	1-2.4
		Liver steatosis	3	
		Liver tumors	3	> 2.5
		Dilated intrahepatic bile ducts	2	
	Not *	Single calcification	1	1.3
		Multiple focal hyperechoic lesions	1	0.5-2.5
		Haemangioma subdiafragmatic	1	1.2
		Mild steatosis	1	
GALL/ BLADDER STUDY- Overall Accuracy 88%	Yes	Cholesterolosis	1	
		Litiasis	2	
		Gallbladder dilatation	2	
	No	Polyp	1	> 0.5
		Cholestrolosis or microlitisis	4	
		Biliary sludge	1	
KIDNEY STUDY- Overall Accuracy 94%	Yes	Angio-miolipoma	1	1.4
		Renal litiasis	1	0.3 mm
		Pelvic ectasia	2	
		Renal cysts	3	
	No	2 renal litiasis	2	0.3/1.2
		angiomiolipoma	1	1.3
		Cysts	3	< 2.5
		primary tumor	1	3.8
PANCREAS Overall Accuracy 100%	Yes	Tumoral enlargement	1	
		Agreement in all normal cases		
	No	0 cases		
SPLEEN Overall Accuracy 100%	Yes	3 patients with splenomegaly		
		accessory spleen	1	1
	No	0 cases		
BLADDER- Overall Accuracy 100%		No pathology was found		
ABDOMINAL AORTA and INFERIOR VENA CAVA		They were partly seen in 96 % the patients		

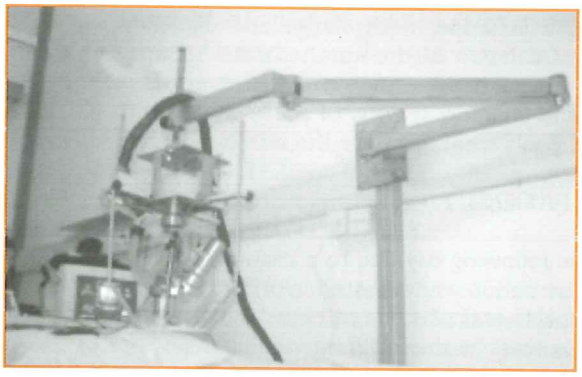

Fig. 5. MARTE Robot holder arm designed and constructed by the MARTE research team of the Higher Technical Institute and installed and used in Kyperounta hospital.

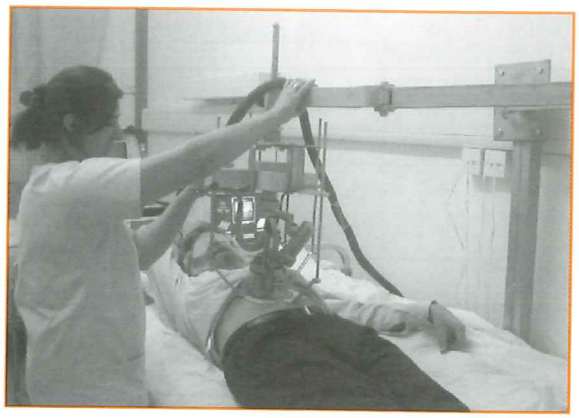

Fig. 6. Use of the MARTE arm during tele-echography examination by expert radiologists in Nicosia General Hospital assisted by a trained paramedic in Kyperounta hospital.

Another novelty during the MARTE validation tests was the use of a mirror on the opposite wall phasing the tele-conferencing unit camera in the patient site.
This mirror gives the opportunity to the expert to view simultaneously two ambient views of the patient site.

Relevant guidance regarding tele-echography examination is given in Figure 7 in combination with table 3.
The validation tele-echography clinical tests were performed by examining real patients in Kyperounta. One examination was performed during an emergency when the patient had strong pain in the abdominal area. The cause was diagnosed both locally using normal echography and remotely using the tele-echography system, by experts in Nicosia hospital. The system apart from tele-control, was also used extensively for the remote training of non-expert-local doctors in Kyperounta and medical staff by experts and engineers situated in the central hospital in Nicosia and/or in France.

The details of remote examination of real patients in Kyperounta using tele-echography are given below:

a) PATIENT1 (Female, 78 years) Casualty Kyperounta hospital.

1. Clinical history/ Examination: Abdominal pain, fever, palpable mass at the right hypochondrium to the mid – epigastrium.
2. Tele-echography examination findings: i) Distended Gall-Bladder with sludge and cholelithiasis. ii) Mild Dilatation of the intrahepadic bile ducts around the portal hepatis.
3. Opinion: i) Signs of acute cholecystitis ii) The palpable mass is due to the distended gall bladder.

b) PATIENT 2 (Re-examination of PATIENT 1)

The following day due to a request by her physician, the examination was repeated in order to clarify whether the palpable area was due to either the distended gall bladder or a mass at the left liver lobe. The findings of the new tele-echography examination were identical to the previous tele-echography examination. Additionally the left liver lobe was found to be with normal echogenicity. The above findings were confirmed the following day at Kyperounya hospital using conventional echography.

c) PATIENT 3 (Male, 65 years old) Inpatient Kyperounta hospital.

1. Clinical history – The incident was followed up after treatment: Patient had a known history of a pelvic abscess, which was confirmed with ultra sonography and CT examination. The patient was under antibiotic treatment for ten (10) days.
2. Tele-echography examination: The abscess was detected and appeared to have much smaller size than the reported size from the previous examinations (of the order of 50 %).
3. Opinion: The treatment was efficient as the abscess decreased in size. A follow-up examination was recommended.

The above tele-echography findings were confirmed the following day using conventional examination.

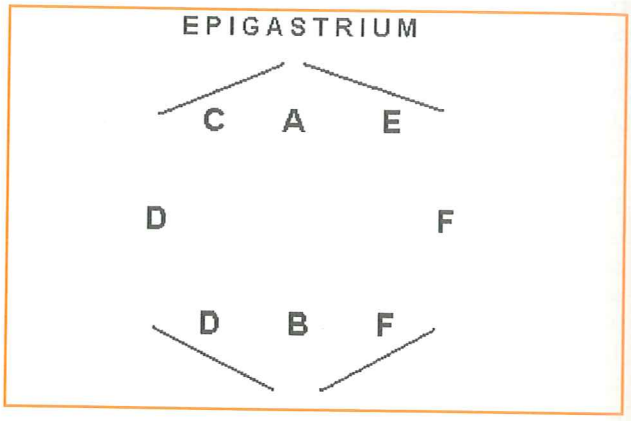

Fig.7. Corporal schema for epigastrium examination

Table 3: Examination guide for tele-echography

		To see...
A	Transversal Longitudinal	Liver (Left Lobe); Pancreas Liver (Left Lobe); Aorta; Cava
B	Transversal Longitudinal	Bladder, prostate, uterus, annexes Bladder, uterus, Douglas
C	Transversal Longitudinal	Liver, portal vein Right kidney, free fluid, paracolic space
D	Transversal Longitudinal	Right kidney, free fluid, paracolic space Free fluid , paracolic space
E	Transversal Longitudinal	Spleen, left kidney Spleen , left kidney
F	Transversal Longitudinal	Free fluid, paracolic space, left kidney Free fluid, paracolic space

4. DISCUSSION

The tele-echography system designed and clinically validated is not a full robotic system, but a robotic arm, which is located and maintained on the patient body by a paramedic or doctor, and induces on the real probe the movements of the expert hand.

A human interface between the robot and the patient

guarantees the safety of the patient. None of the patients refused to be investigated with the robotic system, and none of them complained after being examined by the system. The videoconferencing link allowed the patient and the expert doctor to communicate in real-time, thus contributing towards the quality of the examination and the diagnosis.

Robotic-surgery is probably the most popular application of telerobotics in medicine, where the surgical robotic arm is expected to reproduce very accurately the complex movements of the surgeon's hands. The robot must explore the 3 directions of space (6 degrees of freedom) and perform an invasive action.

In the case of tele- echography the robotic arm has to orientate the probe head at the surface of the patient skin (probe head remains in the same plane). There is a human interface between the robot and the patient and it is a non-invasive process. The medical assistant who handles the robotic arm can position it on or remove it from the patient skin at any moment. The use of the robotic arm, introduced during the MARTE experiments, which holds the weight of the robot, makes this task now easier and without any risk for the patient to be hurt by the echographic robotic arm.

The echo robotic arm can work with wireless links as well (e.g. satellite or UMTS channels) since an interruption of the data transfer will not be dangerous, which unfortunately does not apply in the case of a surgical robot. Therefore the safety problems were limited to the ultrasound safety.

Generally speaking the method used by the various experts is more or less the same, since this telemedicine system allows them to act as if they were examining a patient in their office. The social impact of the full application of this system in tele-echography is tremendous. Patients in rural or isolated hospitals may be examined by the experts anywhere in the world with safety.

This and other similar telemedicine systems can help towards the provision of medical care to the whole population of a country irrespective of the hospital they are admitted. Thus an important reason for making people move to the main cities will be weakened. The economic benefit for the health care system is obviously very important as well.

5. CONCLUSIONS

The clinical evaluation of the overall tele-operated chain was presented and the experimentation on abdominal patients was described and commented. The clinical evaluation carried out at the Corporaci½ Sanitaria Clinic (Barcelona) and the Nicosia and Kyperounta hospitals in Cyprus (MARTE project) were reported and discussed. The ergonomy of the overall system was also discussed, as this is a critical issue for the accurate interactivity between both remote and expert sides for the purpose of real-time diagnosis.

The use of the MARTE robotic arm will contribute towards improving the quality of the tele-echography examination in motion, since the assistant will concentrate to the medical aspects of the tele-examination rather than on holding the weight of the probe holder robot. In the case of a moving ambulance the absence of the MARTE robotic arm can make the examination difficult.

Successful experiments in the above field can lead us to the conclusion that tele-echography has great prospective with many benefits for the patients, the doctors, the economy and generally the whole society.

The clinical validation of the tele-echography system using the OTELO robot in France, Spain and Cyprus showed that this system is reliable and safe for the performance of remote US examination through satellite and/or UMTS channels.

ACKNOLEDGEMENTS

This project was partly funded through the Program for Bilateral Cooperation, Cyprus-France 2003-2005: "Mobile And Robotised Telemedecine for Emergency vehicle" (MARTE), by the Research Promotion Foundation of Cyprus and by EGIDE of France. ISDN connections were provided by CYTA.

REFERENCES

OTELO clinical and technical validation (2004). Reference D35_WP7_2004_10_1_A.

OTELO Consortium (2002) "OTELO project: mObile Tele-Echography using an ultra Light rObot", Telemed'02, London, UK, poster.

Pierrot F., Dombre E., Dégoulange E., Urbain L., Caron P., BoudetS., Gariépy J., and Mégnien J.-L (1999). "Hippocrate: a safe robot arm for medical applications with force feedback", Medical Image Analysis, vol. 3 (3), pp. 285-300.

Poisson G, P. Vieyres, P. Poignet and A. Gourdon (1999). "Robot à trois degrés de liberté et à un point fixe" (Three degree of freedom and one fixed point) ; French Patent nΓ 9903736, Institut National de la Protection Industrielle « INPI », France.

Smith-Guerin N., L. Al Bassit, G. Poisson, C. Delgorge, P. Arbeille and P. Vieyres (2003). "Clinical validation of a mobile patient-expert tele-echography system using ISDN lines", IEEE-EMBS Information Technology Applications in Biomedicine, Birmingham, UK.

Vieyres P., G Poisson, F Courrege, O Merigeaux and Ph Arbeille (2003). "The TERESA project : from space research to ground tele-echography", Industrial Robot: An International Journal, 30 (1), pp. 77-82.

Vilchis A, et al. (2001). "TER: a system for robotic tele-echography," Proc. of International Conference of Medical Image Computing and Computer- Assisted Intervention, Utrech, The Netherlands, pp. 326-334.

Voskarides S., N. Smith-Guerin, C. Novales, Josserand L. and G. Mourioux (2004) "Marte tele-echography manual, MTE 1_V_5", Nicosia.

AN HONORARY AWARD TO THE HTI

The "Solar energy e-learning laboratory (Solar e-lab)" of the Higher Technical Institute was awarded the "Diploma for Excellence in the use of Information Technology" by the "Stockholm Challenge Award 2006", during a ceremony that took place in the Stockholm City Hall in Sweden, on the 11th of May 2006. Of the 1165 originally registered projects in this international competition, the Challenge Award jury identified 151 projects, including the "Solar e-lab", acknowledged as Challenge finalists. Dr Ioannis Michaelides, Head of the Mechanical Engineering Department, and Dr Polyvios Eleftheriou, lecturer, represented HTI in the above event and also participated in the workshops and conference that took place during 9-10 May 2006, at the Royal Institute of Technology in Stockholm.

The "Solar Energy e-Learning Laboratory" was the product of a research project financed by the European Commission within the Leonardo da Vinci programme. The value of this e-lab is that it goes beyond usual e-learning and virtual courses; it provides access to remotely located students (anywhere in the world) to perform live experiments through the internet. The e-lab has already been accessed and used by many users from many Universities all over the world.

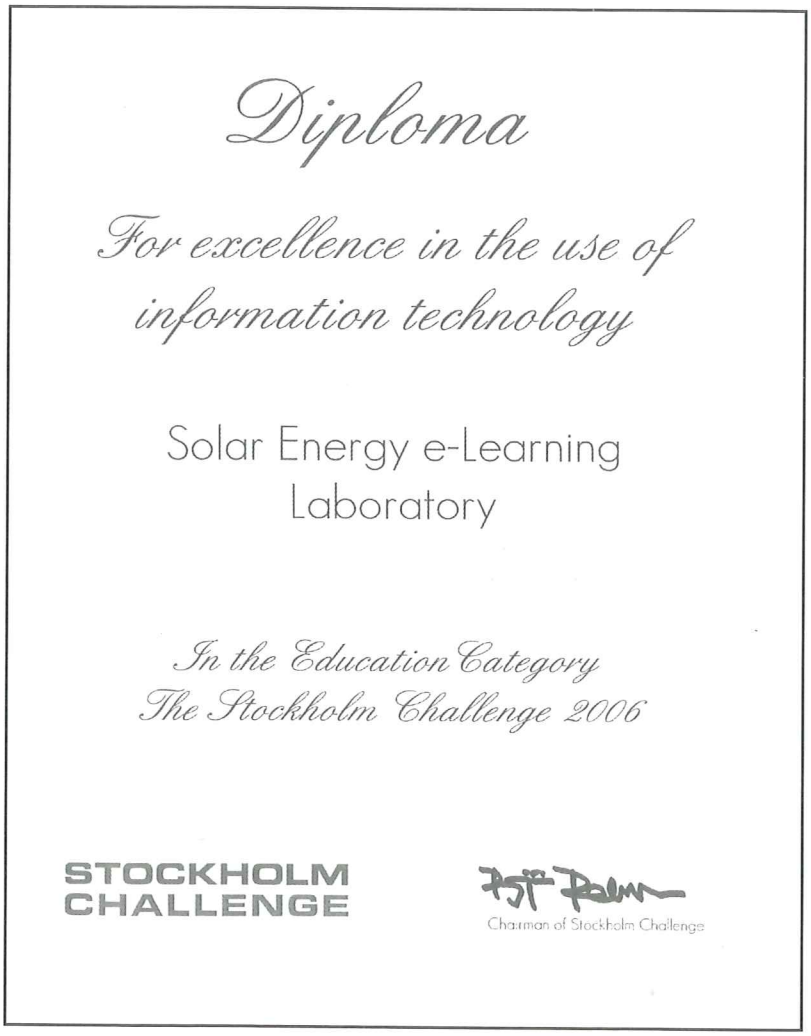

DR. SOTERIS KALOGIROU, INTERNATIONAL WREC AWARD RECIPIENT

During the 9th World Renewable Energy Congress (WREC) which took place in Florence, Italy from 19 to 25 August 2006, there was a competition for awards in various renewable energy categories. More than 1100 scientists from 110 countries participated in the competition. The award in the category Scientists and topic Solar Energy was received by Dr. Soteris Kalogirou, who is an instructor of Mechanical Engineering. The award was presented during a special Awards Ceremony which took place on Friday 25th of August in Palazzo Vecchio (old palace) in Florence.

The proceeding of the award is as follows:

The award in the category Scientists and topic Solar Energy is given to Dr. Soteris Kalogirou from Higher Technical Institute in Nicosia, Cyprus. Since 1985 Dr. Kalogirou has been involved in research dealing with the use of solar energy collectors and systems. He also pioneered in applying artificial intelligence methods for the modelling and performance prediction of energy and solar energy systems. He has 15 book contributions and published 146 papers out of which 60 in international scientific journals. Until now he has received 550 citations on this work.

Dr. Kalogirou (right) with Professor Ali Sayigh, Chairman of WREN in the awards ceremony

The awards ceremony in Palazzo Vecchio

PUBLICATIONS FOR THE YEAR 2005-2006

CIVIL ENGINEERING DEPARTMENT

1. Serghides, D. 2006 Bioclimatic Designs for the New University of Cyprus: A Student Housing, Proceedings of EPEQUB 2006 Conference, Milos Island, Greece.

2. Kathijotes N. Marinova S. Petrov K. "Effects of Treated Wastewater and Sludge in Agriculture: Environmental and Growth Evaluation of Selected Cultures". International Scientific Conference, Agricultural Engineering Problems, Latvian University of Agriculture, 2-3 June 2005 Jelgava, Latvia

3. Marinova S., Tsolova V., Kathijotes N. "Chemical Changes in Alluvial Lawn Soils, Fertilized by Sediments from Wastewater Treatment Stations" International Conference – Balkan Economic Reconstruction and Ecology -2005" The Balkan Academy of Sciences and Culture, 8-10 June 2005 Sofia," Ecology and Industry " Vol. VII N 1, 2005. BG

4. Koleva M. Kathijotes.N 'Reclamation of Disturbed Terrain by Using Biological Active Humic Meliorates: Cyprus Asbestos Mines" International Scientific Conference UNITECH '05 Technical University of Gabrovo, Nov 2005 Gabrovo, BG

5. Kathijotes N. "Wastewater Reuse for Irrigation: an Acceptable Soil Conditioner?" Conference on Water Observation and Information System for Decision Support BALWOIS 2006, 23-26 May 2006 Ohrid, F.Y.Republic of Macedonia

6. Kathijotes N. "Wastewater Reuse for Irrigation: A Preview of the Cyprus Experience". Balcanereco '06, The Balkan Academy of Sciences and Culture, June 2006 Sofia, BG

7. Marinova S., Kathijotes N., "Requirements and Possibilities for Utilization of Sewage Sludge in Agriculture" Balcanereco '06, The Balkan Academy of Sciences and Culture, June 2006, Sofia, BG

8. Kathijotes N., "Wastewater Reuse for Irrigation: Ecological Concerns and Constraints." HydroEco 2006, International Multidisciplinary Conference Hydrology and Ecology, Sept.2006 Karlovy Vary, Czech Republic

MECHANICAL and MARINE ENGINEERING DEPARTMENT

1. Michaelides I., Eleftheriou P., and Economides K. Solar energy e-learning laboratory – Remote experimentation over the Internet. International Journal of Online Engineering, Vol. 1, No. 2 (2005), www.i-joe.org (2005).

2. Μιχαηλίδης Ι., Ελευθερίου Π., Οικονομίδης Κ. Εργαστήριο Ηλιακής Ενέργειας για εξ Αποστάσεως Εργαστηριακές Δοκιμές μέσω Διαδικτύου, 8ο Εθνικό Συνέδριο για τις Ήπιες Μορφές Ενέργειας, Θεσσαλονίκη 29-31 Μαρτίου, 2006.

ELECTRICAL ENGINEERING DEPARTMENT

1. Spyros P Spyrou, Biomedical Engineering in Cyprus: An Overview IFMBE Proceedings, Vol 14, (World Congress on Medical Physics and Biomedical Engineering 2006), Editors: Sun I Kim and Tae Suk Suh, Aug. 2006 Springer Publications, ISBN 3-540-36839-6

GENERAL STUDIES DEPARTMENT

Book Contribution
Invited Review Chapter

1. Andreas Othonos, Kyriacos Kalli, David Pureur, and Alain Mugnier "Fibre Bragg gratings" in "Wavelength Filters for Fibre Optics", editor: Herbert Venghaus, FhG-HHI. Publisher: Springer, Springer Series in Optical Sciences, Volume 123, 2006.

Journal Publications

2. C.Themistos, B. M. A. Rahman, M. Rajarajan, K. Kalli and K.T.V. Grattan "Characterization of surface plasmon modes in metal-clad optical waveguides" Applied Optics, Volume 45, Number 33, 8 pages, 2006.

3. K. Kalli, G. Simpson, K. Zhou, L. Zhang, D. Birkin, T. Ellingham and I. Bennion [Special Issue on Optical Fibre Sensors] "Spectral modification of type IA fibre Bragg gratings by high power near infra-red lasers" Measurement Science and Technology, Volume 17, pages: 968-974, 2006.

4. J. S. Petrovic, V. Mezentsev, H. Dobb, D. J. Webb, K. Kalli, and I. Bennion [Special Issue on Optical Waveguide Theory and Numerical Modelling] "Multiple Period Resonances in Long Period Gratings in Photonic Crystal Fibres" Optical and Quantum Electronics, Volume 38, Numbers 1-3, pages 209-216, 2006.

Conference Publications

5. D. J. Webb, H. Dobb, K. Carroll, K. Kalli, A. Argyros, M.C. Large, M.A. van Eijkelenborg "Fibre Bragg gratings recorded in microstructured polymer optical fibre" 18th International Conference on Optical Fiber Sensors Topical Meeting. October 23-27, 2006, Cancun, Mexico

6. K. Kalli, H. L. Dobb, D. J. Webb, M. Komodromos, C. Themistos, G.-D. Peng, Q. Fang, I. W. Boyd "Electrically Tunable Bragg Gratings in Single Mode Polymer Optical Fiber" 18th International Conference on Optical Fiber Sensors Topical Meeting. October 23-27, 2006, Cancun, Mexico.

7. [Invited Paper] K Kalli, H L Dobb, D J Webb, G-D Peng, Q Fang and I Boyd "Progress towards a tunable FBG POF-based filter" 5th International Conference on Optical Communications and Networks/ the 2nd International Symposium on Advances and Trends in Fiber Optics and Applications (ICOCN/ATFO 2006) September 18-22, 2006, Chengdu, China.

8. H. Dobb, K. Carroll, D. J. Webb, K. Kalli, M. Komodromos, C. Themistos, G. D. Peng, A. Argyros, M.

Large, M. van Eijkelenborg, Q. Fang, and I. Boyd "Thermal response of Bragg gratings in POF" 15th International Conference on Plastic Optical Fiber, Seoul, Korea, September 2006

9. K. Kalli, G. Simpson, K. Zhou, L. Zhang, and I. Bennion "Impact of hydrogenation conditions on the temperature and strain discrimination of Type I and Type IA Bragg grating sensors" SPIE Photonics Europe 2006, EPE108 Optical Sensing II, April 2006

10. T. Allsop, H. Dobb, A. Main, A. Martinez, M. Dubov, K. Kalli, D.J. Webb, I. Bennion "A comparison of the spectral properties of high temperature annealed long-period gratings inscribed by femtosecond laser, UV and fusion-arc" SPIE Photonics Europe 2006, EPE112 Reliability of Optical Fiber Components, Devices, and Systems, and Networks III, April 2006

11. K. Kalli, G. Simpson, K. Zhou, L. Zhang, D. Birkin, T. Ellingham and I. Bennion "Spectral modification of type IA fibre Bragg gratings by high power near infra-red lasers" SPIE Photonics Europe 2006, EPE112 Reliability of Optical Fiber Components, Devices, and Systems, and Networks III, April 2006

12. Kyriacos Kalli, George Simpson, Helen Dobb, Michael Komodromos, David Webb and Ian Bennion "Annealing and temperature coefficient study of Type IA fibre Bragg gratings inscribed under strain and no strain - implications to optical fibre component reliability" SPIE Photonics Europe 2006, EPE112 Reliability of Optical Fiber Components, Devices, and Systems, and Networks III, April 2006

13.[Invited paper] Helen Dobb, Karen Carroll, David Webb, Kyriacos Kalli, Michael Komodromos, Christos Themistos, Gang-Ding Peng, Alex Argyros, Maryanne Large, Martijn van Eijkelenborg "Reliability of fibre Bragg gratings in polymer optical fibre" SPIE Photonics Europe 2006, EPE112 Reliability of Optical Fiber Components, Devices, and Systems, and Networks III, April 2006

14. [Invited paper] Helen Dobb, Karen Carroll, David Webb, Kyriacos Kalli, Michael Komodromos, Christos Themistos, Gang-Ding Peng, Alex Argyros, Maryanne Large, Martijn van Eijkelenborg, Qi Fang, and Ian Boyd "Grating based devices in polymer optical fibre" SPIE Photonics Europe 2006, EPE108 Optical Sensing II, April 2006

15. T. Allsop, H. Dobb, R. Neal, K. Kalli, C. Themistos, B.M.A. Rahman, D. Webb, D. Mapps and I. Bennion "Enhanced Spectral Sensitivity of Fibre Long Period Gratings to Refractive Index of Aqueous Solutions Utilising Copper Patterned Coatings" Proceedings of SPIE Volume: 6083, Optical Fibers and Sensors for Medical Diagnostics and Treatment Applications VI, Biomedical Optics BiOS 2006

MONOGRAPH

16. C.Harakis (editor), P.Christodoulides Anti-social Behavior of the Cypriot Youth: Racist tendencies (in greek), Ant. N. Sakkoulas Publishers, 2005.

JOURNAL ARTICLES

17. D.Leonidou, M.Vassiliou, P.Christodoulides & A.Georgiou, Drug abuse in the Cypriot youth: Characteristics of users, Cyprus J. Sci. Tech., 4(4) 98-114, 2005.
D.Leonidou, M.Vassiliou, A.Georgiou & P.Christodoulides, Drug abuse in the Cypriot youth: Sources of information and prevention, Cyprus J. Sci. Tech., 4(4) 81-97, 2005.

ENGINEERING PRACTICE DEPARTMENT

Journals

1. Kalogirou, S., 2006. Prediction of Flat-Plate Collector Performance Parameters Using Artificial Neural Networks, Solar Energy, Vol. 80, No. 3, pp. 248-259.

2. Mellit, A., Benghanem, M. and Kalogirou, S.A., 2006. An adaptive wavelet-network model for forecasting daily total solar radiation, Applied Energy, Vol. 83, No. 7, pp. 705-722.

3. Kalogirou, S. and Tripanagnostopoulos, Y., 2006. Hybrid PV/T Solar Systems for Domestic Hot Water and Electricity Production, Energy Conversion and Management, Vol. 47, No. 18-19, pp. 3368-3382.

4. Mellit, A. Benghanem M. and Kalogirou S.A., 2007. Modeling and simulation of a stand-alone photovoltaic system using an adaptive artificial neural network: Proposition for a new sizing procedure, Renewable Energy, Vol. 32, No. 2, pp. 285-313.

Conferences

1. Kalogirou, S. and Tripanagnostopoulos, Y., 2006. Applications of PV/T Solar Energy Systems, Proceedings of the 8th National Conference for the Renewable Energy Sources on CD-ROM, Thessaloniki, Greece.

2. Kalogirou, S., 2006. Review on the Use of Solar Energy in Cyprus, Proceedings of the 8th National Conference for the Renewable Energy Sources on CD-ROM, Thessaloniki, Greece.

3. [Invited] Kalogirou, S., 2006. Artificial Neural Networks and Genetic Algorithms for the Optimisation of Solar Thermal Systems, Proceedings of the IX World Renewable Energy Congress on CD-ROM, Florence, Italy.

4. Kalogirou, S., Florides, G., Lalot, S. and Desmet, B., 2006. Development of a Neural Network-Based Fault Diagnostic System, Proceedings of the IX World Renewable Energy Congress on CD-ROM, Florence, Italy.

5. Florides, G. and Kalogirou, S., 2006. Thermal performance of a U-tube borehole heat exchanger, Proceedings of the IX World Renewable Energy Congress on CD-ROM, Florence, Italy.

6. Mellit, A. and Kalogirou, S., 2006. An ANFIS-based Modeling for a Photovoltaic Power Supply (PVPS) System, Proceedings of the IX World Renewable Energy Congress on CD-ROM, Florence, Italy.

7. Mellit, A. and Kalogirou, S., 2006. Application of Neural Networks and Genetic Algorithms for Predicting the Optimal Sizing Coefficient of Photovoltaic Supply (PVS) Systems, Proceedings of the IX World Renewable Energy Congress on CD-ROM, Florence, Italy.

Participation of Staff in Short Courses/Conferences and Educational Exchange Programmes for the Year 2005 – 2006

Conferences/ Seminars attended by HTI Academic Staff:

1. Mr Marinos Ioannides, Lecturer in the Computer Studies Department, participated in the National Conference **"CIPA 2005"**, held in Torino, Italy, 27 September 2005 – 2 October 2005.

2. Dr George Florides, Senior Instructor in the Engineering Practice Department and Dr Soteris Kalogirou, Instructor in the Engineering Practice Department, participated in the National Conference **"CLIMA 2005"** in Lozanne, Switzerland, 9 – 12 October 2005.

3. Mr Constantinos Loizou, President of IAESTE Cyprus and Mr Theodoros Symeou, National Secretary of IAESTE Cyprus, attended the **Annual Conference of IAESTE**, held in Malta, 21 – 27 January 2006.

4. Mr Sotos Voskarides, Lecturer in the Electrical Engineering Department, visited University of Neuchatel for research cooperation, Switzerland, 30 January 2006 – 3 February 2006.

5. Dr Ioannis Angeli, Lecturer in the Mechanical Engineering Department, presented a paper in the "2nd Balkan Quality Forum" titled: **"Hierarchy of actions for Improvement – a Case Study of how CAF can be implemented using Quality Function Deployment"**, Sofia, Bulgary, 17 – 18 March 2006.

6. Dr Ioannis Michaelides, Head of the Mechanical Engineering Department, participated in the 8th National Conference on Renewable Energy Sources where he presented a paper titled: "**Solar Energy e-learning Laboratory – Remote Experimentation over the Internet**", Thessaloniki, Greece, 29 – 31 March 2006.

7. Dr Kyriacos Kalli, Lecturer in the General Studies Department, participated in the European Conference "**Photonics Europe 2006**" in Strasbourg, France, 3 – 7 April 2006.

8. Dr Nicholas Kathijiotes, Lecturer in the Civil Engineering Department, participated in the International Conference "BALWOIS 2006" where he presented a research titled: "**Wastewater Re-use for Irrigation: An acceptable soil conditioner?**" in Ohrid, F.Y.R.O.M, 23 – 26 May 2006.

9. Dr Costas Neocleous, Senior Lecturer in the Mechanical Engineering Department, presented a paper in the "7th World Scientific and Engineering Academy and Society Multiconference: NN'O6, FS'06, EC'06, AMTA'06, MCBC'06, ICAI'06" { International Conference on NEURAL NETWORKS (NN'06) } titled: "**A comparison of classical, neural and fuzzy control for an underwater vehicle**" in Cavtat, Croatia, 12 – 14 June 2006.

10. Mrs Anastasia Mouskou – Peck, Lecturer of English and Technical Report Writing in the General Studies Department, attended a conference on "**Diversity in Language Learning and Teaching**" at the Chalmers University of Technology in Goteborg, Sweden, 15 – 17 June 2006.

11. Dr George Florides, Senior Instructor in the Engineering Practice Department and Dr Soteris Kalogirou, Instructor in the Engineering Practice Department, took part in the meeting concerning the "**Development of an artificial neural network based fault diagnostic system for solar systems**" in Valenciennes, France, 19 – 23 June 2006.

12. Mr Savvas Savvides, Head of the Engineering Practice Department, attended the Annual General Meeting of **European Higher Engineering Education and Technical Professionals Association (EurEta)** in Kaliari, Italy, 16 – 20 June 2006.

13. Dr Marios Kassinopoulos, Lecturer in the Electrical Engineering Department, attended a seminar on "**The Three Cycle System**" at Napier University in Edinburgh, Scotland, 22 – 23 June 2006.

14. Dr Despina Serghides, Senior Lecturer in the Civil Engineering Department, presented a paper in the International Workshop: "EPEQUP 2006" titled: "**Bioclimatic Designs for the Student Housing of the New University of Cyprus**", Milos, Greece, 5 – 7 July 2006.

15. Dr Costas Neocleous, Senior Lecturer in the Mechanical Engineering Department, participated in the "**Euroscience Open Forum 2006**" in Munich, Germany, 15 – 19 July 2006.

16. Dr George Florides, Senior Instructor in the Engineering Practice Department and Dr Soteris Kalogirou, Instructor in the Engineering Practice Department, participated in the "**IX World Renewable Energy Congress – WREC 2006**", where Dr Soteris Kaloyirou received the "WREC 2006 Award" in the topic of Solar Energy, Florence, Italy, 19 -25 August 2006.

Short Courses attended by HTI Academic Staff:

1. Dr Kyriacos Kalli, Lecturer in the General Studies Department, participated in the workshop: "**Gratings in Polymer Optical Fibre**" at Aston University in Birmingham, UK, 7 – 11 November 2005.

2. Mrs Pagona Katsouri, Lecturer in the Computer Studies Department, participated in the educational programme: "**Microsoft.NET Framework and the VB.NET and C# Programming Languages**" held in London, 14 – 17 November 2005.

3. Mr Spyros Spyrou, Senior Lecturer in the Electrical Engineering Department, attended the training programmes: "**TT1 – Bioinstrumentation**", "**TT2 – Bioelectromagnetism**" and "**TT3 – Bioinformatics and Computational Biology**" which took place in Prague, Czech Republic, 18 – 22 November 2005.

4. Dr Pavlos Christodoulides, Lecturer in the General Studies Department, participated in the educational programme "**Rogue Waves**" at ICMS in Edinburgh, UK, 12 – 15 December 2005.

5. Mr Costas Ioannou, Lab Assistant in the Electrical Engineering Department, attended "**Modern Digital Communications**" at Surrey University, UK, 27 – 31 March 2006.

6. Mr Constantinos Christofi, Instructor in the Engineering Practice Department and Mr Charalambos Tsioutis, Instructor in the Engineering Practice Department, attended the training programme: "**CNC Lathe Combi 2000**", UK, 5 – 12 June 2006.

7. Dr Despina Serghides, Senior Lecturer in the Civil Engineering Department, attended the educational programme "**Solar and Bioclimatic Architecture**" at Glasgow Caledonian University in Scotland, UK, 26 – 30 June 2006.

8. Mr Spyros Spyrou, Senior Lecturer in the Electrical Engineering Department, participated in the educational programme for **Medical Engineering/ Medical Physics** in Seoul, Corea, 28 August – 1 September 2006.

Visits/ Educational Exchange Programmes

1. Mr George Katodrytis, Lecturer in the Mechanical Engineering Department, visited the Aristotle University under the Staff Exchange Programme, Thessaloniki, Greece, 17 – 21 October 2005.

2. Dr Herodotos Stavrides, Head of the Civil Engineering Department, participated in the Staff Exchange Programme and visited Surrey University , UK, 7 – 11 November 2005.

3. Dr Christos Marouchos, Lecturer in the Electrical Engineering Department, participated in the Staff Exchange Programme and visited Brunel University, UK, 7 – 11 November 2005.

4. Dr Ioannis Michaelides, Head of the Mechanical Engineering Department, participated in the Staff Exchange Programme and visited Surrey University, UK, 14 – 17 November 2005.

5. Dr Chrysis Papaleontiou, Lecturer in the Civil Engineering Department, visited the Poushkarov Institute of Soil Sciences under the Staff Exchange Programme, Bulgary, 21 – 25 November 2005.

6. Dr Pavlos Christodoulides, Lecturer in the General Studies Department, visited University College London (UCL) under the Staff Exchange Programme, UK, 26 – 31 March 2006.

7. Dr George Florides, Senior Instructor in the Engineering Practice Department, visited Brunel University under the Staff Exchange Programme, UK, 26 March 2006 – 2 April 2006.

8. Mr Spyros Spyrou, Senior Lecturer in the Electrical Engineering Department, visited the Derby University within the Erasmus – Socrates Programme. He gave lectures on **Medical Electronics** and **Analogue Electronics**, UK, 1 – 5 May 2006.

9. Mr Ioannis Demetriou, Lecturer in the Electrical Engineering Department, visited the Tours University within the Erasmus – Socrates Programme, France, 22 – 26 May 2006.

10. Mr Savvas Savvides, Head of the Engineering Practice Department, visited the University of Latvia under the Staff Exchange Programme, 29 May – 4 June 2006.

11. Mr Charalambos Chrysafiades, Senior Lecturer in the Electrical Engineering Department, visited the Tallinn University of Technology, under the **PROTOCOL** of the **First Session of the Cypriot – Estonian Intergovernmental Commission on Economic, Scientific, Technical and Industrial Cooperation**, Esthonia, 30 May 2006 – 3 June 2006.